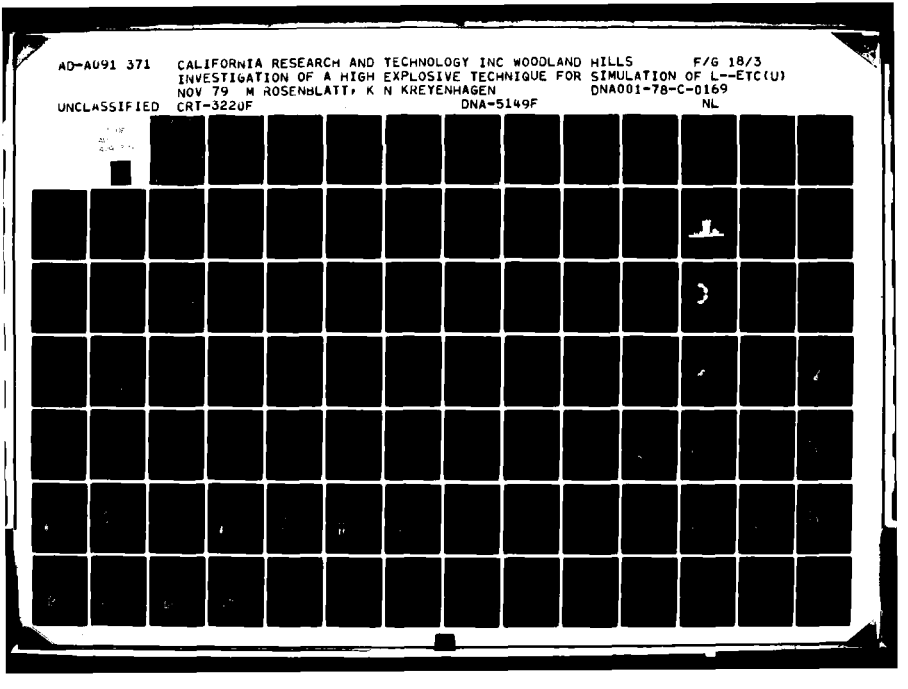
AD-A091 371
CALIFORNIA RESEARCH AND TECHNOLOGY INC WOODLAND HILLS F/G 18/3
INVESTIGATION OF A HIGH EXPLOSIVE TECHNIQUE FOR SIMULATION OF L--ETC(U)
NOV 79 M ROSENBLATT, K N KREYENHAGEN DNA001-78-C-0169
UNCLASSIFIED CRT-3220F DNA-5149F NL

DNA 5149F

INVESTIGATION OF A HIGH EXPLOSIVE TECHNIQUE FOR SIMULATION OF LOCAL FALLOUT FROM SHALLOW-BURIED BURSTS

California Research and Technology, Inc.
6269 Variel Avenue, Suite 200
Woodland Hills, California 91367

1 November 1979

Final Report for Period 1 March 1978—31 July 1979

CONTRACT No. DNA 001-78-C-0169

THIS WORK SPONSORED BY THE DEFENSE NUCLEAR AGENCY
UNDER RDT&E RMSS CODE B344078464 Y99QAXSA00210 H2590D.

Prepared for
Director
DEFENSE NUCLEAR AGENCY
Washington, D. C. 20305

Destroy this report when it is no longer needed. Do not return to sender.

PLEASE NOTIFY THE DEFENSE NUCLEAR AGENCY, ATTN: STTI, WASHINGTON, D.C. 20305, IF YOUR ADDRESS IS INCORRECT, IF YOU WISH TO BE DELETED FROM THE DISTRIBUTION LIST, OR IF THE ADDRESSEE IS NO LONGER EMPLOYED BY YOUR ORGANIZATION.

UNCLASSIFIED

SECURITY CLASSIFICATION OF THIS PAGE (When Data Entered)

(19) REPORT DOCUMENTATION PAGE

READ INSTRUCTIONS BEFORE COMPLETING FORM

(18) 1. REPORT NUMBER: DNA 5149F

2. GOVT ACCESSION NO: AD-A091 371

3. RECIPIENT'S CATALOG NUMBER:

(6) 4. TITLE (and Subtitle): INVESTIGATION OF A HIGH EXPLOSIVE TECHNIQUE FOR SIMULATION OF LOCAL FALLOUT FROM SHALLOW-BURIED BURSTS.

(9) 5. TYPE OF REPORT & PERIOD COVERED: Final Report for Period 1 Mar 78—31 Jul 79

(14) 6. PERFORMING ORG. REPORT NUMBER: CRT-3220F

(10) 7. AUTHOR(s): M. Rosenblatt, K. N. Kreyenhagen, S. H. Schuster, R. J. Schlamp, P. J. Hassig, A. S. Porton

(15) 8. CONTRACT OR GRANT NUMBER(s): DNA 001-78-C-0169 NEW

9. PERFORMING ORGANIZATION NAME AND ADDRESS:
California Research & Technology, Inc.
6269 Variel Avenue, Suite 200
Woodland Hills, CA 91367

10. PROGRAM ELEMENT, PROJECT, TASK AREA & WORK UNIT NUMBERS:
Subtask Y99QAXSA002-10

(16)

(11) 11. CONTROLLING OFFICE NAME AND ADDRESS:
Director
Defense Nuclear Agency
Washington, DC 20305

12. REPORT DATE: 1 Nov 79

13. NUMBER OF PAGES: 118 (17) A002

(12) 14. MONITORING AGENCY NAME & ADDRESS (if different from Controlling Office):

15. SECURITY CLASS. (of this report): UNCLASSIFIED

15a. DECLASSIFICATION/DOWNGRADING SCHEDULE: N/A

16. DISTRIBUTION STATEMENT (of this Report)

Approved for public release; distribution unlimited.

17. DISTRIBUTION STATEMENT (of the abstract entered in Block 20, if different from Report)

18. SUPPLEMENTARY NOTES

This work sponsored by the Defense Nuclear Agency under RDT&E RMSS Code B344078464 Y99QAXSA00210 H2590D.

19. KEY WORDS (Continue on reverse side if necessary and identify by block number)

Radioactivity
Fallout
Buried Nuclear Bursts
Cratering
Finite Difference Calculations
Multiphase Flow

20. ABSTRACT (Continue on reverse side if necessary and identify by block number)

Detonation of a shallow-buried nuclear device creates a strong shock wave in the surrounding soil, leading to formation of a crater and ejection of soil and radioactive weapon debris into the atmosphere. Predictions of local fallout depositions of this radioactive debris are important in developing tactical doctrines. Currently, predictions of local fallout from low-yield subsurface bursts in wet soils are very uncertain because the relevant nuclear tests were performed in dry alluvial soil at NTS.

DD FORM 1 JAN 73 1473 EDITION OF 1 NOV 65 IS OBSOLETE

UNCLASSIFIED

SECURITY CLASSIFICATION OF THIS PAGE (When Data Entered)

A 391 223 mt

In this investigation, computer code numerical solutions were performed and analyzed to examine the HE Local Fallout Simulation Technique used in the Diamond Ore and Essex Tests. In this experimental technique, iridium-coated tracer particles are mixed with the HE charge. Three numerical solutions were analyzed: a 10-ton HE burst buried 6 meters in wet soil (i.e., the Essex 6MS test), a 10-ton HE burst buried 6 meters in dry alluvial soil, and a 20-ton nuclear burst buried 6 meters in dry alluvial soil. Comparisons between the solutions indicate important effects on early lofting of tracers or radioactive debris due to differences in wet vs dry soil properties and differences in HE vs nuclear sources. Good agreement was obtained between the HE/Wet Media case and the observed early lofted cloud from Essex Test 6MS.

These conclusions are drawn:

1. The nominal 10-ton HE charges used in the Essex I test series did not adequately simulate the local fallout from shallow-buried 20-ton nuclear bursts; the vented energy was too small and the energy densities of vented material were too low. The most significant physical process of a nuclear burst which is not simulated by an HE charge is the release of the heat of vaporization upon condensation of soil which is vaporized by the shallow-buried nuclear burst. Most of this energy release occurs after venting as the soil vapor mixes with air above the burst, resulting in intense heating of the air and consequent buoyant lofting of the hot air plus entrained soil and radioactive material.
2. The ejecta plume from Essex 6MS was primarily a "throw out" cloud dominated by ballistic processes, aerodynamic drag filtering, and shedding of small particles from larger clumps. Buoyant lofting was minimal.
3. Because of buoyant lofting, radioactive material from a shallow-buried nuclear burst will reach a significantly higher altitude than the altitude reached by iridium tracers in the Essex 6MS test.
4. For HE sources, the dust cloud and iridium tracers in a dry soil remain at a lower altitude but reach a larger radius than in a wet soil. Additional analyses will be required before conclusions can be drawn about local fallout from nuclear bursts in wet and dry media.
5. Development of a satisfactory HE simulator for local fallout from buried nuclear bursts appears feasible, but the technique needs to be specifically designed to reproduce those phenomena which govern early lofting. The HE simulator needs to be designed on the basis of equivalent energy venting. This will probably mean using an explosive system with total energy greater than the nuclear yield. Extreme pressures from a nuclear burst result in vaporization of the device and surrounding soil. Transfer of the latent heat to air above the burst produces buoyant lofting. HE cannot vaporize the soil, but the equivalent energy from the heat of vaporization can probably be simulated.
6. The CRALE and DICE numerical models adequately treated the processes which determine the visible characteristics of the ejecta plume from Essex 6MS. Fallout deposition on the ground was not calculated or compared with observations, but the final positions of still-lofted tracers appeared consistent with test data.
7. Analyses of possible modifications to the HE Local Fallout Simulation Technique should be made towards improving simulation accuracy and confidence levels.

TABLE OF CONTENTS

LIST OF ILLUSTRATIONS

LIST OF ILLUSTRATIONS (Continued)

LIST OF ILLUSTRATIONS (Continued)

LIST OF ILLUSTRATIONS (Continued)

LIST OF ILLUSTRATIONS (Continued)

LIST OF TABLES

SECTION 1

INTRODUCTION AND SUMMARY

1.1 BACKGROUND OF HE LOCAL FALLOUT SIMULATION TECHNIQUE

Detonation of a shallow-buried nuclear device, such as an Atomic Demolition Munition (ADM) or Tactical Earth Penetrating Weapon (TEPW) will create a very strong shock wave in the soil, leading to formation of a crater and ejection of soil and radioactive weapon debris. Definition of expected crater dimensions, ejecta fallback characteristics, and radioactive fallout depositions are needed as a basis for developing tactical doctrines for the possible employment of such weapons. Inevitably, though not always explicitly stated, there are uncertainties associated with such definitions. In particular, current predictions of radioactive fallout from low-yield subsurface bursts in *wet* soils are very uncertain because the only available shallow-buried nuclear data are from tests performed in the relatively *dry* alluvial soil at the Nevada Test Site.

To help reduce this uncertainty, a high explosive concept for simulating local radiation fallout from subsurface nuclear bursts has been evolving in connection with the Middle Course II, Diamond Ore, and Essex programs. This concept, which will be referred to here as the HE Local Fallout Simulation Technique, makes use of iridium-tagged quartz particles distributed in the explosive charge.

Using this technique, tests have been fired in relatively dry media at Trinidad, Colorado (Middle Course II),[1] in wet shale at Ft. Peck, Montana (Diamond Ore),[2] and in wet soil at Ft. Polk, Louisianna (Essex I)[3].

1.2 ESSEX I LOCAL FALLOUT SIMULATION TESTS

The most comprehensive use of the HE Local Fallout Simulation Technique has been in the Essex I series. For these tests, the iridium tracer particles were uniformly distributed in gelled nitromethane explosive. Eight tests were performed to examine effects of depth of burial, stemming, and hole size upon the deposition of the tracer particles recovered in the ground. The test conditions are summarized in Table 1.1.

Different quantities of the explosive, varying between 8.0 and 12.4 tons, were used for the different DOB and stemming conditions. These quantities were established on the basis of series of calculations by Thomsen[4] and by Blake and Wilkins[5], in which the masses of explosive required to couple the same kinetic energy to the soil as occurs in nuclear bursts under the same conditions were determined. This equivalent kinetic energy criterion was based on the assumption (partially confirmed by cratering calculations) that it would lead to *equivalent cratering and ground motions*.

1.3 COMPARISON OF HE AND NUCLEAR LOCAL FALLOUT DATA IN WET AND DRY MEDIA

Figure 1.1 (adapted from Reference 3) shows the vent fraction* vs scaled DOB for several nuclear tests and for several HE tests using the Local Fallout Simulation Technique. Tests fired in wet

---

* Vent fraction from HE tests is defined[3] as the ratio of the tracer element (iridium) deposited beyond the limit of continuous ejecta in the local fallout area, divided by the initial iridium in the HE charge. Vent fraction in the nuclear events is the fraction of the total device activity deposited beyond the limit of continuous ejecta in the local fallout area. Long range or global nuclear fallout is not included in either vent fraction. The limit of continuous ejecta is that boundary within which the ground is completely covered by explosion-produced ejecta and debris. For craters in soil media, the area within this limit is of the order of ten times the crater area (i.e., out to ~3 crater radii).

Table 1.1 ESSEX I EVENTS[3]

(All tests were to simulate 20t nuclear burst)

Event	DOB (m)	Mass (t)	Density (g/cm^3)	Shape	Dia (m)	Height (m)	Stemming Condition
12MS	12	12.4	1.19	Cyl	2.29	2.29	Fully stemmed
6MS*	6	12.4	↓	↓	↓	↓	↓
6MU	6	9.9	↓	↓	↓	1.82	Unstemmed, 1.8 m dia hole
12MPS	12	12.4	↓	↓	↓	2.29	Partially stemmed, 0.18 m dia hole
12MU	12	8.0	0.96	↓	2.63	1.39	Unstemmed, 1.8 m dia hole
6MWS	6	10.0	0.98	↓	2.28	2.28	Stemmed with 1.71 m of water in 0.6 m dia hole
3MS	3	11.5	0.96	↓	2.65	1.98	Fully stemmed
3MU	3	9.0	0.94	↓	↓	1.57	Unstemmed, 1.8 m dia hole

* This event was numerically simulated by Case 3221 in current study

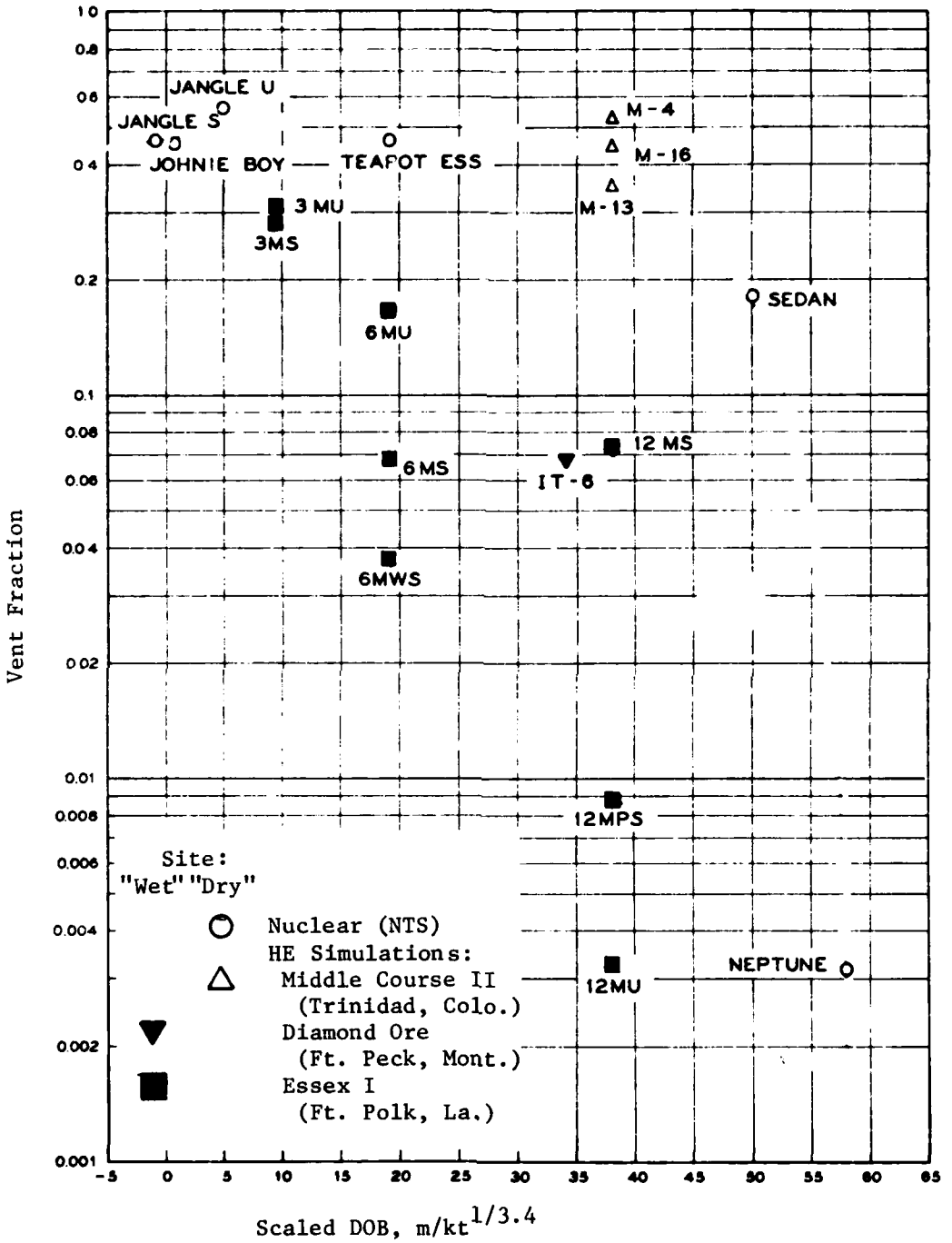

Figure 1.1 Vent Fraction vs Scaled DOB for Several NTS Nuclear Tests and HE Local Fallout Simulation Tests (adapted from Ref. 3)

media are designated by filled-in symbols, while those in dry media have open symbols. There is a strong perception from Figure 1.1 of a media dependence, with bursts in wet media producing much smaller vent fractions than bursts in dry media. If real, such a pronounced difference would have important implications, inasmuch as many targets of interest for shallow-buried low yield devices are in areas of wet soil. However, note that:

- All nuclear data in Figure 1.1 are from tests in dry media
- All wet media data in Figure 1.1 are from HE tests.

The only data which directly compare local fallout in wet and dry media are from the Essex (wet) and Middle Course II (dry) tests at 35-40 $m/kt^{1/3}$ DOB (i.e., Essex events 12MS, 12MPS, and 12MU vs Middle Course events M-4, M-13, and M-16). The highest vent fraction in the wet media is 7%; the lowest value in the dry media is 35%. This comparison certainly supports the hypothesis of a strong media dependence.

A comparison of local fallout *deposition profiles*, however, indicates that fallout distribution from the HE Local Fallout Simulation Technique may be qualitatively quite different than patterns observed from nuclear bursts. Figure 1.2 compares fallout profiles from Essex event 6MS (HE), Middle Course II event M-13 (HE), and Teapot Ess (Nuclear). In the HE simulation tests in both wet and dry media, the peak of the deposition curves falls well *within* the limit of continuous ejecta. By contrast, the peak in the nuclear test Teapot Ess is well *beyond* the limit of continuous ejecta.

The observation in Figure 1.2 that the deposition profiles from HE simulation tests *in both wet and dry media* have the same general relationship to the limit of continuous ejecta, and that this relationship is *different* than that observed in a nuclear

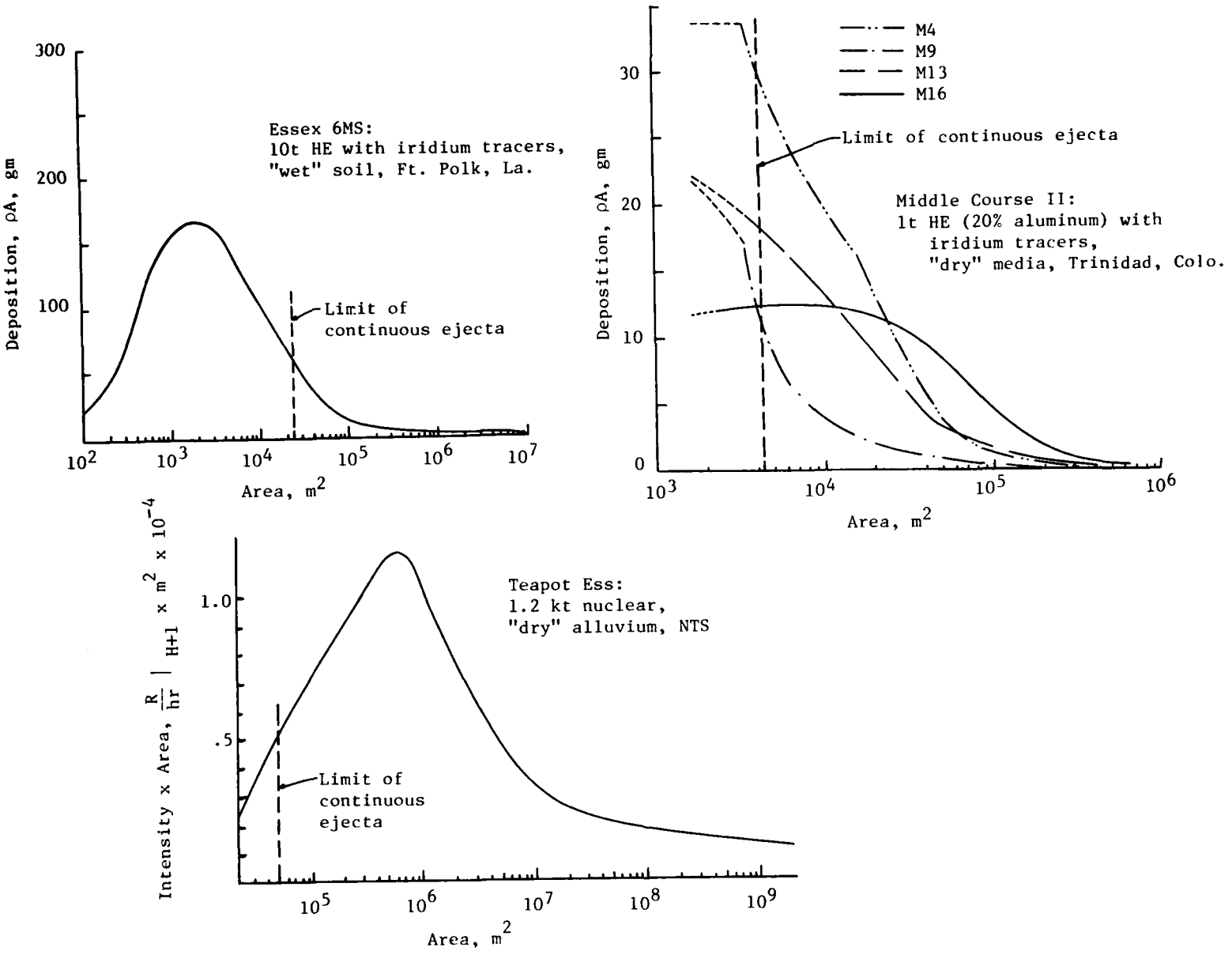

Figure 1.2. Deposition Profiles from Nuclear and HE Simulation Tests.

test, raises the possibility that the sharply reduced vent fraction in the Essex wet media tests could be the result of the specific HE charge design used in the Essex tests to simulate local fallout.

1.4 OBJECTIVES OF CURRENT PROGRAM

Our objectives have been to compare processes affecting local fallout in nuclear bursts and in the HE Local Fallout Simulation Technique, and to suggest modifications, if necessary, for improving this HE simulation technique.

Towards this objective, numerical computer code calculations were performed and analyzed to investigate the nature of shallow-buried nuclear and HE bursts in wet and dry soils, with emphasis on comparisons between the venting and early lofting dynamics of the radioactive material which becomes fallout in shallow nuclear bursts, and of the iridium tracer particles used in the HE Local Fallout Simulation Technique.

For these analyses, it is convenient to separate the processes into cratering dynamics, and multiphase flow of ejecta and air, as shown in Figure 1.3. With this separation, the cratering dynamics can be modeled using CRALE, an arbitrary Lagrangian-Eulerian finite difference code of the type which has been used to calculate both HE and nuclear craters[6,7]. Results of the cratering dynamics analyses define the characteristics of ejecta flowing through the ground surface plane from the developing crater. These ejecta characteristics form the lower boundary condition for the subsequent multiphase flow portion of the numerical simulations. Note that in the nuclear case, ejecta includes vaporized soil material, weapon debris, and tracers. In the HE case, ejecta includes HE combustion products and iridium tracers.

Using the ejecta definition from the CRALE cratering dynamic analysis, the DICE code is then used to treat the multiphase flow

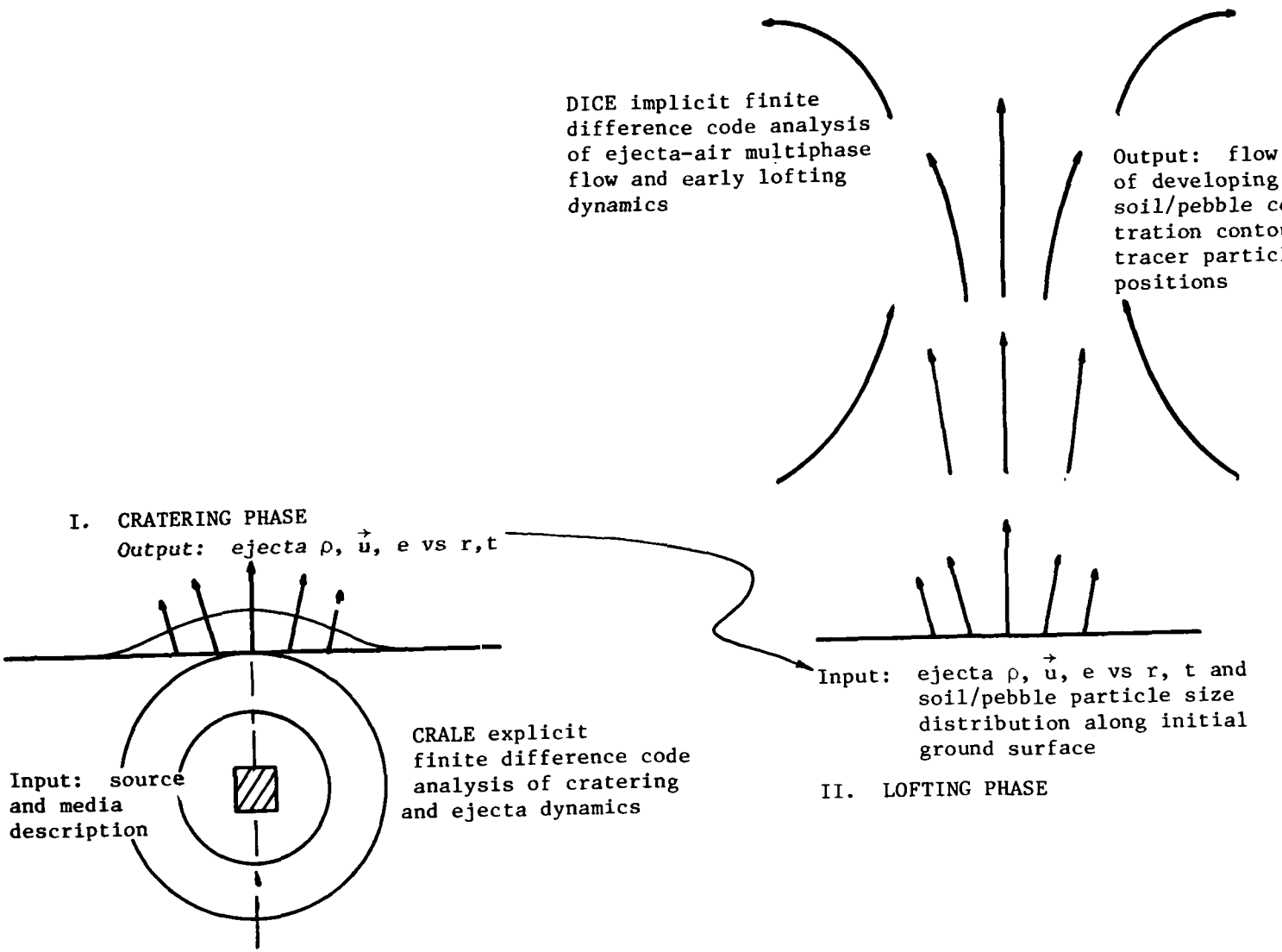

Figure 1.3 Approach for Modeling of Lofted Ejecta Dynamics from Buried HE and Nuclear Bursts.

characteristics above the original ground surface. DICE was developed to provide a method for analyzing lofted cloud dynamics following a surface burst[8,9,10]. It calculates the coupled multiphase dynamic behavior of the mixture of air and lofted soil particles. The air and particles flow separately while exchanging momentum and energy through drag and thermal interaction mechanisms (including phase changes) as functions of position and time.

Table 1.2 defines the three numerical solutions performed and analyzed in the current study.

One purpose of Case 3221 (HE/Wet) was to demonstrate the feasibility of simulating cratering dynamics and multiphase ejecta-air flow above HE buried bursts using the CRALE and DICE numerical techniques. The results of this calculation can be compared directly with experimental observations of cloud development. The effects of a *wet vs dry media* on venting and early cloud dynamics are investigated by comparing Case 3221 with Case 3222. The effects of an *HE vs nuclear source* (in a dry medium) are investigated by comparing Case 3222 and Case 3223.

In all three cases, tracer particles were distributed throughout the media as well as in the source regions to determine locations and movements of radioactive material in the developing clouds. Figure 1.4 shows the initial location of the indexed iridium tracer particles associated with the HE source in Cases 3221 and 3222, and the location of the tracer particles within the nuclear source in Case 3223. Tracers which flowed through the original ground surface in the CRALE calculation are injected into the DICE phase of the calculations. In all cases, the tracers have diameters between 75 and 175 microns (the size range of the iridium-tagged particles in the Essex tests).

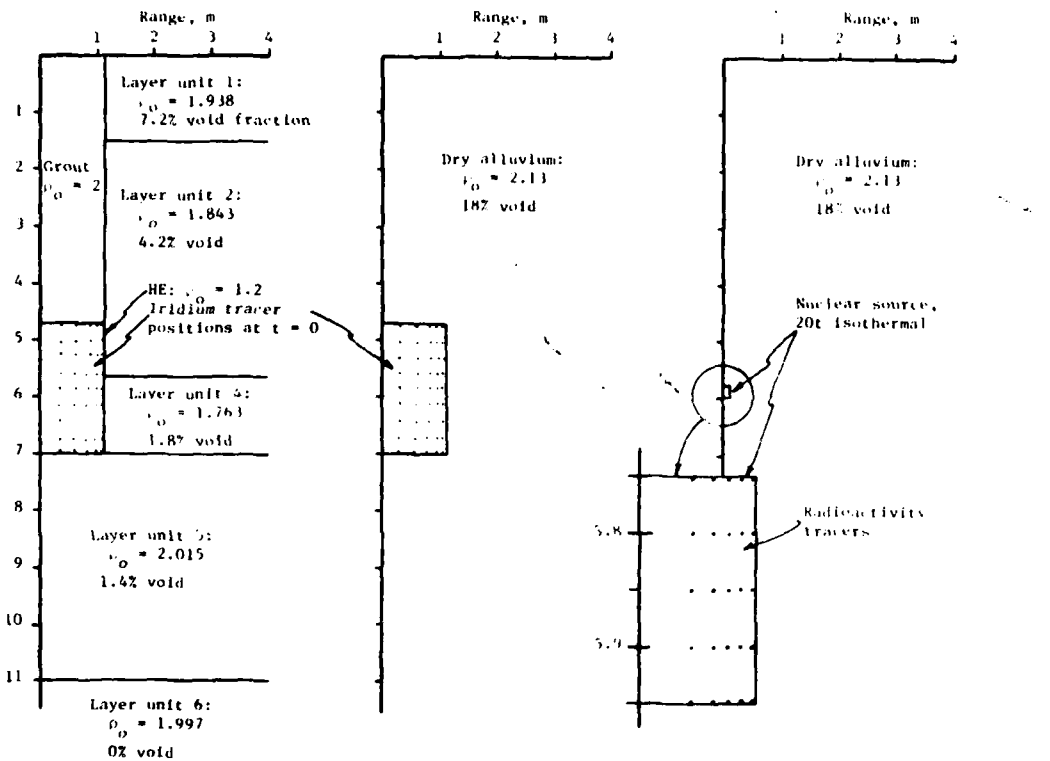

Case 3221 HE Source/ Wet Media

Case 3222 HE Source/ Dry Medium

Case 3223 Nuclear Source/ Dry Medium

Figure 1.4 Conditions for Three Numerical Solutions.

Table 1.2 CONDITIONS FOR CRALE/DICE NUMERICAL SOLUTIONS

	Case 3221 HE Source/ Wet Media (Essex I event 6MS)	Case 3222 HE Source/ Dry Medium	Case 3223 Nuclear Source/ Dry Medium (Scaled Teapot ESS)
Source	10t (equiv. TNT yield) HE cylinder (2.28 m x 2.28 m) centered at 5.85 m depth. Ignited at center. P_{max} ~ 200 Kb.		20t internal energy in isothermal cylinder (20 cm x 20 cm) centered at 5.85 m depth. P_{max} ~ 60 Mb.
DOB	~ 6 meters		
Media	Wet soil, Ft. Polk layering, WT = 12 ft.	Dry NTS alluvium	
Particle size range	5 size groups: .01-100 cm 90% > 1 cm	5 size groups: .005-10 cm 70% < 1 cm	
Objective	Baseline case. Experimental comparison with Essex 6MS	Wet vs dry comparison (3221←→3222)	HE vs nuclear comparison (3222←→3223)

Particle sizes of the incoming ejecta are not a direct output of the cratering dynamics calculations and must be estimated. Figure 1.5 shows the distributions which were used. For the dry-media cases, we used the nominal size distribution for alluvium at the Johnie Boy site[11]. In this distribution, the mass mean diameter (MMD) is .16 cm, and 70% of the mass is in particles smaller than 1 cm. For the wet-media case, the MMD is 18 cm, and 90% of the mass is in particles larger than 1 cm. There is experimental support for this trend in ejecta size distribution for dry vs wet soils[12]. However, the details of the wet soil particle size distribution are estimates. In the DICE analyses, the particles were divided into five size groups, with appropriate drag and heat exchange characteristics, plus a soil "vapor" group.

1.5 SUMMARY OF RESULTS

Figure 1.6 shows a photograph* of the plume of ejecta from Essex event 6MS at 1.5 seconds. Superimposed on the photograph are two cloud boundaries from the CRALE/DICE code analyses. The inner boundary encompasses the 1-10 cm particle size group, while the outer boundary encompasses the 10-100 cm particle size group. (Aerodynamic drag filtering is responsible for the difference.)

Visual perception of the edge of a cloud is affected by particle size, mass concentration, relative location of the observer and the sun, and general meteorological conditions. Given these complications, the agreement between the visible plumes in the photos and the calculated boundaries is considered quite good.

Shedding (aerodynamic stripping from weakly cohesive clumps of wet soil) is quite evident from the larger clumps in Figure 1.6.

---

* Provided to us by John Dishon, Waterways Experiment Station.

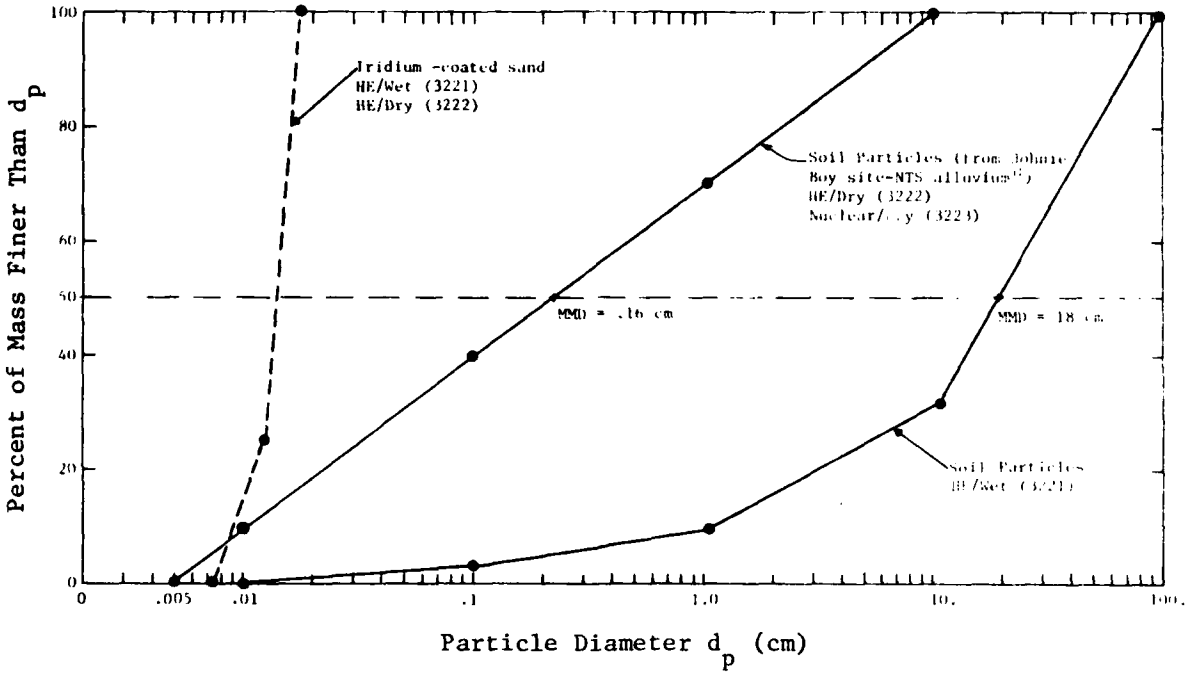

Figure 1.5 Incipient Ejecta Particle Size Distributions used in the Numerical Solutions.

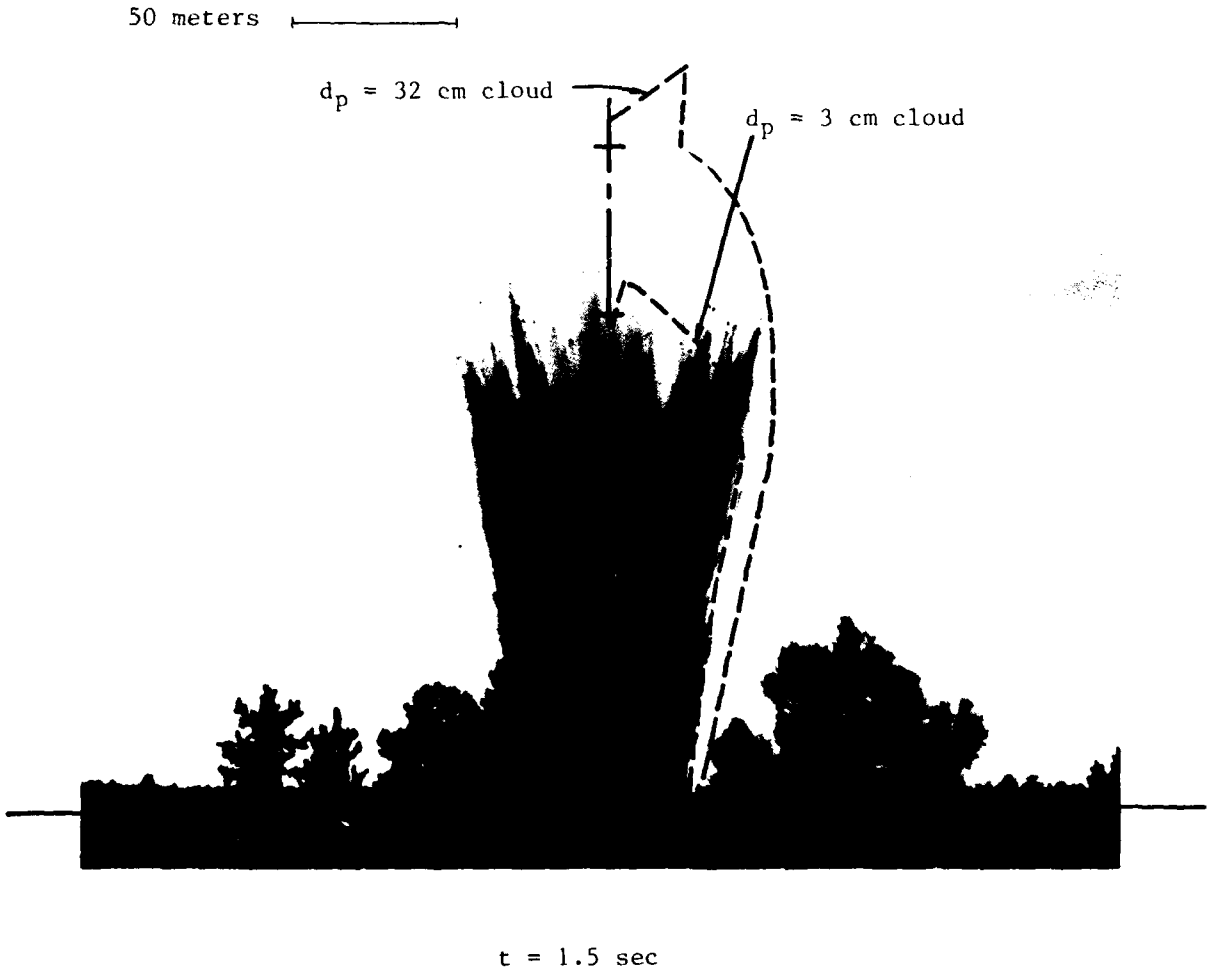

Figure 1.6 Photograph of Essex 6MS Cloud with CRALE/DICE Calculation 3221 Superimposed for Comparison (Dashed Lines).

This mechanism was not modeled in the current analyses. It would have dynamically reduced the large particle sizes, leading to increased drag and reduced upward growth of the calculated plume.

Both the photograph and the calculated profiles in Figure 1.6 suggest that the plume in Essex event 6MS at 1.5 seconds is being pushed up by ejecta momentum, rather than being lofted by the buoyancy of a hot fireball.

Figure 1.7 shows the ejecta cloud altitudes and the maximum tracer particle altitudes as functions of time for the three cases. The radioactivity tracers in the nuclear case are significantly higher than the iridium tracers in either of the HE cases. This behavior is due to differences in the magnitude and form of the vented energy. As described in Section 1.2, the Essex HE charge masses were established so that the same kinetic energy would be coupled to the soil as in a nuclear burst, with the expectation that equivalent cratering and ground motions would result. This is a reasonable approach for designing a *cratering* simulation charge.

Local fallout, however, is influenced by different processes than cratering. Note that the results of the calculations in References 4 and 5, as manifested in the HE charge masses in Table 1.1, indicate that shallow-buried nuclear bursts are only half as efficient as buried HE charges in coupling kinetic energy to cratering action. This is primarily the consequence of the much higher energy densities and pressures in the nuclear source as compared to the explosive detonation, i.e., ~60 Mb vs ~0.2 Mb. These extreme energy densities result in inefficient (for cratering) vaporization of the nuclear device and of surrounding soil.

On the other hand, *this inefficiency of the nuclear burst for cratering means that a larger fraction of energy is available for venting to the atmosphere*, and hence for dispersing and lofting

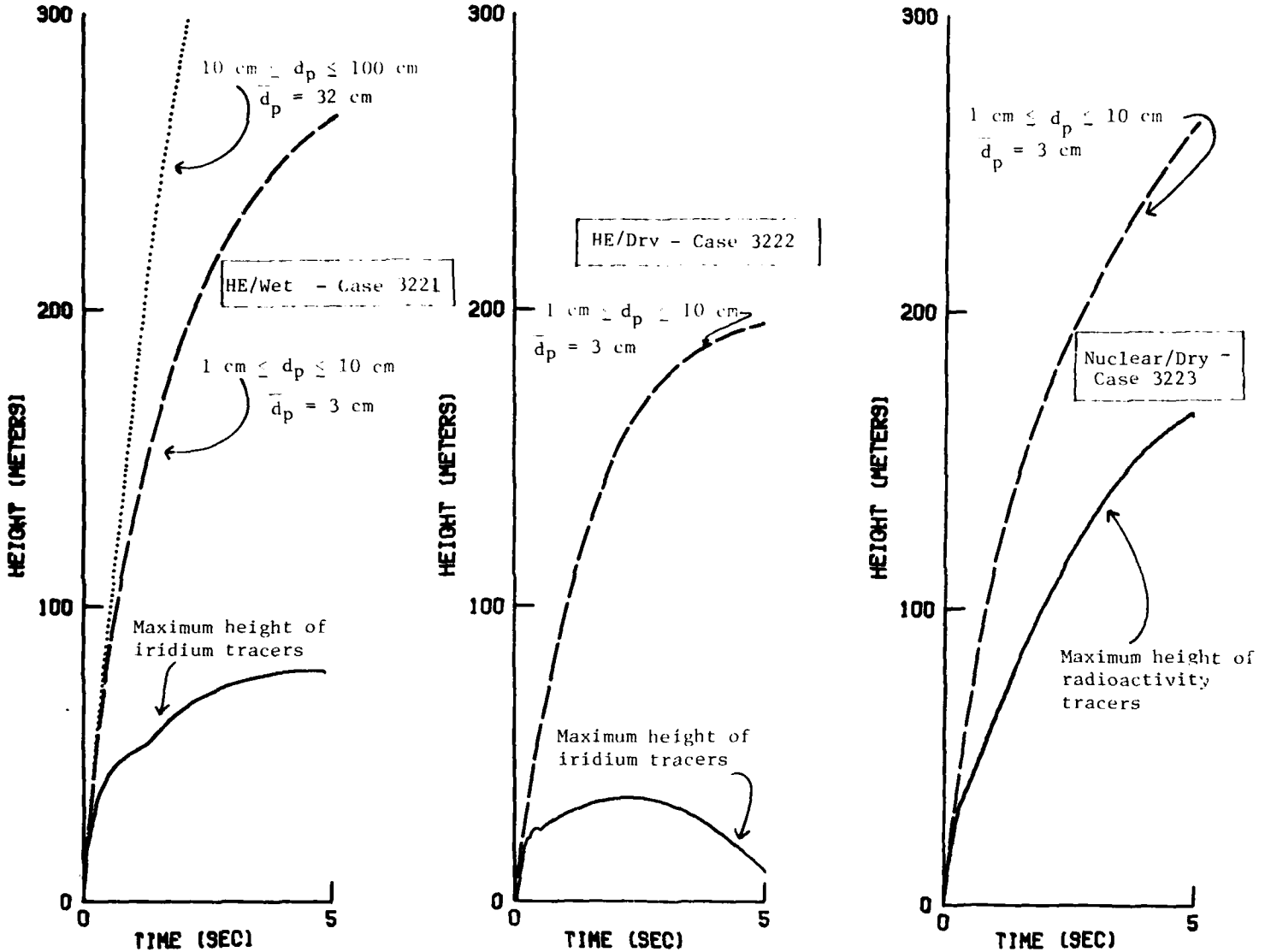

Figure 1.7. Cloud Altitude and Maximum Tracer Altitude Versus Time from the Numerical Solutions.

of radioactive debris. On this simple basis alone, it should not be expected that equating the kinetic energy coupled to the ground by a buried HE charge to that by a buried nuclear burst will lead to the same venting and lofting phenomena above the surface. Rather, the mass and energy of the simulation charge should be chosen such that the *vented energy* is equivalent to the vented energy expected from the nuclear burst being simulated. This means that the total HE energy would probably need to be *larger* than the nuclear yield.

The form and concentration of the vented energy is also very important. Because of the higher initial shock pressures, ejecta from a nuclear burst is much hotter than ejecta from an HE burst, and substantial ejecta mass is vaporized. Approximately 15% of the device yield in the nuclear Case 3223 is in the form of latent heat in soil vapor. Subsequent release of the latent energy (as the soil vapor recondenses) heats the air above the nuclear burst thereby causing buoyant lofting of the radioactivity tracers.

By contrast, ejecta temperatures are relatively low from an HE burst, and no soil vaporization occurs. Calculated temperatures in the vented detonation products in Cases 3221 and 3222 are only a few degrees above ambient (T ~ 300°K). Hence buoyant lofting was very weak in the Essex simulations. The HE ejecta plumes formed as a result of soil and tracer particles being thrown upward *ballistically*. Through drag interactions, the HE-accelerated ejecta particles *pull air* up with them.

Confirmation that particles are dragging air up with them in the HE case is seen in the relative altitudes of large and smaller particles in Case 3221 (HE/Wet) in Figure 1.7. Larger ejecta sizes attain higher altitudes due to drag filtering, i.e., large particles

transfer momentum to the air relatively slowly. Iridium tracers, on the other hand, remain near the bottom of the plume due to their small sizes and the absence of significant thermal lofting.

Comparison in Figure 1.7 of the HE/Wet and the HE/Dry cases (3221 vs 3222) shows that neither the lofted cloud nor the iridium tracers reach as high an altitude in the dry medium burst. This is because of the earlier and stronger aerodynamic drag coupling of the smaller particles used to characterize ejecta from the burst in the dry medium.

Figure 1.8 shows plots of the air velocity fields and the iridium and radioactivity tracer locations for the three cases at the end of the solutions at 5 seconds. In the nuclear burst, there are still upward air velocities of approximately 20 m/sec, and some radioactivity tracers are entrained in this upward flow. In the HE cases, all of the iridium tracers still aloft at 5 seconds are moving downward.

Because iridium tracers were still aloft at 5 seconds in Case 3221, a direct comparison of the predicted iridium deposition profiles on the ground with the experimental profiles from Essex event 6MS shown in Figure 1.2 is not possible. The iridium tracers in Case 3221 are falling close to the source, and many will probably end up within the crater. (The experimental Essex 6MS crater radius was about 25 m.) However, the downward air flow turns outward as it reaches the surface. This flow, plus base surge, could provide additional outward radial motion to the tracers, allowing a final deposition profile similar to that of Essex 6MS in Figure 1.2.

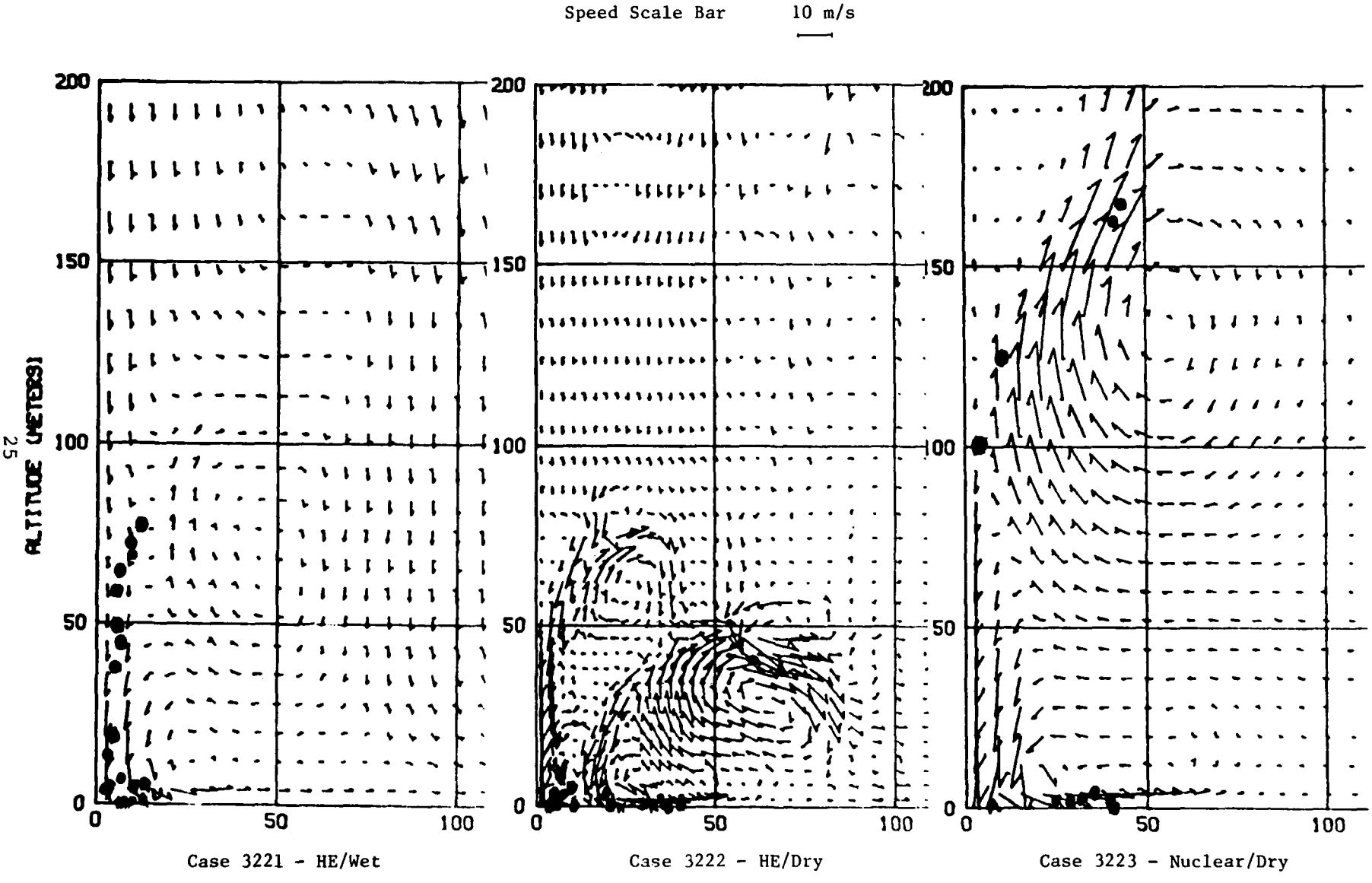

Figure 1.8. Air Velocity and Tracer Positions at 5 seconds for the Three Numerical Solutions.

1.6 CONCLUSIONS AND RECOMMENDATIONS

Regarding the Essex I local fallout simulation tests:

1. *The nominal 10-ton HE charges used in the Essex I test series were too small and the shocked soil temperatures produced were too low to simulate the fallout from shallow-buried 20-ton nuclear bursts.*

These charges were designed to meet an "equivalent kinetic energy" criterion, i.e., to couple the same kinetic energy to the surrounding soil, and hence to cratering and ground motions, as a 20-ton nuclear burst. It takes less total HE than nuclear energy to achieve this equivalence because HE "wastes" less energy on extreme shocking and vaporization of surrounding soil. From the standpoint of fallout simulation, however, the combination of the small charge energy, lower temperatures (with no phase changes), and greater coupling efficiency of the HE charges meant that much less energy was available for venting, and especially for venting of the concentrated internal energy (i.e., latent heat of vaporization) needed for buoyant lofting of iridium tracers. For 10 tons of HE at 6 m DOB, the vented detonation products were too cool to produce significant buoyant lofting.

2. *The ejecta plume from Essex 6MS (and probably from the other tests in the series) was primarily a "throw-out" cloud.*

Major mechanisms involved in the development of such a plume include ballistic throw-out, aerodynamic drag filtering of various particle sizes, air velocities induced by particle drag, and shedding of small particles stripped off of large soil clumps by aerodynamic forces.

3. *Primarily because of buoyant lofting, radioactive material from a shallow-buried nuclear burst will reach a significantly higher altitude (by a factor of 2 or more) than the altitude reached by iridium tracers in the Essex 6MS test.*

Regarding differences between lofting of radioactivity from shallow-buried bursts in wet vs dry media:

4. *For HE sources (the only comparison made in this program), the dust cloud and iridium tracers in a dry soil remain at a lower altitude but reach a larger radius than in a wet soil.*

The typically smaller ejecta particles in dry soil result in earlier and stronger aerodynamic drag coupling with the air than occurs with the larger wet soil clumps. This enhanced coupling results in a substantially lower, broader cloud. Additional comparative analyses will be required before conclusions can be drawn about local fallout from *nuclear* bursts in wet and dry media.

Regarding the feasibility of developing a satisfactory HE Local Fallout Simulation Technique:

5. *Development of a satisfactory HE simulator for local fallout from buried nuclear bursts is feasible, but the HE technique needs to be specifically designed to reproduce those phenomena which govern early lofting.*

The Essex explosive charge was intended to simulate nuclear cratering processes in shallow bursts; its failure to adequately simulate local fallout merely shows that venting, lofting, and local fallout are affected by different processes than cratering.

6. *The HE Local Fallout Simulator should be designed on the basis of equivalent energy which is vented.*

This will probably mean using an explosive system with total energy *greater* than the nuclear yield which is being simulated.

7. *The form and density of the vented energy, not just the quantity, are important.*

The extreme pressures from a nuclear burst result in severe heating and vaporization of soil ejecta mass. Subsequent transfer of this latent and sensible heat to air above the burst produces buoyant lofting.

These energy densities and pressures, with the consequent soil vaporization and transport of latent energy to the surface cannot be produced by an HE charge. However, the *effects* of these processes upon vented energy and early lofting dynamics can be simulated. The following techniques appear promising:

a. Add materials to the explosive to sustain detonation product temperatures through the venting period. Addition of aluminum powder, for example, will produce afterburning, thereby releasing energy into the detonation products at relatively late times. It is noteworthy that the HE charges used in Middle Course II contained 18-20% aluminum powder. As seen in Figure 1.1, these charges produced much higher vent fractions. (While this is not conclusive, since Middle Course II was fired in dry media, the trend is encouraging.)

b. Heat energy could be directly and separately added above the surface. One way would be to center a hemispherical balloon of detonable gas on the surface above the HE charge. It could be initiated by ejecta or by a separate firing system.

Regarding the CRALE/DICE numerical modeling of local fallout processes:

8. *The CRALE and DICE models adequately treat processes which determined the visible characteristics (flow pattern, dimensions) of the ejecta plume from Essex 6MS.*

Fallout deposition on the ground was not complete at the end of the solution at 5 seconds, but the final position of still-lofted tracers appears consistent with the experimental deposition profile. The initial crater ejecta particle size distribution is not calculated, but must be inferred from other data. Shedding was not modeled in the current solutions.

Regarding utilization of numerical solutions for local fallout prediction and to support development of improved simulation techniques:

9. *Analyses of possible modifications (including those suggested in item 7) to the HE Local Fallout Simulation Technique should be made towards improving simulation fidelity. These should precede experimentation.*

10. *The following specific cases should be analyzed:*

    a. A detailed analysis of a NTS buried nuclear event, both to improve understanding of the dominant processes involved, and to provide experimental validation of the analysis technique.

    b. Using the same source and DOB, analyze a nuclear burst in wet media, to provide better understanding of potentially very important wet vs dry media effects which are suggested by vent fraction data from HE tests.

11. *Run numerical solutions to later real times.*

In the current study, the calculations were terminated at 5 seconds. By this time, substantial differences were evident in the qualitative and quantitative behavior of the tracers in the HE and nuclear clouds. Significant differences had also appeared between HE clouds in wet vs dry media. However, these calculations were not run far enough to determine the base surge and final deposition on the ground of the tracers. Future calculations should extend far enough to obtain the local fallout pattern on the ground for an axisymmetric configuration. Effects of atmospheric winds can then be approximated by adding wind transport terms.

12. *Analyze effects of uncertainties in the mass of soil and water vaporized upon local fallout for shallow-buried nuclear bursts in wet and dry soils.*

Latent energy involved in vaporization appears to play a critical role in venting dynamics and in the subsequent lofting processes.

SECTION 2

CRATERING DYNAMICS - CRALE CALCULATIONS

The primary role of the CRALE cratering calculations were to specify the flux of earth material and gas which crosses the initial ground surface into the domain of the DICE lofting calculation. That is, CRALE output provided the lower boundary condition for the DICE solutions.

A discussion of the CRALE cratering studies follows. Initial conditions (soil properties, energy sources, zoning and placement of target tracer points) are described. Then the results of each simulation are described and compared with available experimental data and previous numerical simulations.

2.1 INITIAL CONDITIONS

2.1.1 Soil Properties

The initial soil geologies for the three CRALE simulations are shown in Figure 1.4. Noted for each of the soils in the diagram are the bulk density (ρ_o) and the air-filled void fraction.

Since Case 3221 (HE/WET) is a simulation of the Essex 6MS event, it required the most elaborate soil representation. In addition to five soil strata, there was a column of grout used to back-fill the emplacement shaft. This complex system was designed to match the Essex 6MS experimental conditions as closely as possible. Soil properties can be found in Jackson[13].

The dry ground media (Cases 3222 and 3223) was assumed to be homogeneous NTS desert alluvium, with properties based on Reference 13. Separate back-fill material was not used in these two calculations.

2.1.2 Sources

For Cases 3221 and 3222 an identical 10-ton (equivalent yield) nigh explosive source was used, in the form of a right-circular cylinder, 2.28 meters in height and 1.14 meters in radius, centered 5.85 meters below the ground surface. The HE was ignited at its center and burned with a detonation velocity of .624 cm/μsec and a CJ pressure of 120 kbars.

For Case 3223, the 20-ton (equivalent yield) nuclear source was represented by an isothermal cylinder of normal density alluvium, 10 cm in radius and 20 cm in height, again centered 5.85 meters below the initial ground surface. This energy and volume results in an initial pressure of 50 Mbars.

2.1.3 Tracer Points

Tracer points of two distinct types were included in these calculations. Massless Lagrangian points were located throughout the media to provide time-histories of the velocity, displacement and stress. A subset of these Lagrangian target points was distributed throughout the volume of the initial explosive source. For Cases 3221 and 3222, these points represented the iridium-coated sand particles mixed with the nitromethane explosive. For Case 3223, these Lagrangian points in the initial source region represented radioactive material from the nuclear explosive source. The locations of the source points are shown in Figure 1.4.

Twenty-five Eulerian tracer points were used to collect the information that provided the time- and radius-varying lower boundary condition for the DICE calculation. These points did not flow with the material; they remain equally-spaced in radius, two centimeters above the original ground surface. As the ground rose after the explosion, the radial positions of the Eulerian points were continuously expanded outward in order to observe the

motion of the entire surface mound. The Eulerian points monitored the soil type, particle velocity, specific internal energy and density of the material flowing upward through the original ground surface as a function of time and radial position.

2.2 HE SOURCES IN WET SOIL (ESSEX 6MS) - CASE 3221

Case 3221 was designed to simulate the Essex 6MS experiment at Fort Polk, Louisiana. The experiment consisted of the explosion of 10 tons (equivalent yield) of high explosive buried six meters in wet layered clay. The emplacement shaft was back-filled with a soil-matching grout.

2.2.1 Calculation Result

The soil media respond in a nominally spherical manner until the outrunning shock wave reaches the ground surface, as illustrated in Figure 2.1 by the velocity vector plot at 1.96 msec. The shock wave has induced spherically divergent velocities and the HE gases produced by the cylindrical explosive charge have also become nearly spherical. (The initial HE boundary is indicated on this plot for comparison.)

In Figure 2.1 the shock wave has just reached the ground surface. As a relief wave now propagates back into the soil, the symmetry of the solution is destroyed. As integration proceeds, the ground surface accelerates and the gas cavity grows. Figure 2.2a* illustrates the development at 6.06 msec. The surface has risen near the axis to form a mound. In this weak soil, explosive gases easily continue their nearly spherical growth, producing distortion in the surrounding grout and soils. By t ~21 msec,

---

*Figures 2.2, 2.3 and 2.4 include plots from both the HE/Wet Media (Case 3221) and HE/Dry Media (Case 3222) solutions, so that these solutions can be easily compared. Case 3222 is discussed in Section 2.3.

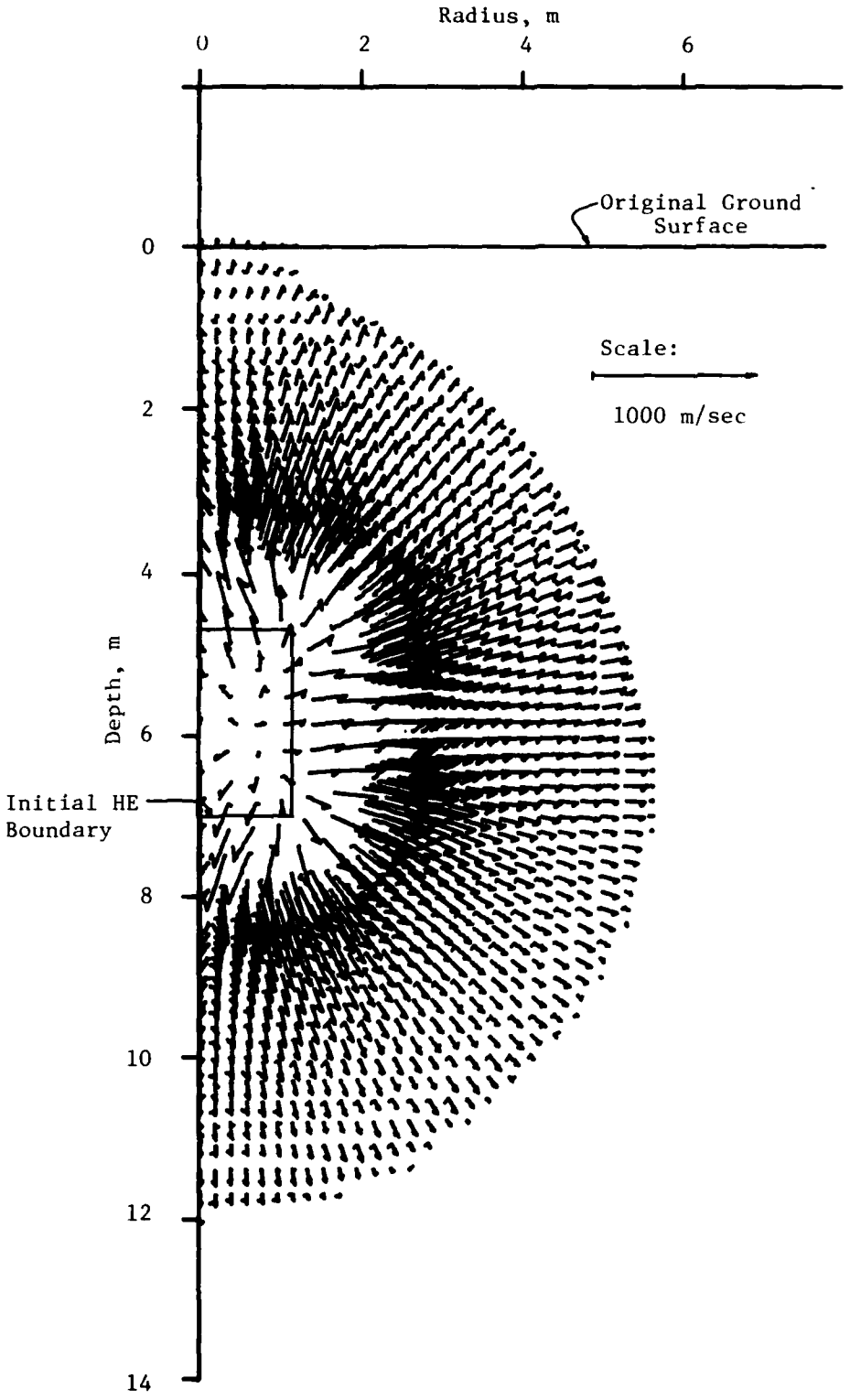

Figure 2.1 Velocity Vector Field at t = 1.96 msec for Case 3221 (Essex 6MS, HE/Wet Media).

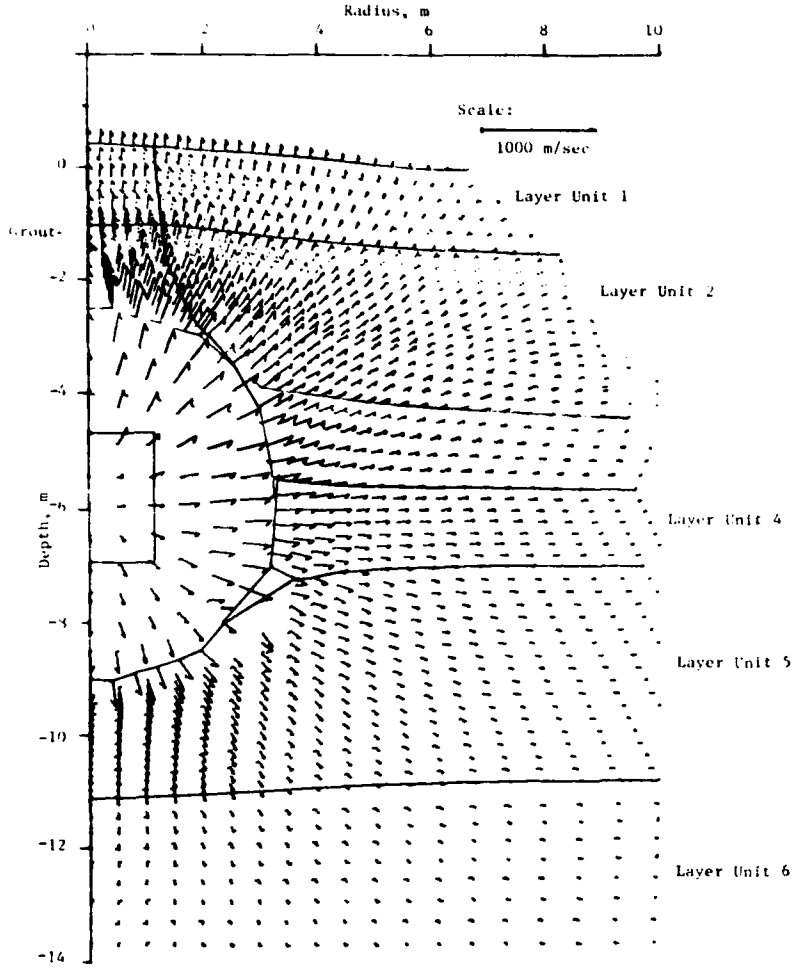

Figure 2.2a. Velocity Vector Field at t=6 msec, Case 3221 (Essex 6MS, HE/Wet).

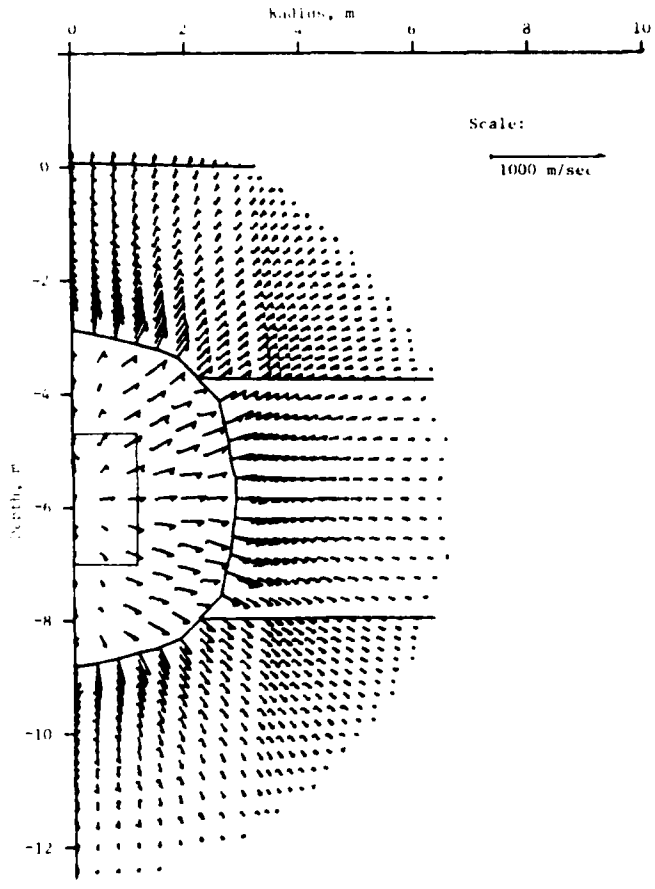

Figure 2.2b. Velocity Vector Field at t=4.8 msec, Case 3222 (HE/Dry).

the gases have broached the original ground surface (Figure 2.3). The cavity is no longer spherical as the gases have found upward expansion easier than lateral expansion. However, gas velocities near the bottom of the cavity are still downward.

CRALE integration proceeded until approximately 50 msec. At that time ballistic extrapolation was used to provide the DICE calculation with an estimate of the ejecta field to 200 msec.

Of particular interest for the continuing DICE calculation was the location of the Lagrangian tracer particles representing the iridium tracers in the high-explosive charge. Figure 2.4a traces the paths of these Lagrangian points. Approximately half of the points were driven downward from the surface by the initial explosion. These particles will probably remain in the crater, or perhaps be carried out at very low velocities at late times.

2.2.2 Experimental Comparisons

Comparison of this CRALE integration with experimental data from the Essex 6MS test is useful for evaluating the numerical approach, including material models. In Figures 2.5 and 2.6, peak stress and velocity versus range at shot depth are shown. The dashed CRALE curve agrees well with measured values of both quantities.

Time-histories at CRALE Lagrangian target points also compare favorably with experimental data from Essex 6MS gauges similarly located. Figure 2.7 is the stress history for a station at shot depth and a radius of three meters. The CRALE stress timing and magnitude are extremely close to the experimental values. Unfortunately experimental data are not reported after the peak.

A comparison of calculated versus measured motion of the surface above the charge bears directly on the realism of the calculated ejecta history. Figure 2.8 compares the vertical

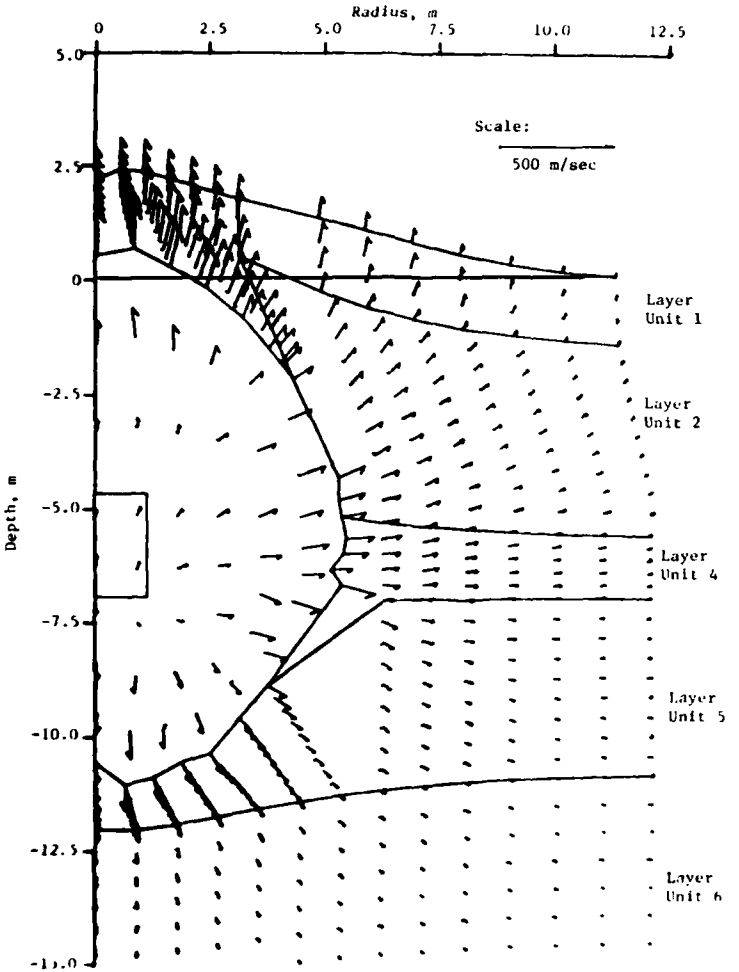

Figure 2.3a. Velocity Vector Field at t=21 msec, Case 3221 (Essex 6MS, HE/Wet).

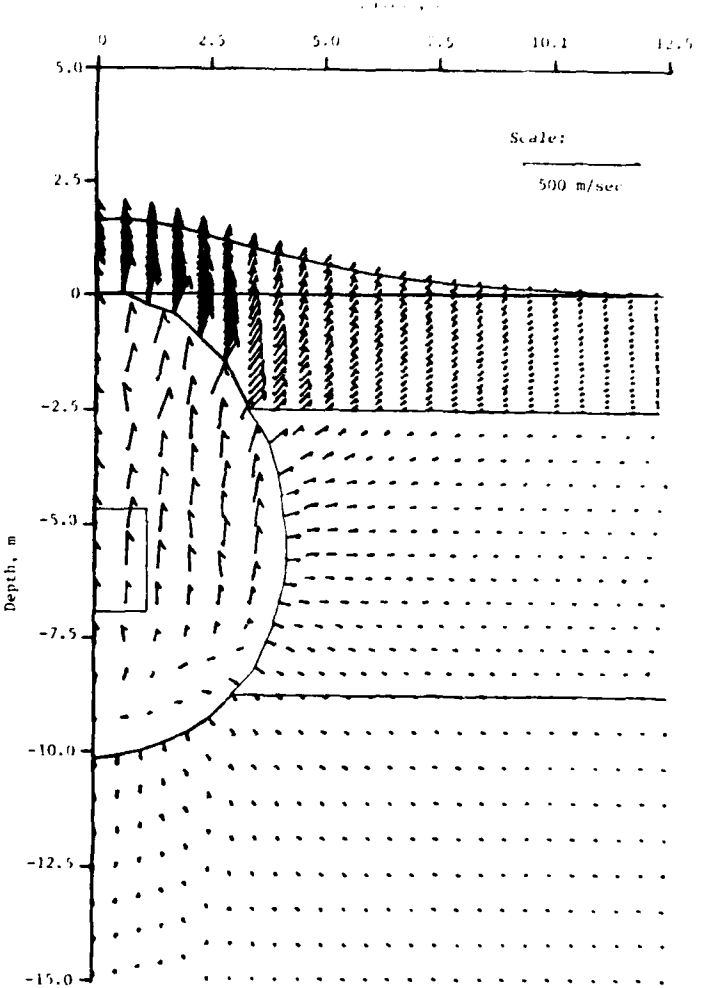

Figure 2.3b. Velocity Vector Field at t=22 msec, Case 3222 (HE/Dry).

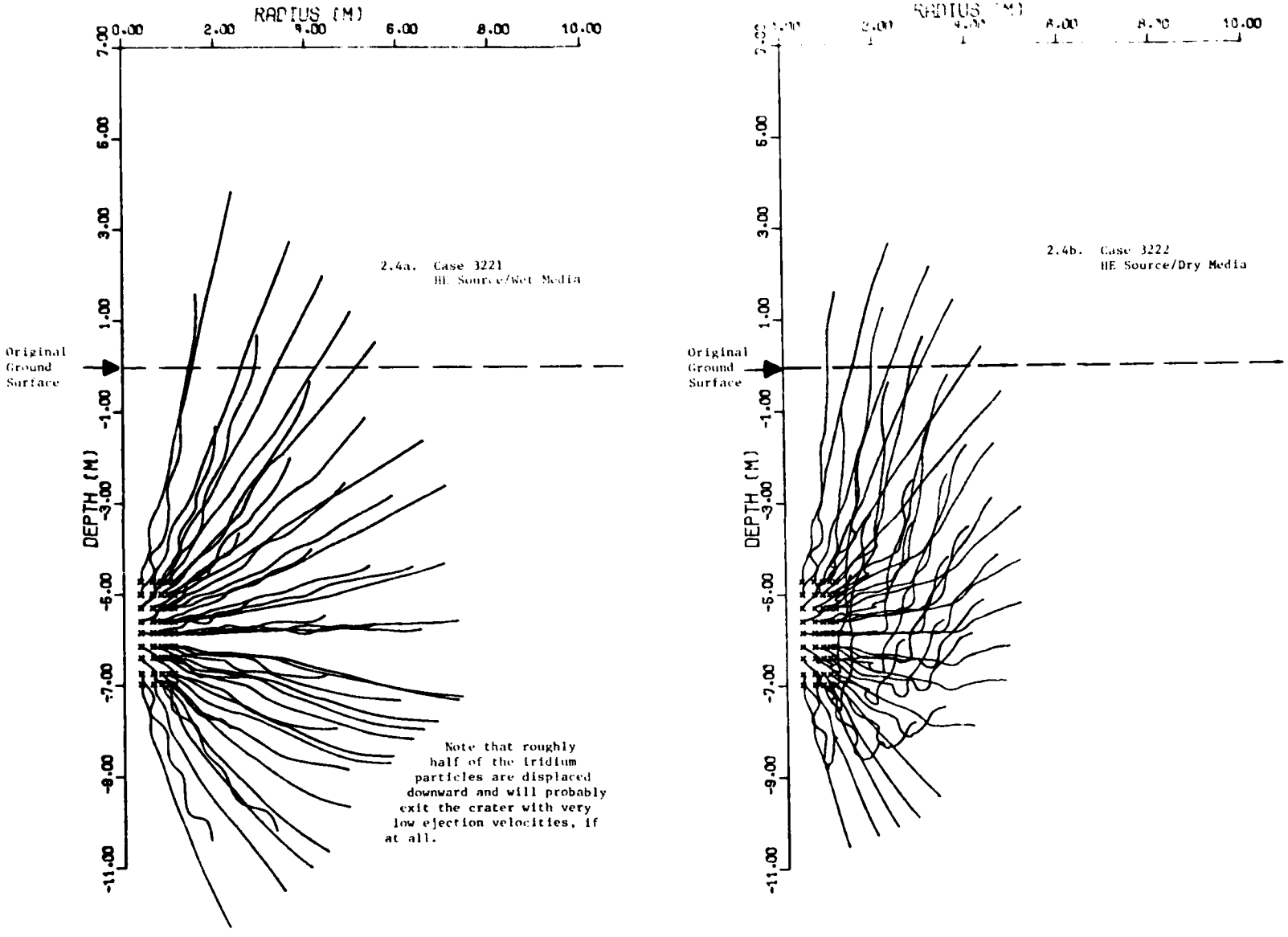

Figure 2.4 Particle Paths for ~ 50 msec Lagrangian Tracers in HE Charges.

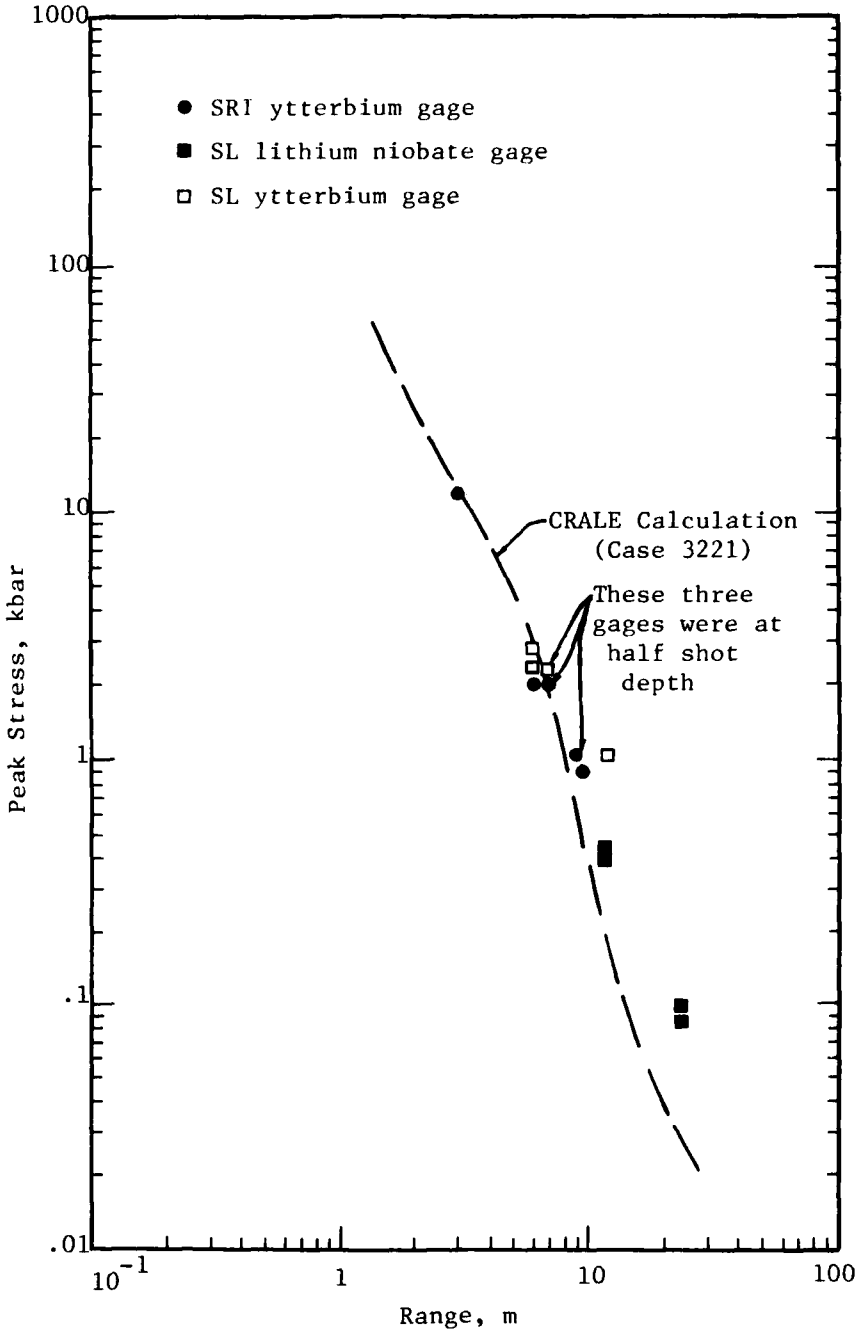

Figure 2.5 Comparison of Calculated and Measured[5] Peak Stresses for Essex 6MS.

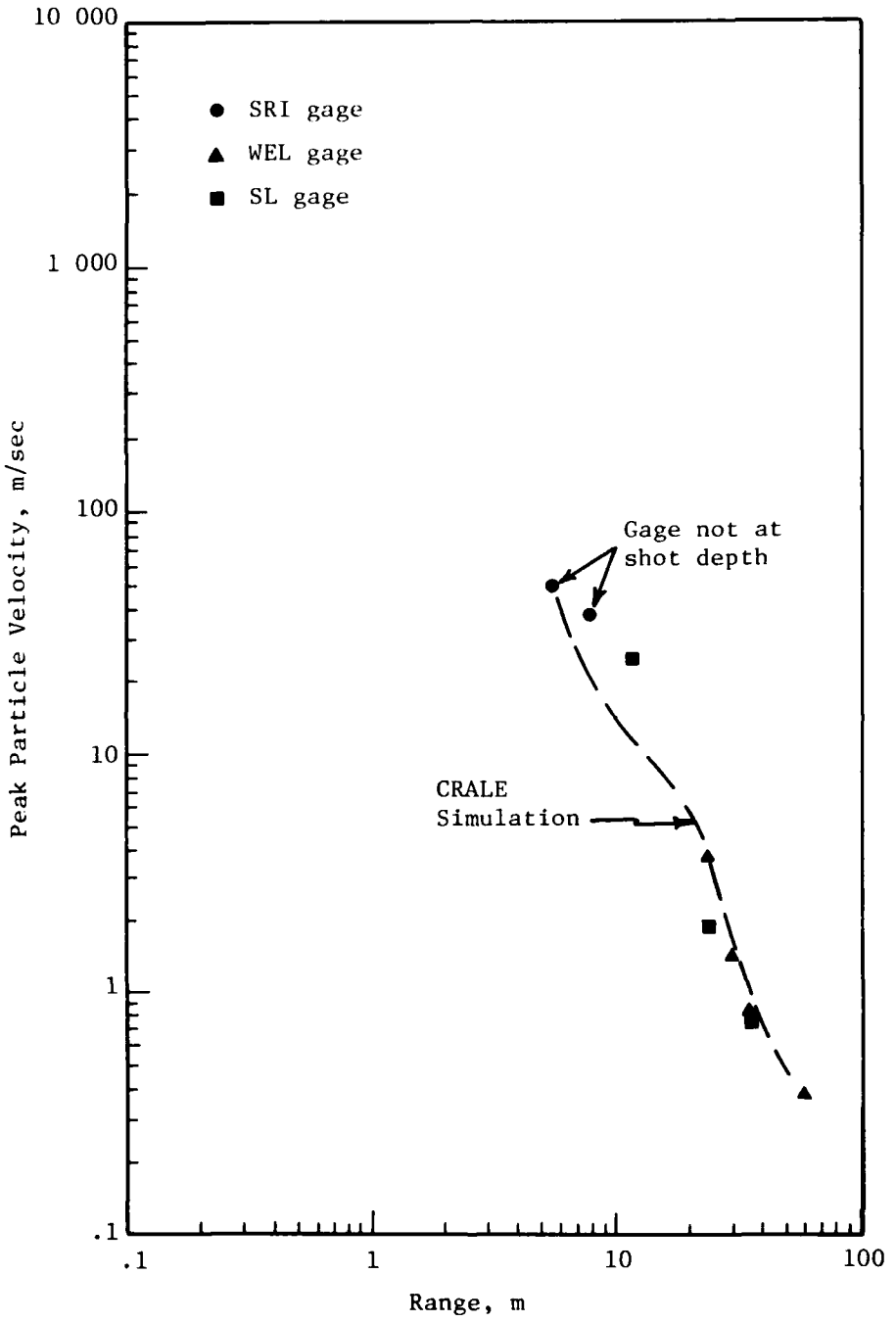

Figure 2.6 Comparison of Calculated and Measured[5] Peak Particle Velocity for Essex 6MS.

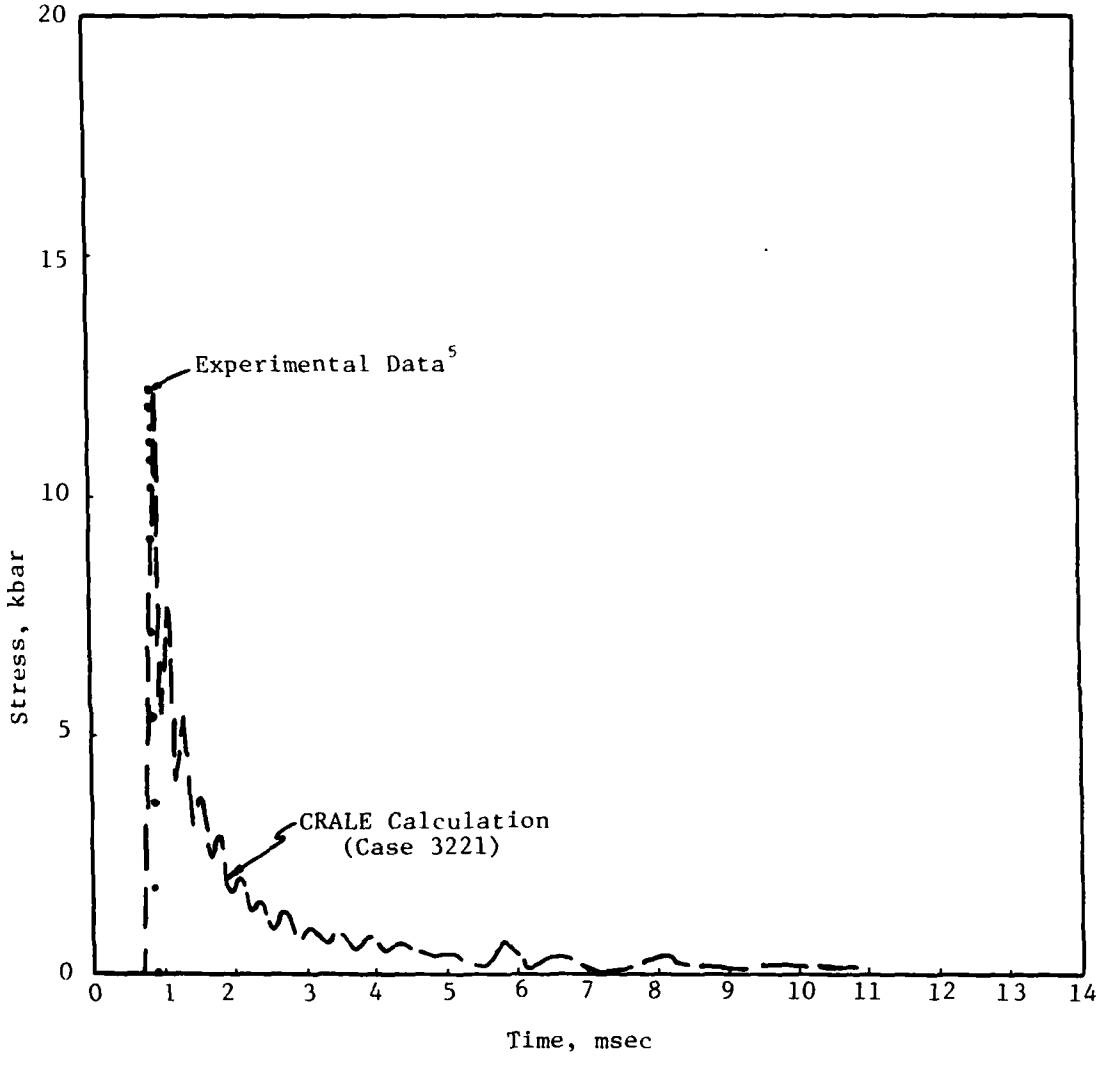

Figure 2.7 Stress History of 3 Meter Station at Shot Dept for Essex 6MS.

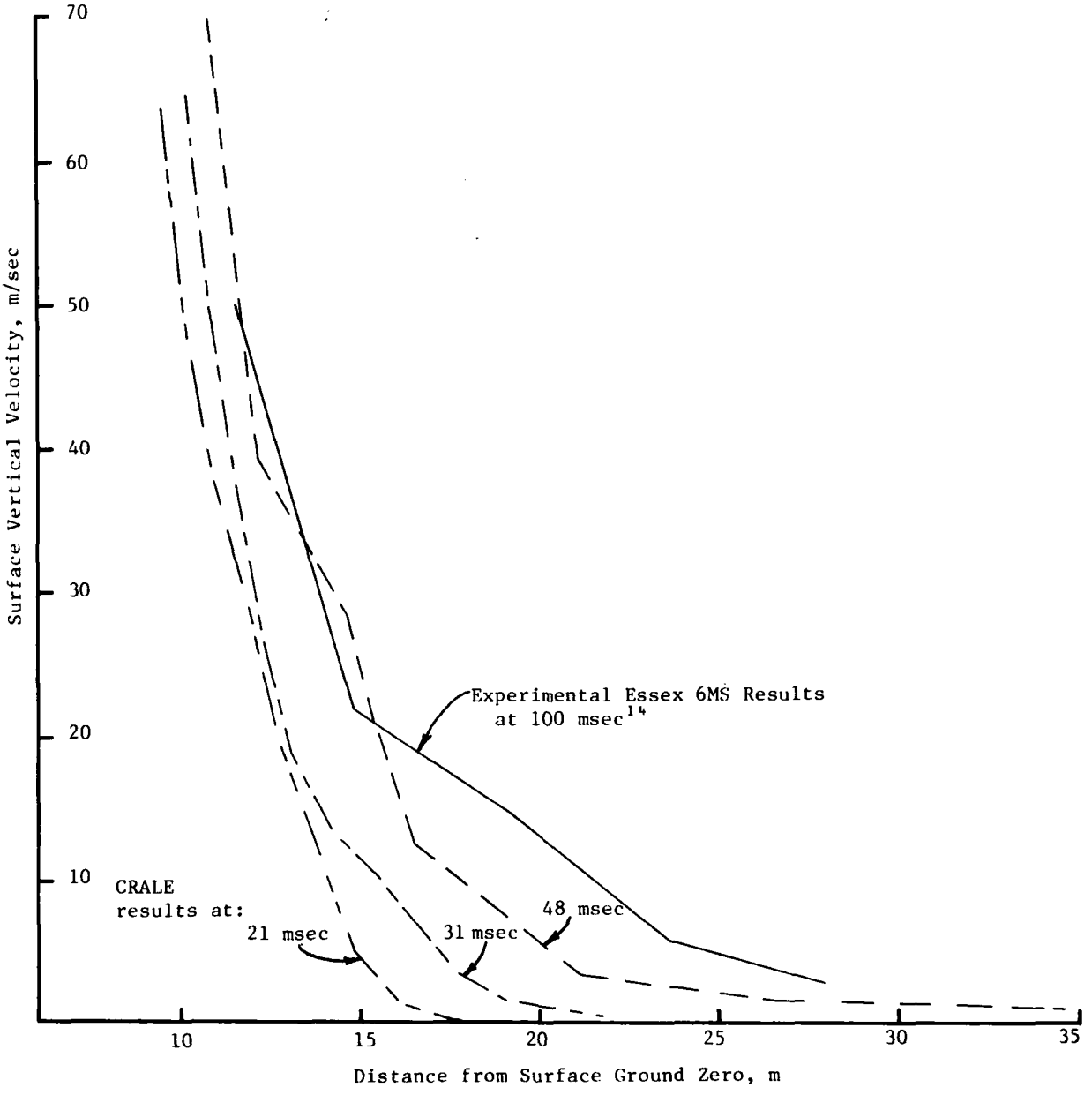

Figure 2.8 Comparison of Surface Vertical Velocity vs Distance from Surface Ground Zero at Various Times for an HE Burst Buried in Wet Soil (Case 3221).

velocity profile of the surface as measured at 100 msec with the CRALE results at 21, 31, and 48 msec. Extrapolation of the early CRALE profiles appears consistent with the 100 msec experimental profile.

Finally, an adequate crater simulation is useful in validating the CRALE incipient ejecta predictions. At various times in CRALE integration a ballistic extrapolation was made to predict the crater profile. Figure 2.9 shows the results of such extrapolations at 19, 27, 38, and 48 msec. For comparison, the apparent crater observed in the Essex 6MS experiment is shown. The predicted CRALE volume at 48 msec is 5640 m^3, versus a measured 6046 m^3. However, the predicted crater radius is smaller, and it is deeper than the flat-floored experimental crater. We attribute this difference to late-time slumping of the saturated soil. Note that the HE charge was located <u>below</u> the floor of the measured crater.

2.3 HE SOURCE IN DRY SOIL - CASE 3222

Case 3222 was run to evaluate the effects of soil properties on a buried, stemmed burst. Rather than the wet, layered clay used in 3221, the medium for 3222 was a dry NTS alluvium. This difference lead to significant differences in the ejection of iridium tracer points.

The early stages of Cases 3221 and 3222 are similar in appearance. Figure 2.2 shows velocity vector fields for Case 3222 (Dry) at 4.84 msec and Case 3221 (Wet) at 6.06 msec. In both plots the ground surface is beginning to accelerate and the HE cavity has expanded to a spherical shape. Distinctions between the two calculations appear in Figure 2.3; this figure shows the velocity vector fields for Case 3222 (Dry) at t = 22.1 msec and for Case 3221 (Wet) at 21.1 msec. This comparison shows that the cavity in the

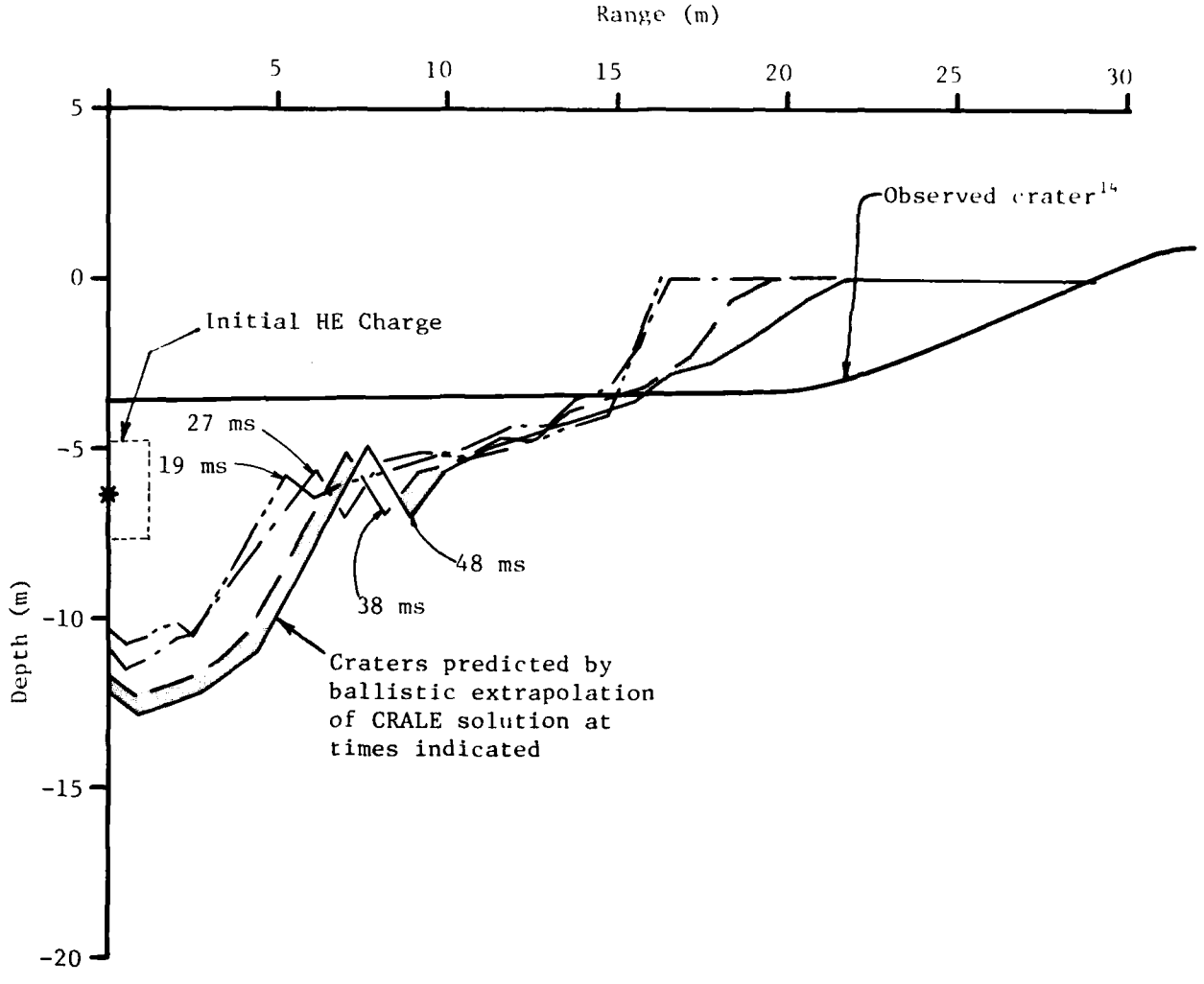

Figure 2.9 Ballistic Extrapolation Craters (which do not include fallback and slumping) at Various Times for Case 3221 (Essex 6MS HE/Wet).

wet soil at this time is much larger and more nearly spherical than the cavity in the dry soil. A comparison of cavity profiles shown in Figure 2.10 provides a likely explanation for the differences. At any particular time the cavity in the wet soil is much larger than the cavity in the dry soil, primarily because wet soil is weaker. The average yield strength of the wet soil is y = ~50 bars compared to a y = 600 bars for the dry alluvium. Having done a greater amount of expansion work, the cavity pressure in the wet soil is lower than the pressure in the dry soil *at the same time*.

The differences in the cavity gas velocity fields observed in Figure 2.3 are a result of the difference in pressure in the two cavities (20 bars in 3221 versus 50 bars in 3222). When the relief wave moves down from the surface into the cavity, the average upward acceleration produced is roughly proportional to the difference between cavity pressure and atmospheric pressure. Since the relief-wave arrival times are comparable and since the cavity pressure in Case 3222 (dry soil) is greater than that in Case 3221 (wet soil), greater upward accelerations occur in the dry case than in the wet. Indeed, the particle paths of the Lagrangian points representing the iridium tracers in Figure 2.4b show that all but the bottom row of points have begun moving upward in the dry media case. This is very different from the behavior in the wet case, shown in Figure 2.4a, wherein half the particles are still moving downward. This differing behavior could contribute to the contrasting vent fractions observed between the Essex (wet media) and Trinidad (dry) tests.

2.4 NUCLEAR SOURCE IN DRY SOIL - CASE 3223

Case 3223 was run to examine the nature of phenomena involved in venting and early lofting dynamics of radioactive material from a 20-ton buried nuclear burst. Results of solutions of this type

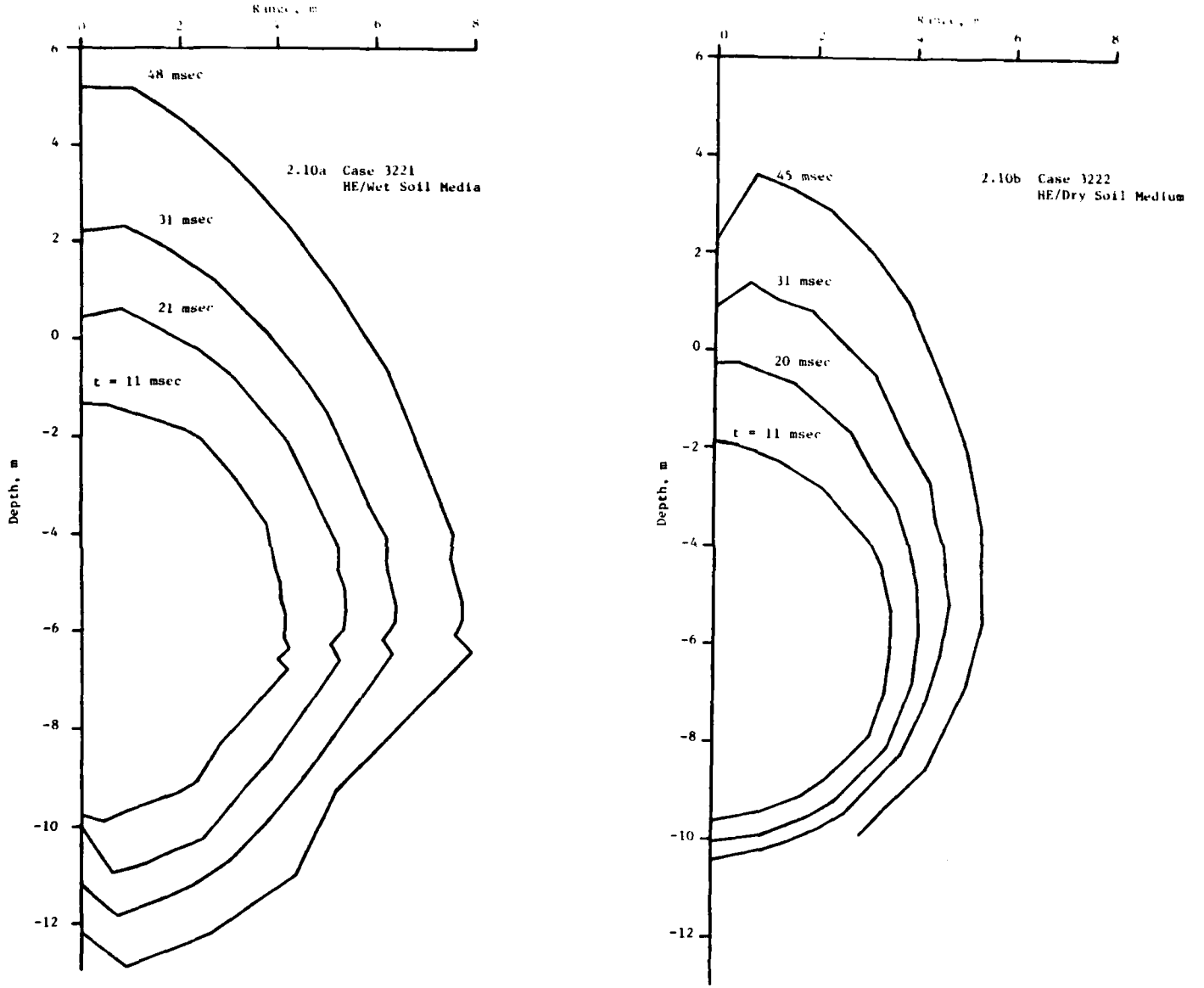

Figure 2.10 Explosive Cavity Profiles (Boundary between HE Detonation Products and Soil Material).

can provide the understanding needed to develop test techniques for realistically simulating local fallout from buried nuclear bursts.

Twenty tons was chosen as the yield, since the 10-ton Essex HE charge was intended to simulate effects of a 20-ton nuclear burst.

The calculations started with 20 tons of internal energy in an isothermal cylinder of alluvium (Figure 1.4). This produces an energy density of 62.7 Mb-cc/gm, and an initial pressure of 59 Mb in the source cylinder. The source region expands rapidly, pushing a shock into the surrounding soil as it transfers energy to that soil. By 50 μsec (Figure 2.11), the source region has expanded by more than a factor of 100. Up until 50 μsec, the computational zoning was Lagrangian, resulting in the severe net distortion seen in Figure 2.11. Thereafter the grid was altered using the ALE technique to preserve more rectangular zones.

The velocity field at 6.4 msec (Figure 2.12) is similar to the prior HE cases (Figures 2.2a and 2.2b) for material beyond the source. Within the source region, the very low density vaporized alluvium is more turbulent than the HE detonation gases. This is also illustrated in Figure 2.13 by the particle paths out to 50 msec for the tracer points originally located in the source region to represent radioactive debris.

A portion of the 20 tons of energy in the source region goes into vaporization of soil as a strong shock propagates out from the source. However, after the cratering calculations for Case 3223 had been completed, a problem with the equation of state was found, in that only a relatively small latent heat of vaporization was required to vaporize soil. As a consequence, only a few hundred kilobars shock pressure was required to vaporize soil,

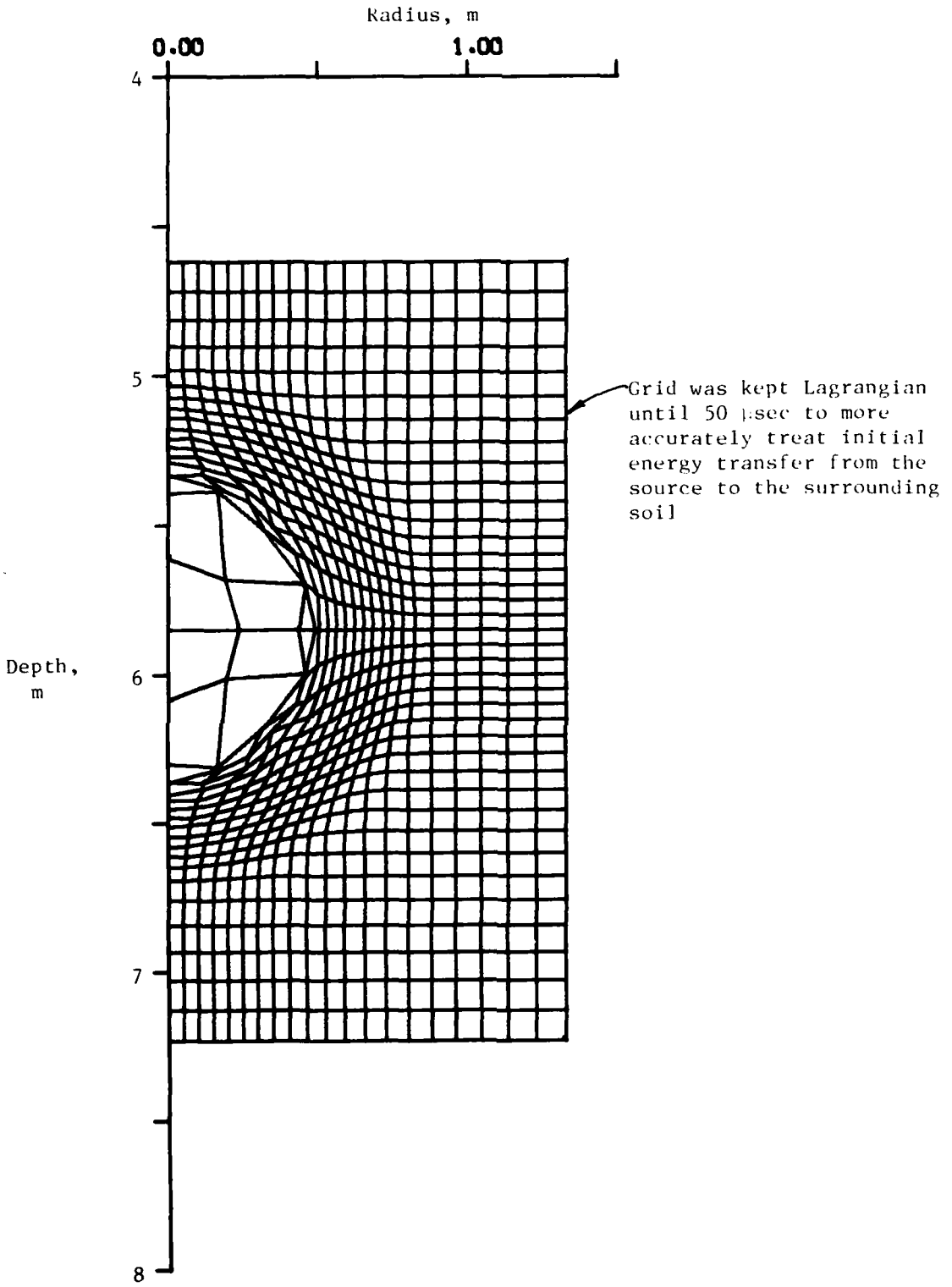

Figure 2.11 Computational Grid Distortion at 50 μsec in Case 3223 (Nuclear Source/Dry Medium).

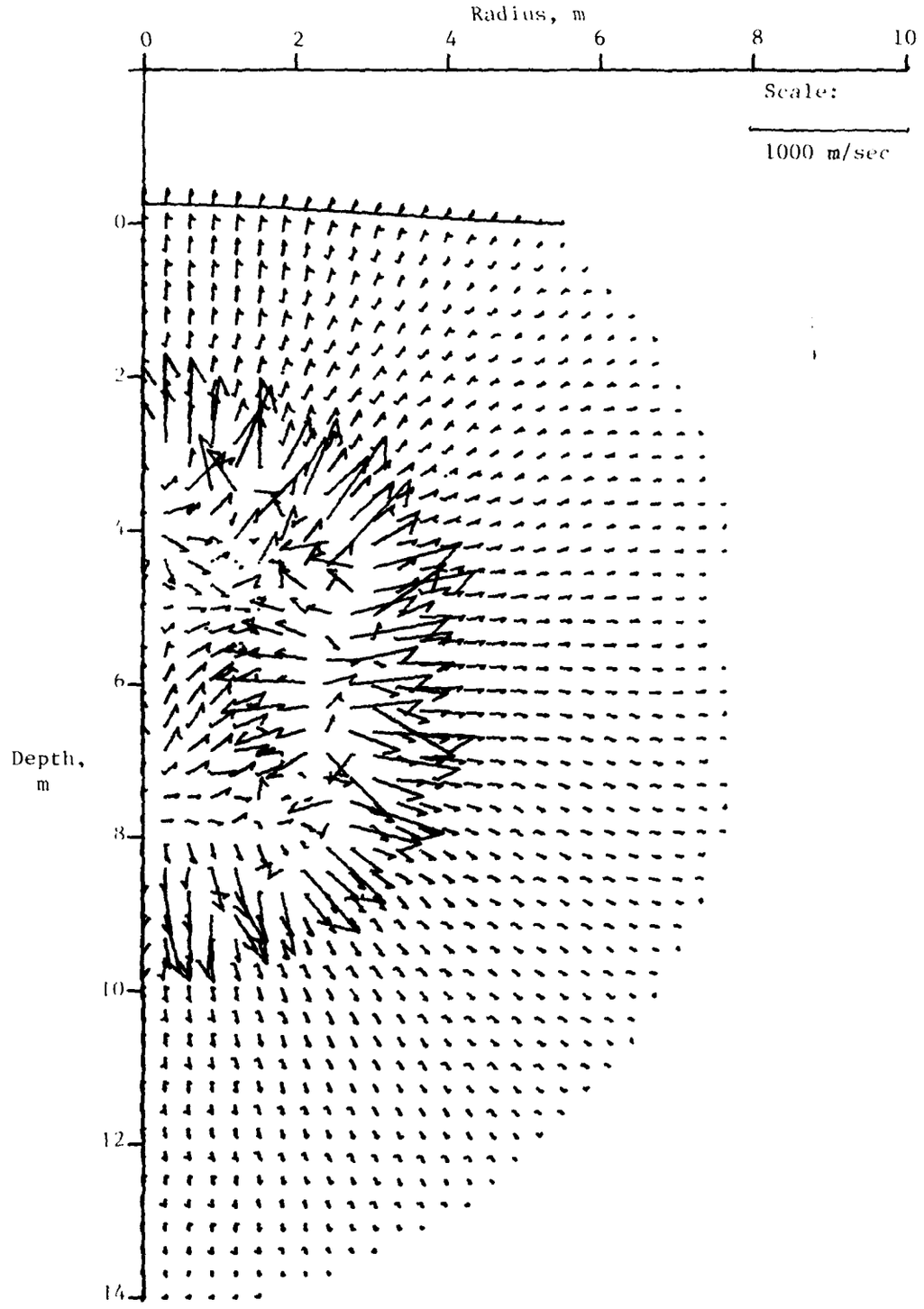

Figure 2.12 Velocity Field at t = 6.4 msec, Case 3223 (Nuclear/Dry).

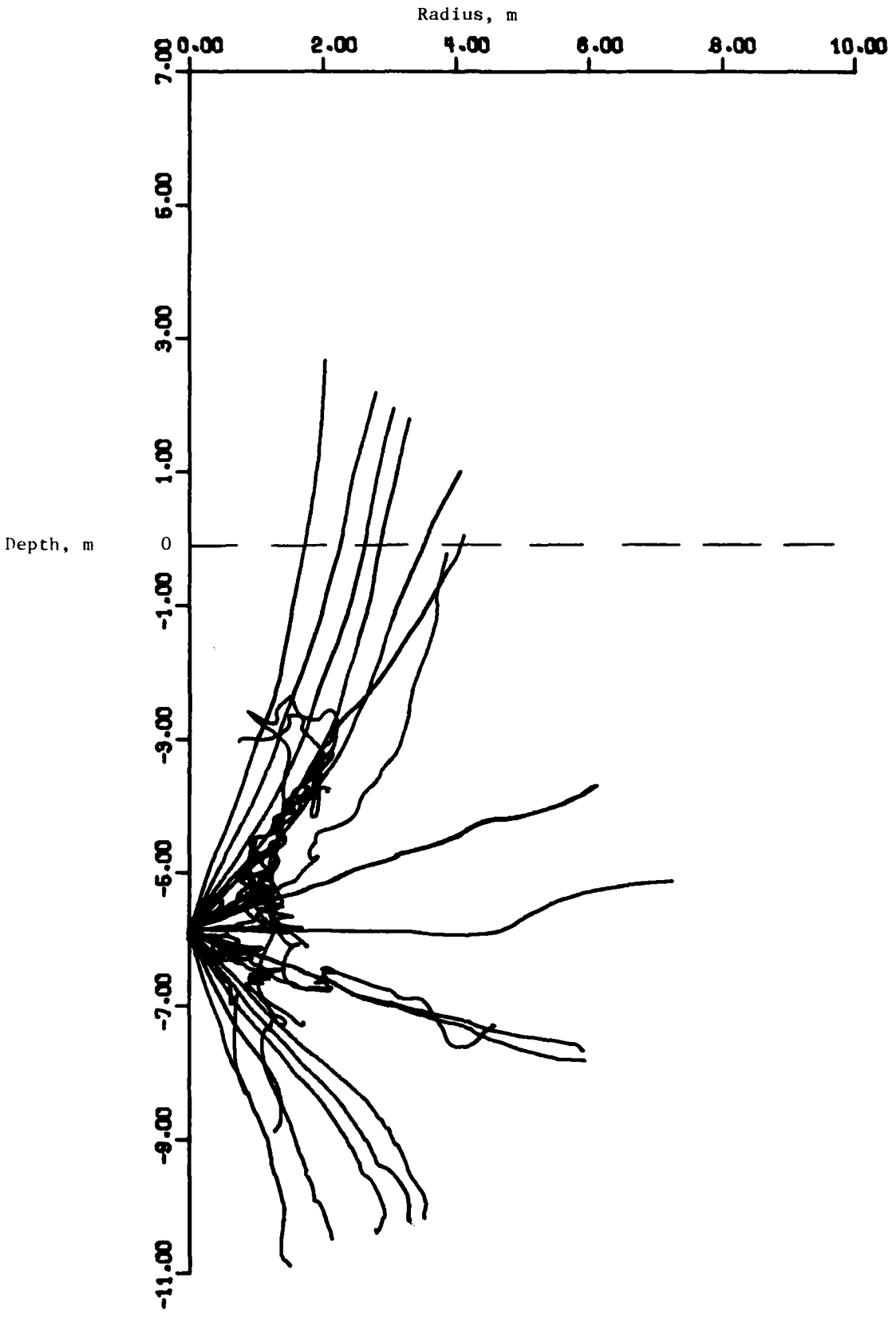

Figure 2.13 Particle Paths of the Radioactive Debris up to ~50 msec for Case 3223 (Nuclear/Dry).

rather than the nominal 1 Mbar normally used. The effect of this problem on the crater was relatively small. Primarily, it allowed somewhat more energy to be available for heating and excavating solid-phase soil. However, the venting of soil vapor without sufficient latent heat of vaporization would have meant that the energy available for subsequent lofting was unrealistically small.

Time did not permit repeat of the CRALE analysis of Case 3223. However, a reasonable compensation for the problem was made in the following way: The mass of soil exposed to peak shock pressures above 1 Mbar was determined from the CRALE analysis, and this mass, approximately 1 metric ton, was taken to have been vaporized. Using an estimated heat of vaporization of $H_v = 14 \times 10^{11}$ ergs/gm[15], the latent heat required to vaporize 1 ton of soil is 1.4×10^{11} ergs/gm $\times 10^6$ gm = 3.3 tons*. The 3.3 tons of energy are approximately 17% of the 20-ton device yield used in Case 3223; this vaporization energy was added to a ton of ejecta vapor entering the DICE code solution.

2.5 SUMMARY OF CRATERING CALCULATIONS

The final crater profiles (from ballistic extrapolation) are shown in Figure 2.14. Table 2.1 compares the calculated dimensions and volumes with available experimental data. Reasonable agreement was obtained. As discussed in Section 2.2.2 and illustrated in Figure 2.9, the calculated crater shape for the HE/Wet case (3221) was much deeper and narrower than the observed crater for Essex 6MS. However, the calculated and observed volumes agreed to within 7%. The shape discrepancy is probably due to late-time slumping in the saturated soil which was not modeled in the code solution. (Some slumping must have occurred, since the HE charge was located below the observed crater floor.)

---

* 1 ton energy = 4.2×10^6 ergs.

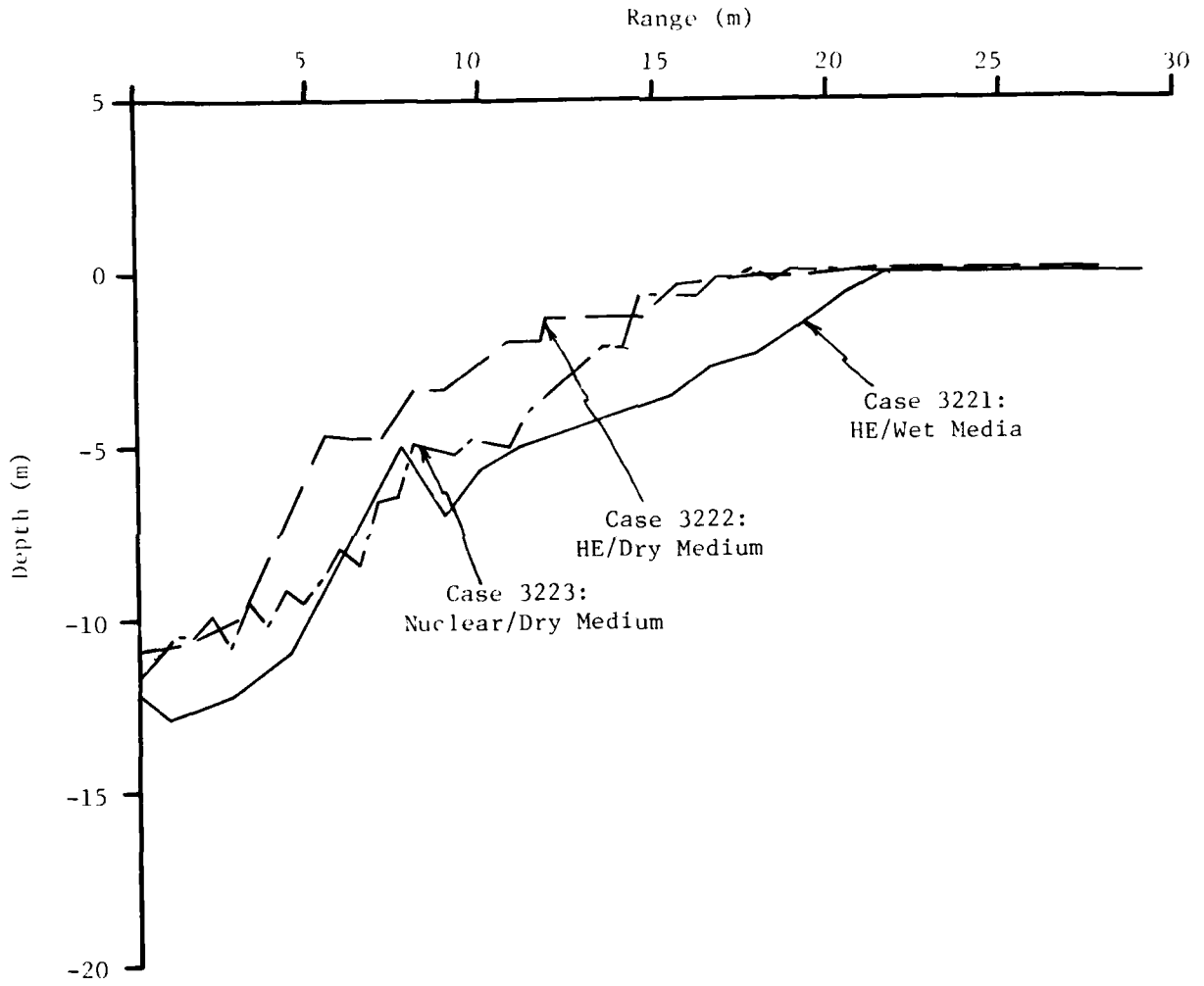

Figure 2.14 Predicted Crater Profiles from the CRALE Solution.

Table 2.1

COMPARISON OF THE CALCULATED CRATER
DIMENSIONS WITH EXPERIMENTAL RESULTS

Calculation				Experiment				
Case	Radius (m)	Depth (m)	Volume (m^3)	Radius (m)	Depth (m)	Volume (m^3)	$\frac{Vcalc}{Vexp}$	Source
3221 HE/Dry	22	13	5640	26.2	3.7	6046	.93	Essex 6MS experiment
3222 HE/Dry	21	10.8	2410					
3223 Nuclear/Dry	18.8	11.8	3510	11.4	7.0	1534* (1227)†	2.29 (2.86)	Teapot Ess, reduced to 20 tons by cube root scaling.

*true

†apparent

Results of the Nuclear/Dry calculation are compared with results for Teapot Ess (scaled to 20-ton yield using $W^{1/3}$). The calculated volume is larger than the scaled Teapot Ess volume by a factor of over two; the depth/diameter ratios are nearly the same.

The flux of material across the ground surface was the major output of the cratering calculation, as this data was required as input to the DICE calculations discussed in the following section. The differences in initial ejecta are summarized in Figure 2.15, which shows the velocity profiles at selected times along the ground surface for the three cases. While the ejecta in the two HE cases appear to have similar initial velocity distributions, the vaporized material in the nuclear case escapes more rapidly.

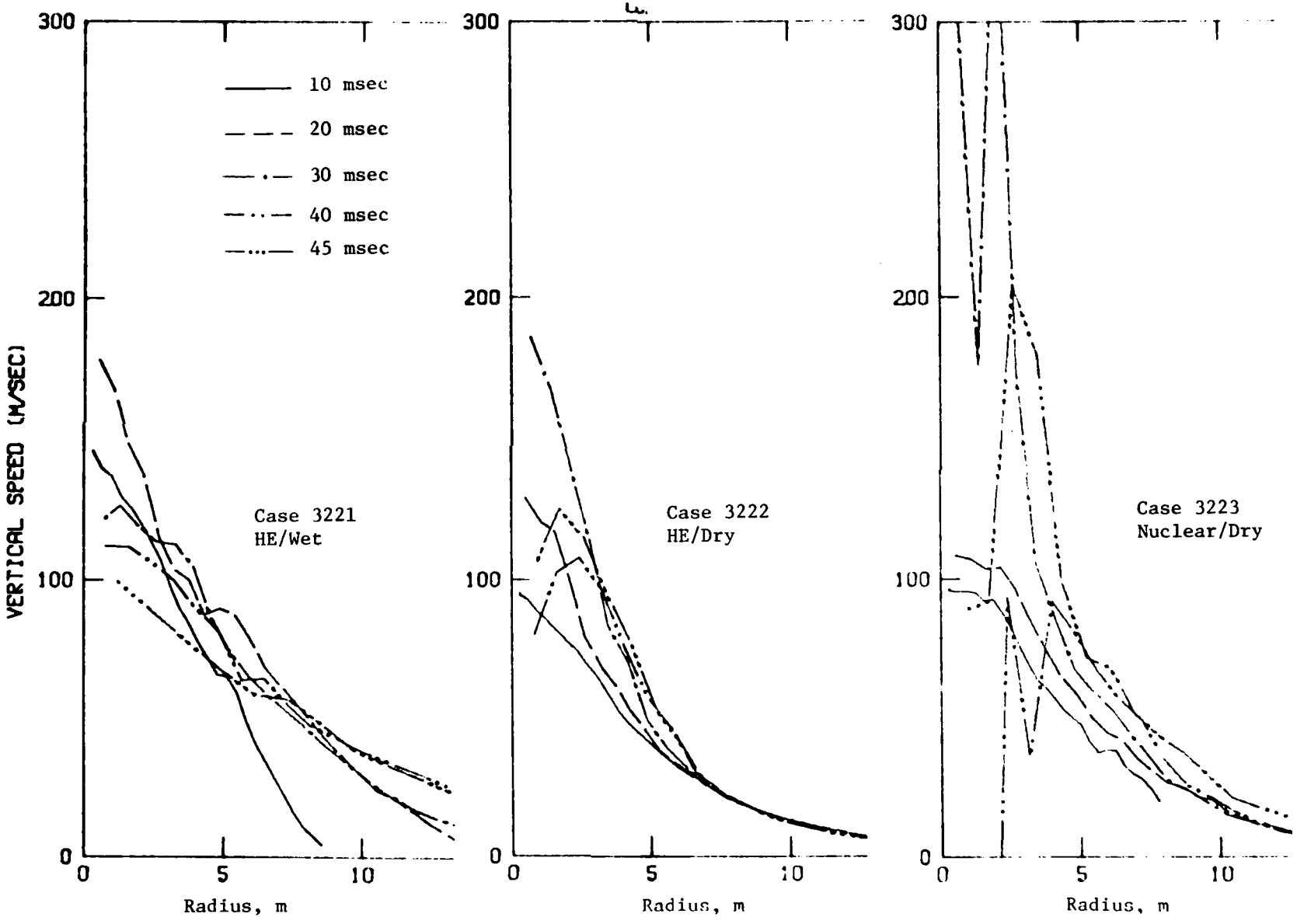

Figure 2.15 Comparison of the Ejecta Velocity Profiles along the Ground Surface at Selected Times for the Three Calculations.

SECTION 3

EJECTA-AIR MULTIPHASE FLOW - DICE CALCULATIONS

The multiphase DICE code was used to analyze the cloud lofting and air flow characteristics. Soil and iridium-coated sand particles were supplied to the DICE code from the CRALE cratering analyses described in the preceding section.

3.1 HE SOURCE IN WET SOIL (ESSEX 6MS) - CASE 3221

The particle size characteristics of the soil and iridium tracers are indicated in Table 3.1. The iridium tracer particles are represented by DICE particle size groups 1 and 2. The iridium tracer particle diameters are between 75 and 175 μm. The particle size distribution of the soil incipient ejecta is not currently predicted by CRALE or any other cratering code. Break-up or agglomeration of soil "clumps" during the cratering process has not been investigated; therefore, the soil incipient ejecta particle size distribution must be estimated based on meager ejecta data. Particle size groups 3-6 represent the soil. Soil particles range in diameter between 100 μm and 100 cm.

Figure 3.1 shows the ejecta mass flowed into the air versus time and particle size group for the wet media (3221). The CRALE cratering simulation provided incipient ejecta density, velocity, and specific internal energy to the DICE code for times up to t = 200 msec. The decrease in the mass of all groups after about 1 sec is due to particle fallout. Iridium-coated sand particles entered the atmosphere at t ~20 msec. Total soil mass ejected into the atmosphere was 5.2 kton, with about 0.5 ton, or 0.01% of this total being the iridium-coated sand.

Figure 3.2 shows a velocity vector field plot and the location of the soil and iridium boundaries at 26 msec after detonation. Below the soil boundary, there is a region of

Table 3.1

PARTICLE SIZE CHARACTERISTICS FOR A WET GEOLOGIC MEDIA AND IRIDIUM-COATED SAND (CASE 3221)

Group	Particle Type	Diameter d_p (cm)			Mass Fraction of Solid Incipient Ejecta
		Minimum	Maximum	Representative Diameter	
1	Iridium	.0075	.0125	.01	.256
2	Iridium	.0125	.0175	.015	.744
3	Soil	.01	.1	.032	.032
4	Soil	.1	1	.32	.068
5	Soil	1	10	3.2	.218
6	Soil	10	100	32	.684

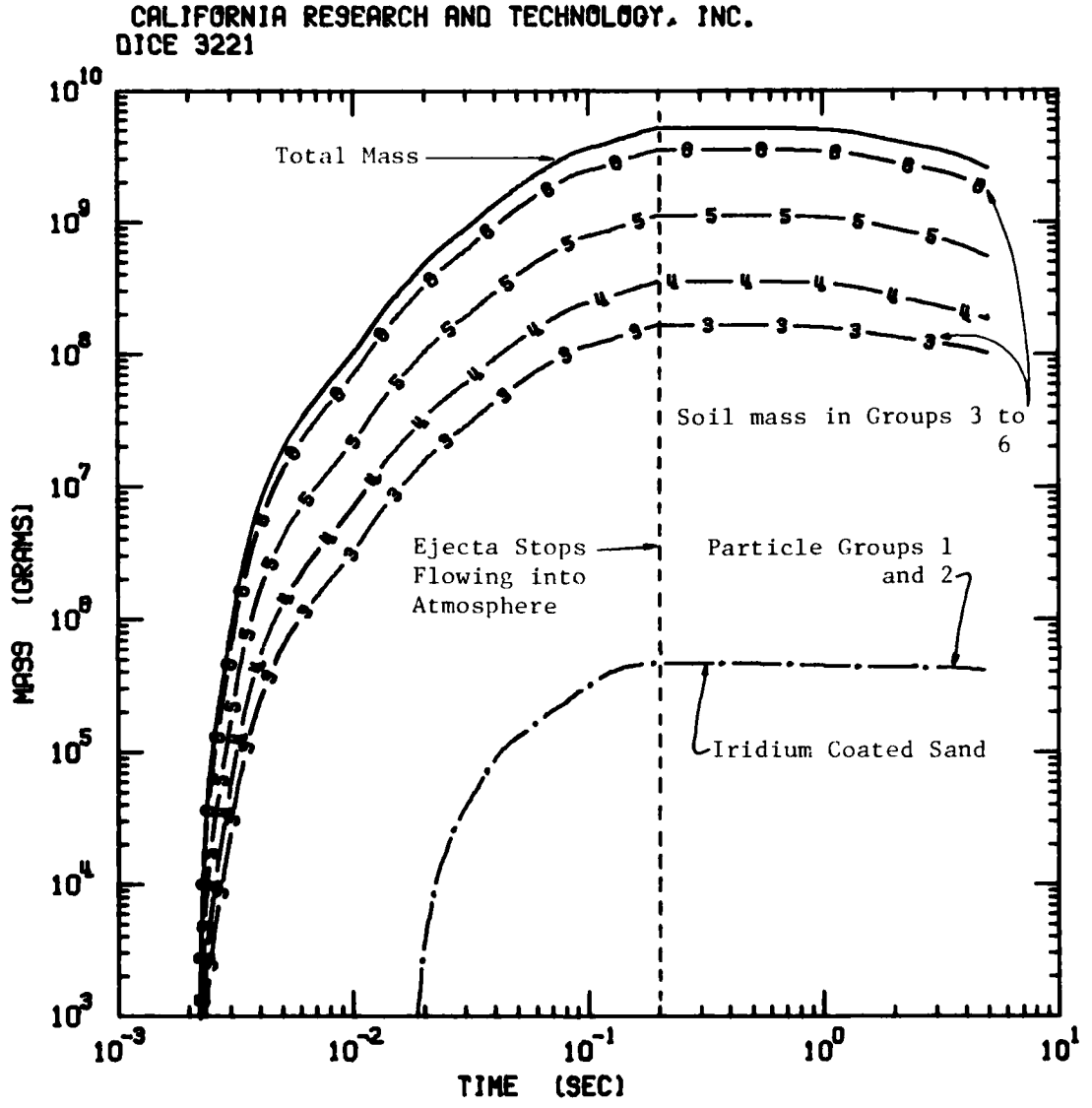

Figure 3.1 Ejecta Mass Flowed into the Atmosphere as a Function of Time and Particle Size Group for Case 3221 - HE Source in Wet Media Representing Essex 6MS.

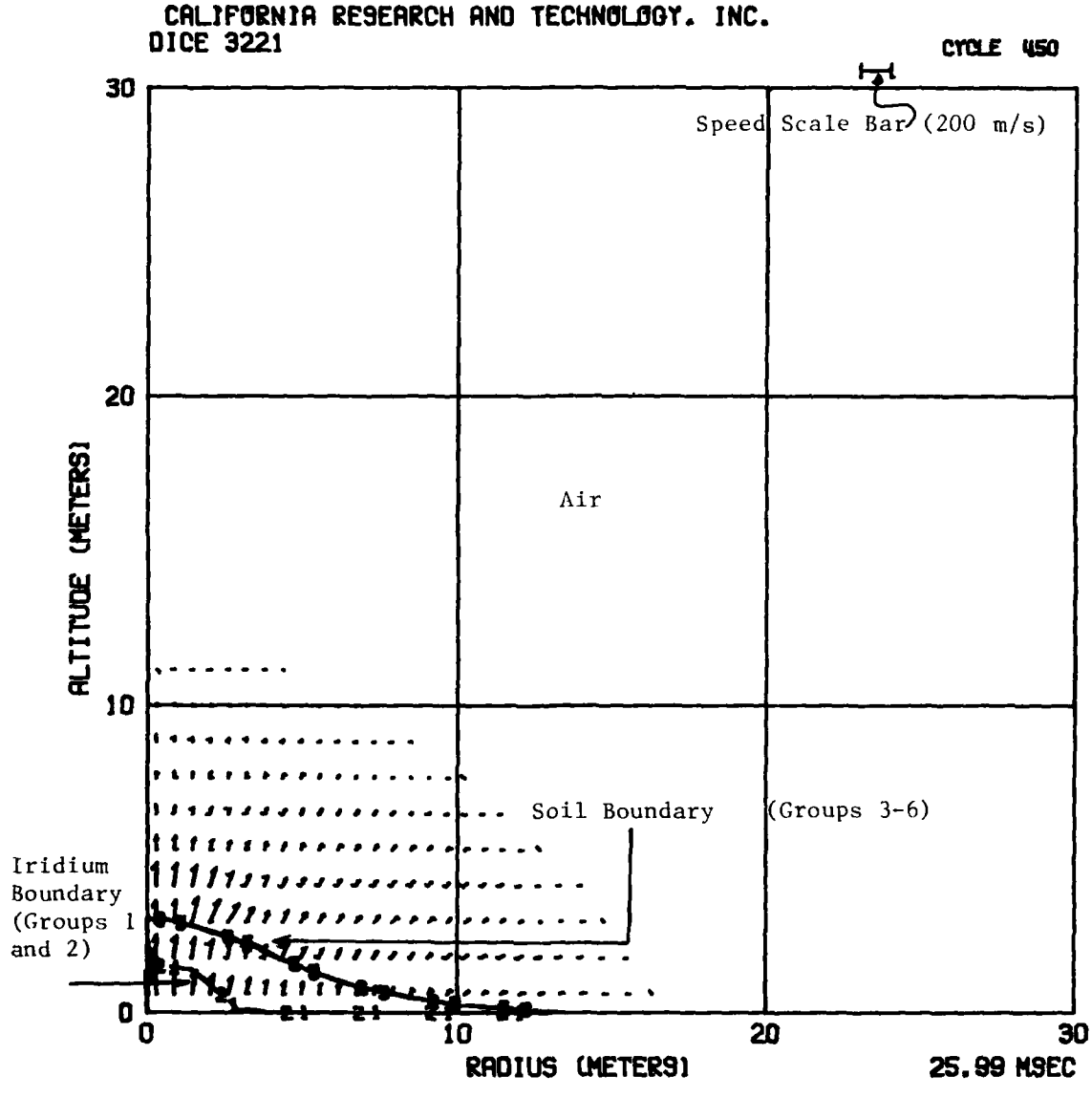

Figure 3.2 Air Velocity Field at 26 msec for HE Burst Buried in a Wet Soil (Essex 6MS, Case 3221).

multiphase flow involving soil particles and air which are dynamically coupled by drag and thermal interactions. The iridium boundary position is below the soil boundary because the iridium was initially buried with the HE charge. The upward moving ground surface accelerates the air to velocities greater than 200 m/sec.

By 45 msec (Figure 3.3), the iridium-coated sand particles have caught up with the soil particles and the two boundaries nearly coincide at the axis of symmetry. This is a consequence of the iridium particles being located in the HE charge and flowing with the detonation products; the detonation gases flowing from the crater region are accelerated to higher velocities than the soil particles once venting begins.

Figure 3.4 shows that by 72 msec, the smallest particles (groups 1, 2, and 3) are at the highest altitudes. This is an aerodynamic drag effect caused by the venting of the detonation gases through the incohesive soil overburden. At this time the upward velocities near the vertical axis are approximately 300 m/sec. The peak upward velocities occur prior to 100 msec and exceed 300 m/sec.

As seen in Figures 3.5 and 3.6 (t = 100 msec and 300 msec, respectively), drag filtering causes the larger soil particles to overtake the smaller particles when the detonation gases begin to decelerate and gas speeds fall below soil particle speeds. (Note the 50 m/sec scale bar in Figure 3.6.)

Figures 3.7 and 3.8 show the lofted cloud and air flow fields at 1.5 sec using two different fields of view. Figure 3.7 shows that ascending size groups reach progressively higher altitudes. For example, the 10 to 100 cm diameter particles (group 6) have attained an altitude of over 200 m and a maximum radius of 50 m. The largest "particles" flow ballistically with

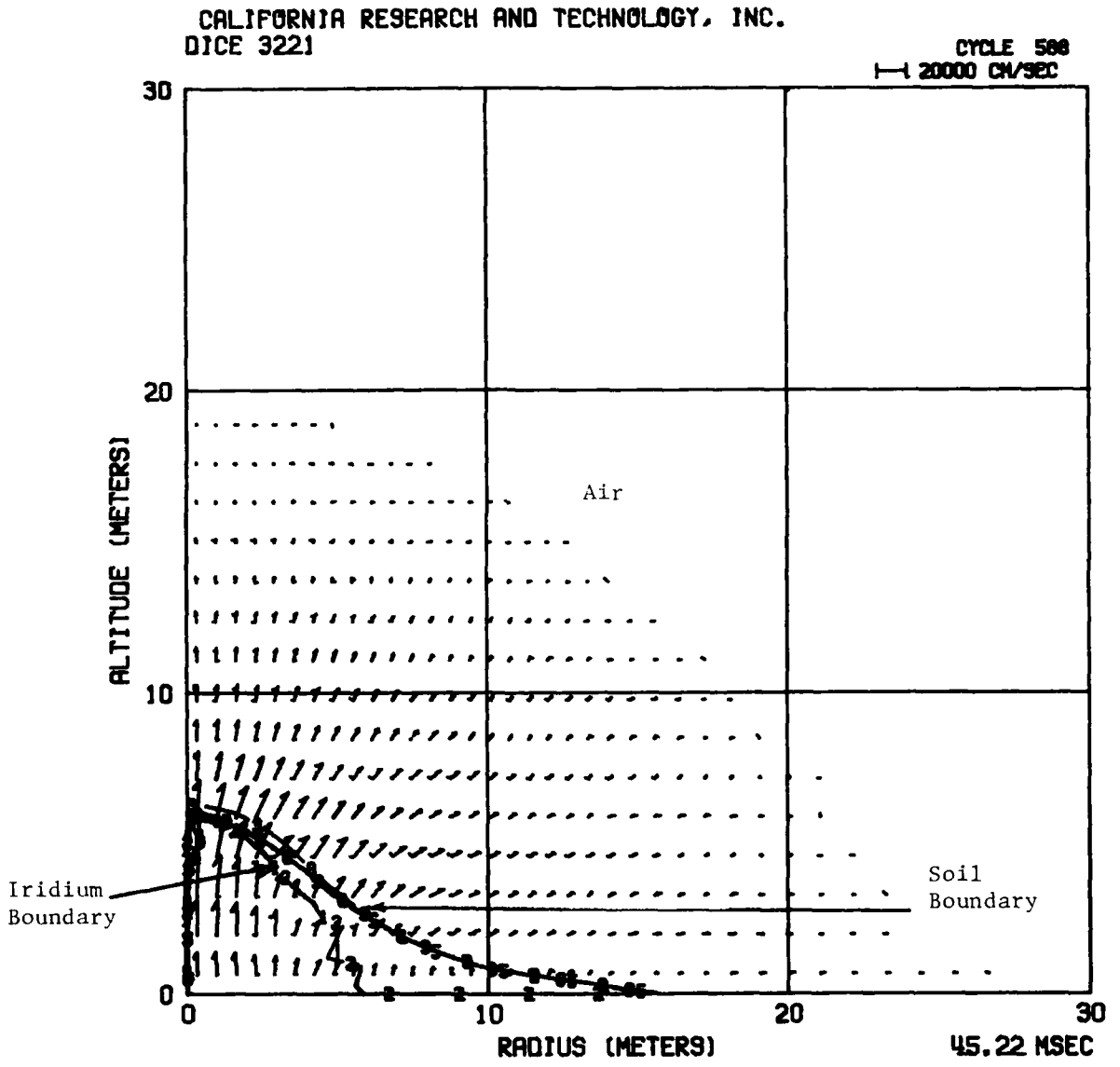

Figure 3.3 Air Velocity Field at 45 msec for HE Burst Buried in a Wet Soil (Essex 6MS, Case 3221).

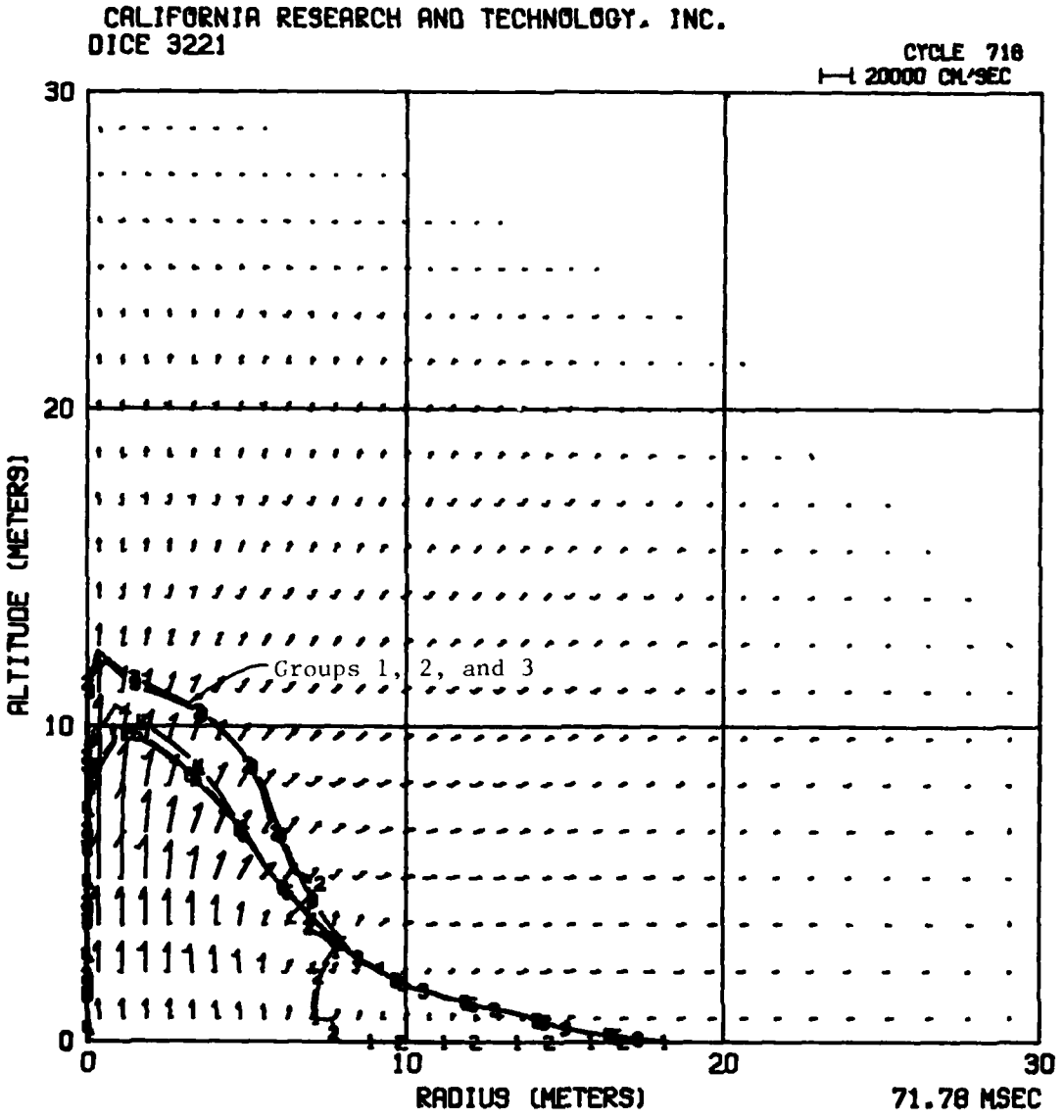

Figure 3.4 Air Velocity Field at 72 msec for HE Burst Buried in a Wet Soil (Essex 6MS, Case 3221).

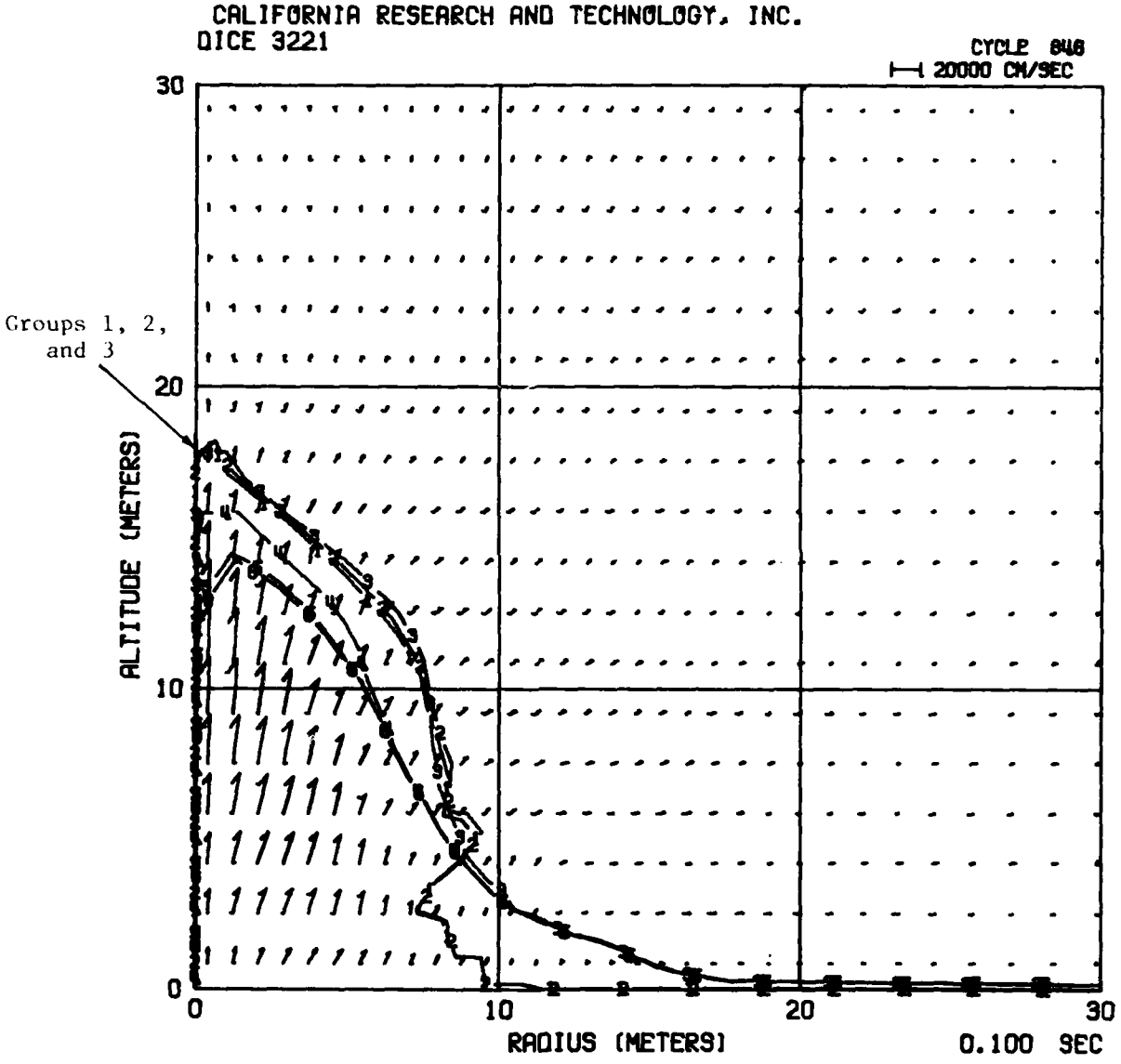

Figure 3.5 Air Velocity Field at .1 Seconds for HE Burst Buried in a Wet Soil (Essex 6MS, Case 3221).

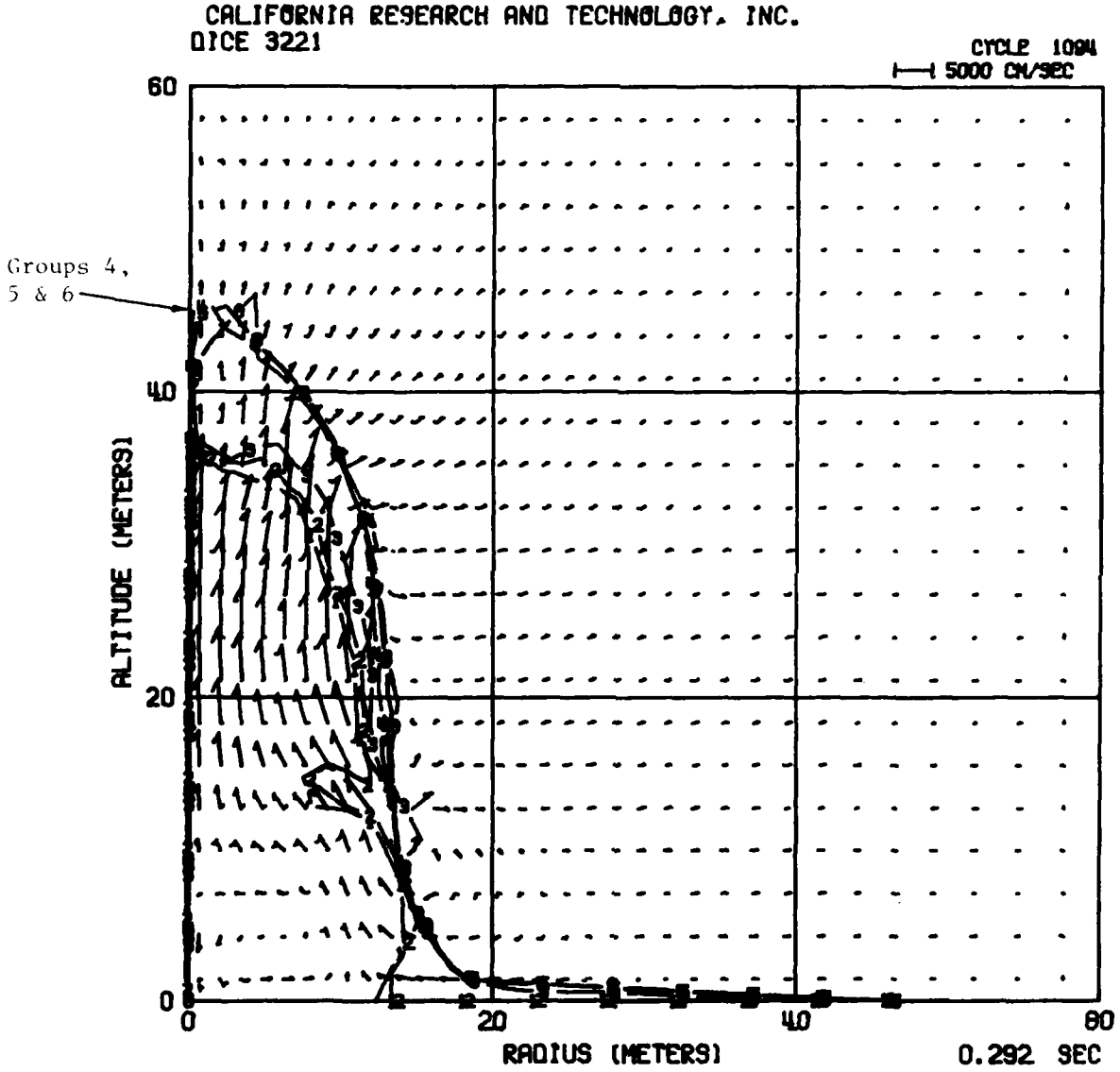

Figure 3.6 Air Velocity Field at .3 Seconds for HE Burst Buried in a Wet Soil (Essex 6MS, Case 3221).

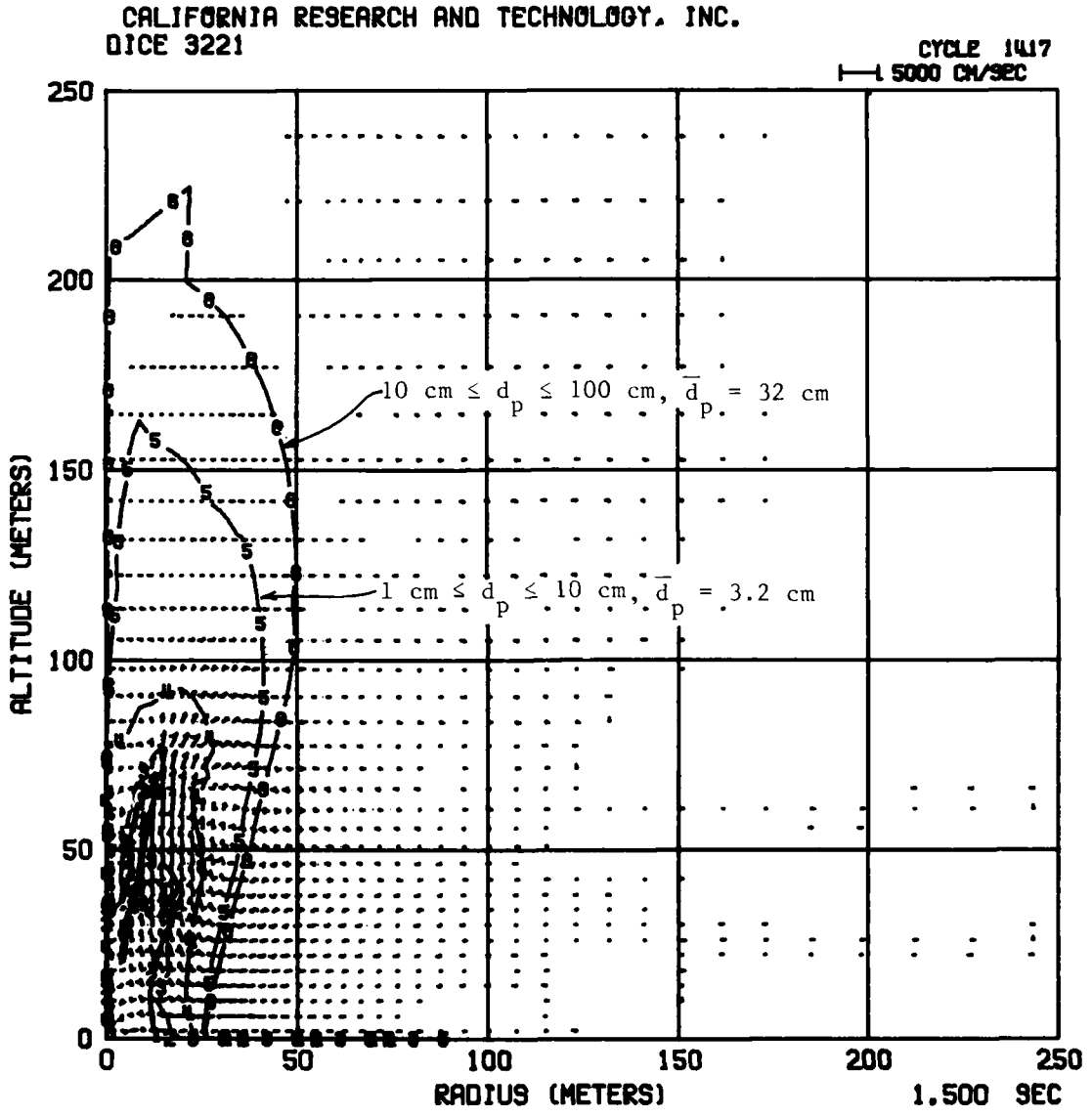

Figure 3.7 Air Velocity Field at 1.5 Seconds for HE Burst Buried in a Wet Soil (Essex 6MS, Case 3221).

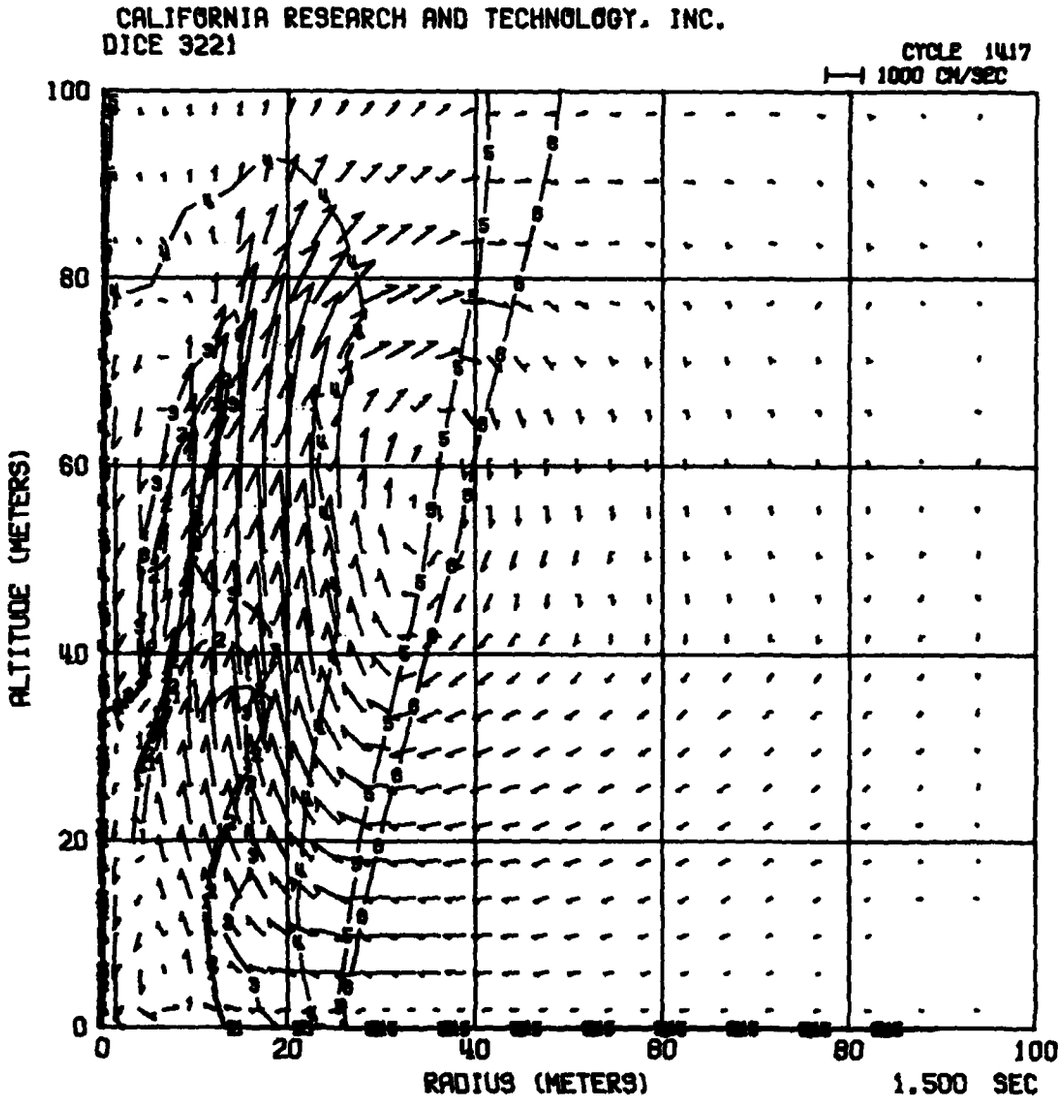

Figure 3.8 Air Velocity Field at 1.5 Seconds for HE Burst Buried in a Wet Soil (Essex 6MS, Case 3221).

a minimum of aerodynamic drag interactions. The separation between groups 4, 5, and 6 is due to greater aerodynamic drag decelerations for the small size particles.

A more detailed view of the evolving air flow pattern is shown in Figure 3.8. A main vortex has formed giving a toroidal circulation; however, there is downflow of air below 80 m near the axis of symmetry. The small iridium particles (groups 1 and 2) are strongly affected by this downflow.

Figures 3.9 and 3.10 show analogous spatial fields of view at a time of 2.5 sec. The 10-100 cm diameter clumps of soil reach altitudes of 350 m. Note that shedding and break-up of soil clumps was not modeled in these calculations. Figure 3.10 shows that the main vortex persists, confining the iridium particles to a narrow region near the axis.

Figures 3.11 and 3.12 show two fields of view of the cloud and air flow fields at 5.0 sec when the computation was stopped. At this time downflow dominates the entire field. Only particles greater than 1 cm diameter (groups 5 and 6) continue to rise in the descending air. The 10-100 cm particles (group 6) have reached an altitude of 550 m while attaining a radius of nearly 150 m. The maximum altitude of the 1-10 cm soil particles is 270 m. Figure 3.12 shows an air flow pattern with only weak upward velocities (less than 5 m/sec) in the main vortex.

3.2 HE SOURCE IN DRY SOIL - CASE 3222

The particle size characteristics used in this solution are indicated in Table 3.2. Alluvium[11] has a relatively small particle size distribution as compared to the wet soil in Case 3221; soil particle diameters ranged between .005 cm to 10 cm in groups 3 through 6. The iridium particles (groups 1 and 2) have sizes identical to those in Case 3221.

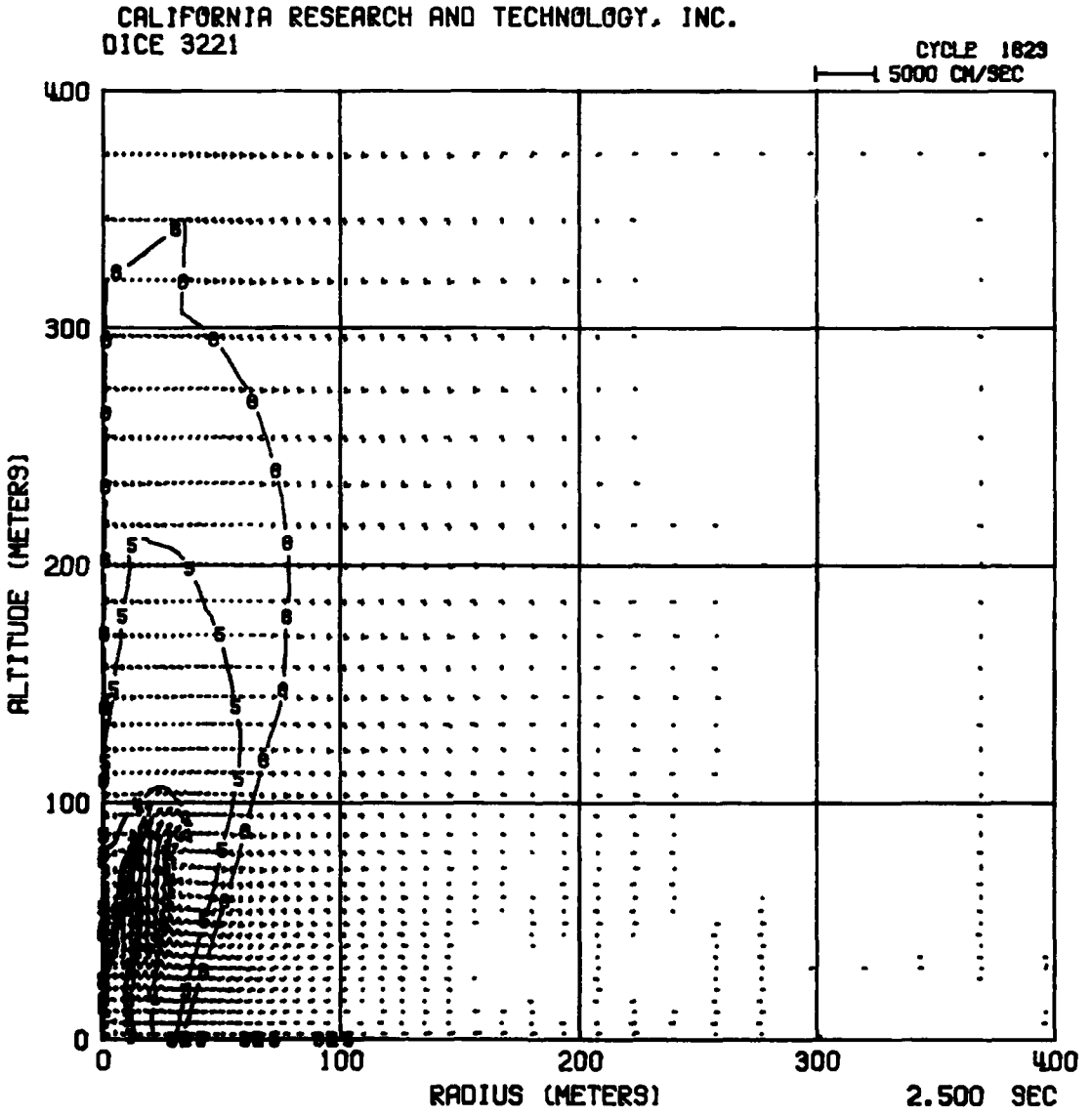

Figure 3.9 Air Velocity Field at 2.5 Seconds for HE Burst Buried in a Wet Soil (Essex 6MS, Case 3221).

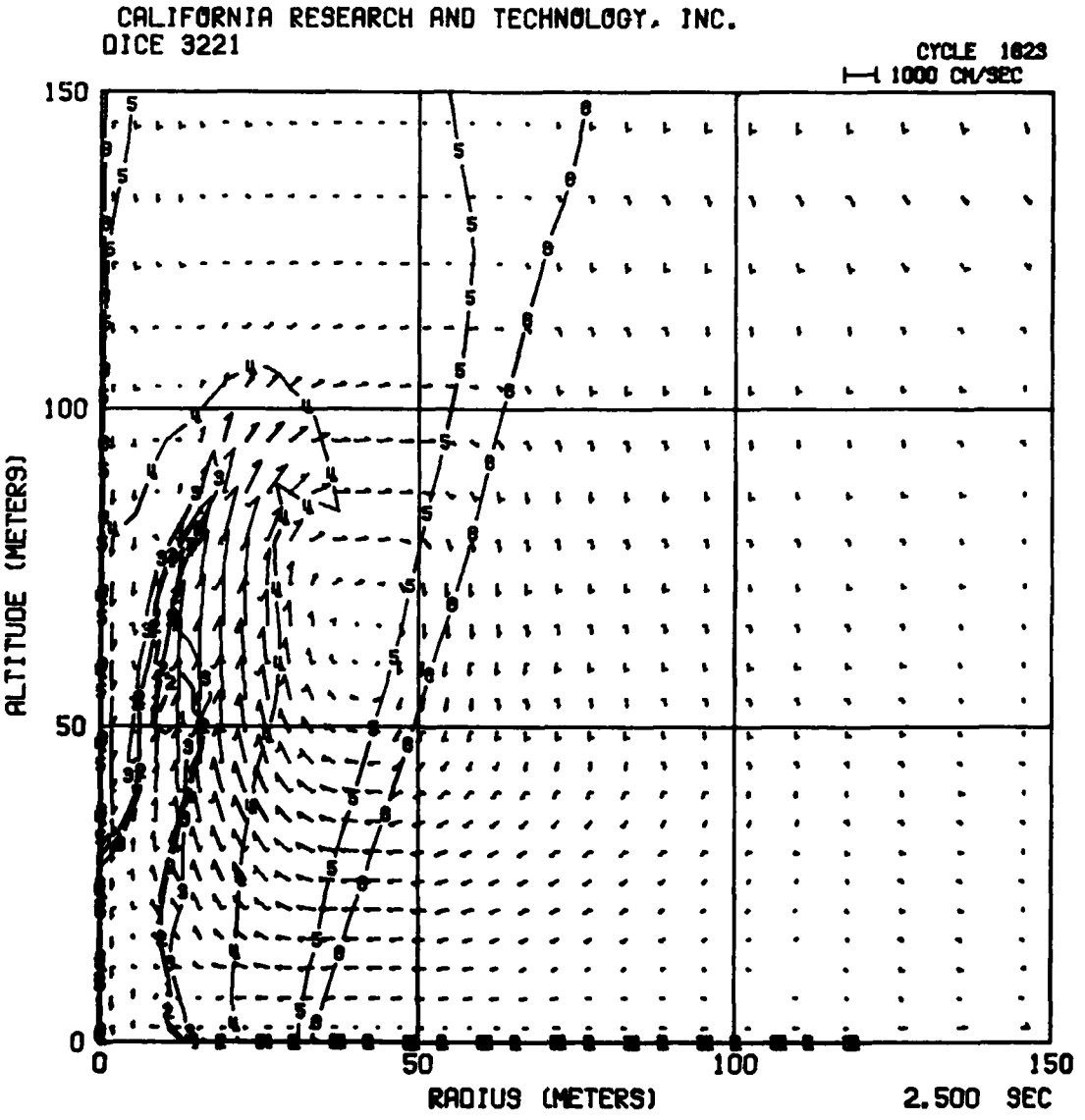

Figure 3.10 Air Velocity Field at 2.5 Seconds for HE Burst Buried in a Wet Soil (Essex 6 MS, Case 3221).

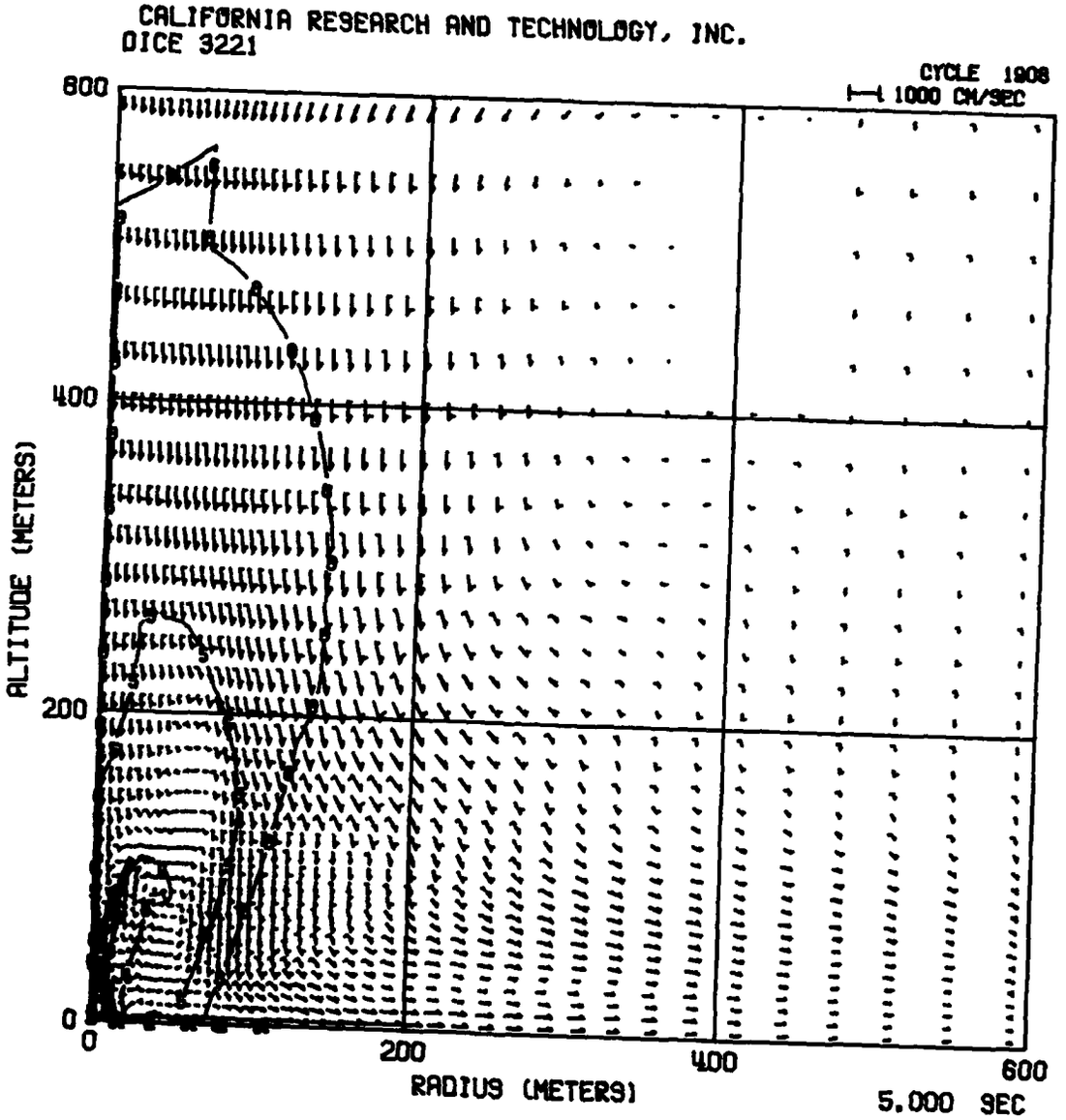

Figure 3.11 Air Velocity Field at 5 Seconds for HE Burst Buried in a Wet Soil (Essex 6MS, Case 3221).

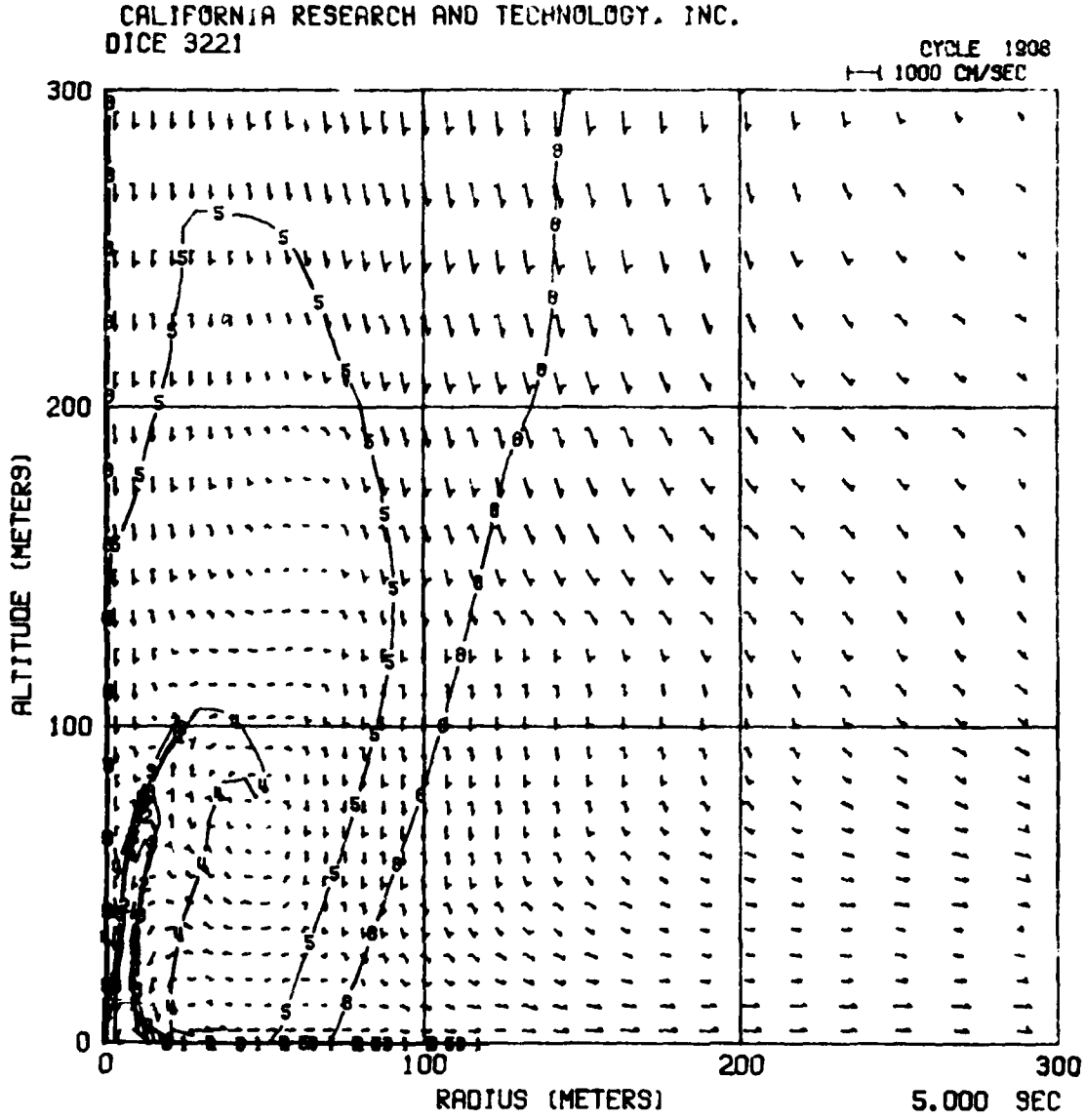

Figure 3.12 Air Velocity Field at 5 Seconds for HE Burst Buried in a Wet Soil (Essex 6MS, Case 3221).

Table 3.2

PARTICLE SIZE CHARACTERISTICS FOR ALLUVIUM[11]
AND IRIDIUM-COATED SAND (CASE 3222)

Group	Particle Type	Diameter d_p (cm)			Mass Fraction of Solid Incipient Ejecta
		Minimum	Maximum	Representative Diameter	
1	Iridium	.0075	.0125	.010	.256
2	Iridium	.0125	.0175	.015	.744
3	Soil	.0050	.01	.007	.1
4	Soil	.01	.1	.032	.3
5	Soil	.1	1	.32	.3
6	Soil	1	10	3.2	.3

Figure 3.13 shows the CRALE-supplied ejecta mass flux into the air. Incipient ejecta crossed the ground surface for times up to 200 msec. Total soil mass ejected into the atmosphere was 2.4 kt as compared with 5.2 kt in the HE/Wet case (3221). About 1 ton, or 0.05% of the total particle mass, was in the form of iridium-coated sand for Case 3222. This is twice as much iridium as was ejected from the crater in the wet case (3221).

Figures 3.14 to 3.20 show the air velocity field with the lofted soil particle size boundaries at t = .03, .05, .1, .25, 1.0, 2.0, and 5.0 seconds.

Figure 3.21 shows the air velocity field with a smaller field of view at 5.0 sec. Two main vortices are apparent, with general downflow elsewhere in the field. Strong downflow is especially noticeable near the axis of symmetry. Note that the overall flow characteristics for this case are quite complicated with a few smaller vortices being apparent.

The relatively small particle size distribution in this dry alluvium as compared to the wet soil in Case 3221 causes a much stronger aerodynamic coupling between the ejected soil and air. The cloud dynamics are strongly affected by this difference; for example, compare Figures 3.2 to 3.12 from Case 3221 (wet soil) with Figures 3.14 to 3.21 from Case 3222 (dry soil). Comparisons between these cases are described in Section 4.

3.3 NUCLEAR SOURCE IN DRY SOIL - CASE 3223

The soil particle size characteristics are given in Table 3.3. Soil groups 1-4 in Case 3223 were identical to groups 3-6 in Case 3222. Group 5 is the soil vapor group.

A portion of the 20 tons of device energy released in this nuclear burst goes into vaporization of soil which is shocked by very high pressures (P > 1 megabar). As the cratering dynamics

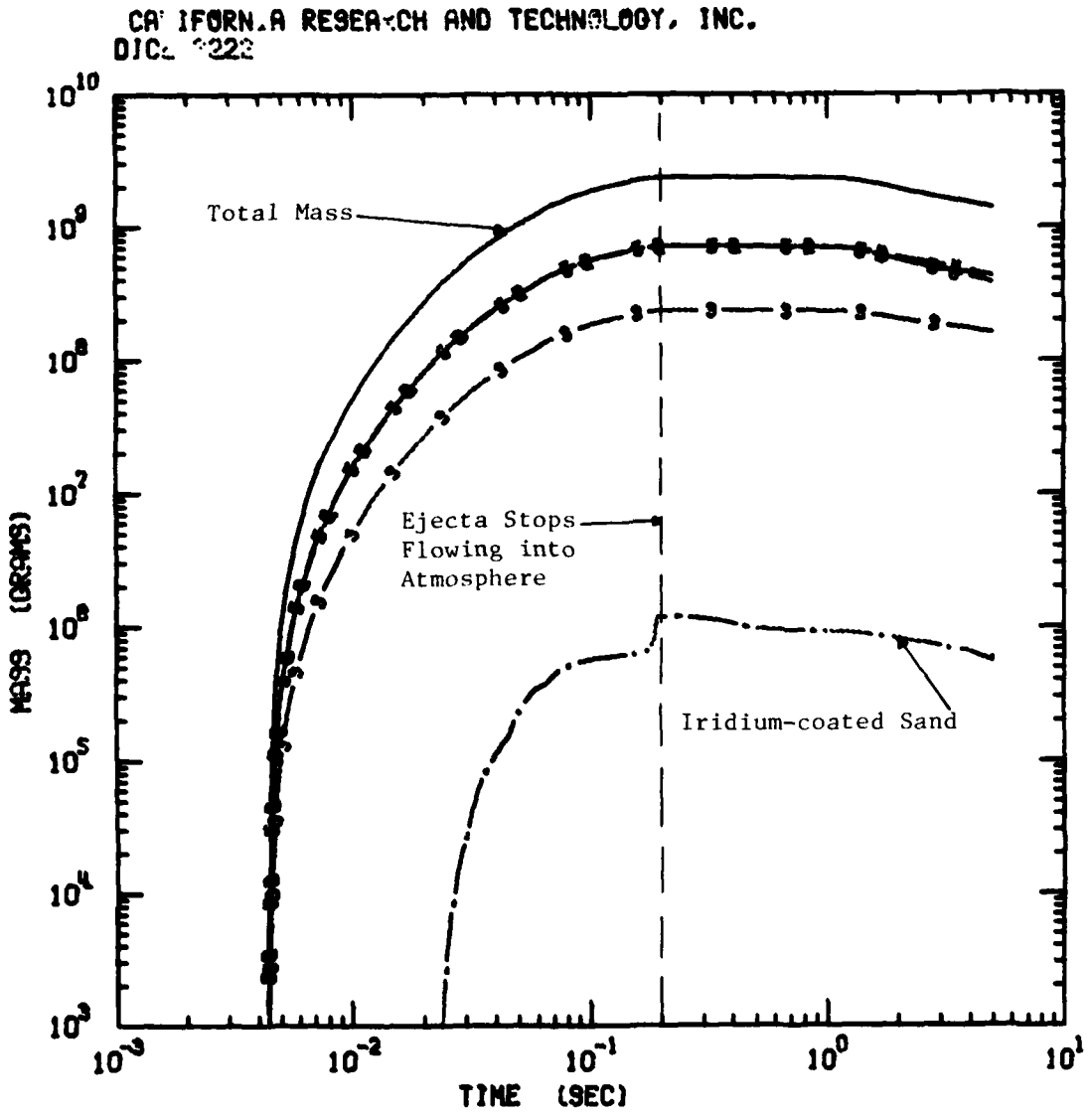

Figure 3.13 Ejecta Mass Flowed into the Atmosphere as a Function of Time and Particle Size Group for HE/Dry Numerical Simulation (Case 3222).

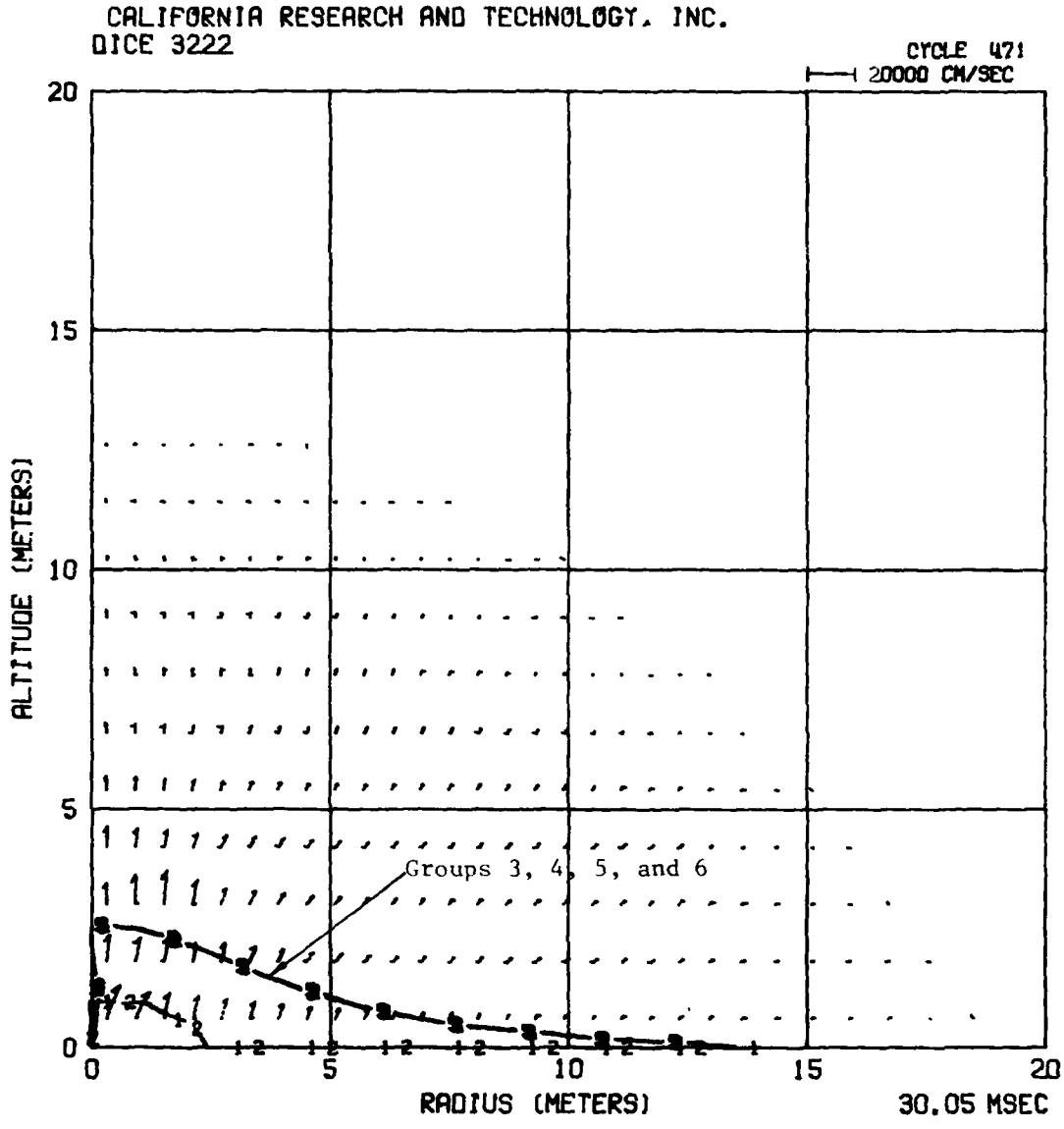

Figure 3.14 Air Velocity Field at 30 ms for a 10-ton HE Burst Buried 6 Meters in a Dry Soil (Case 3222).

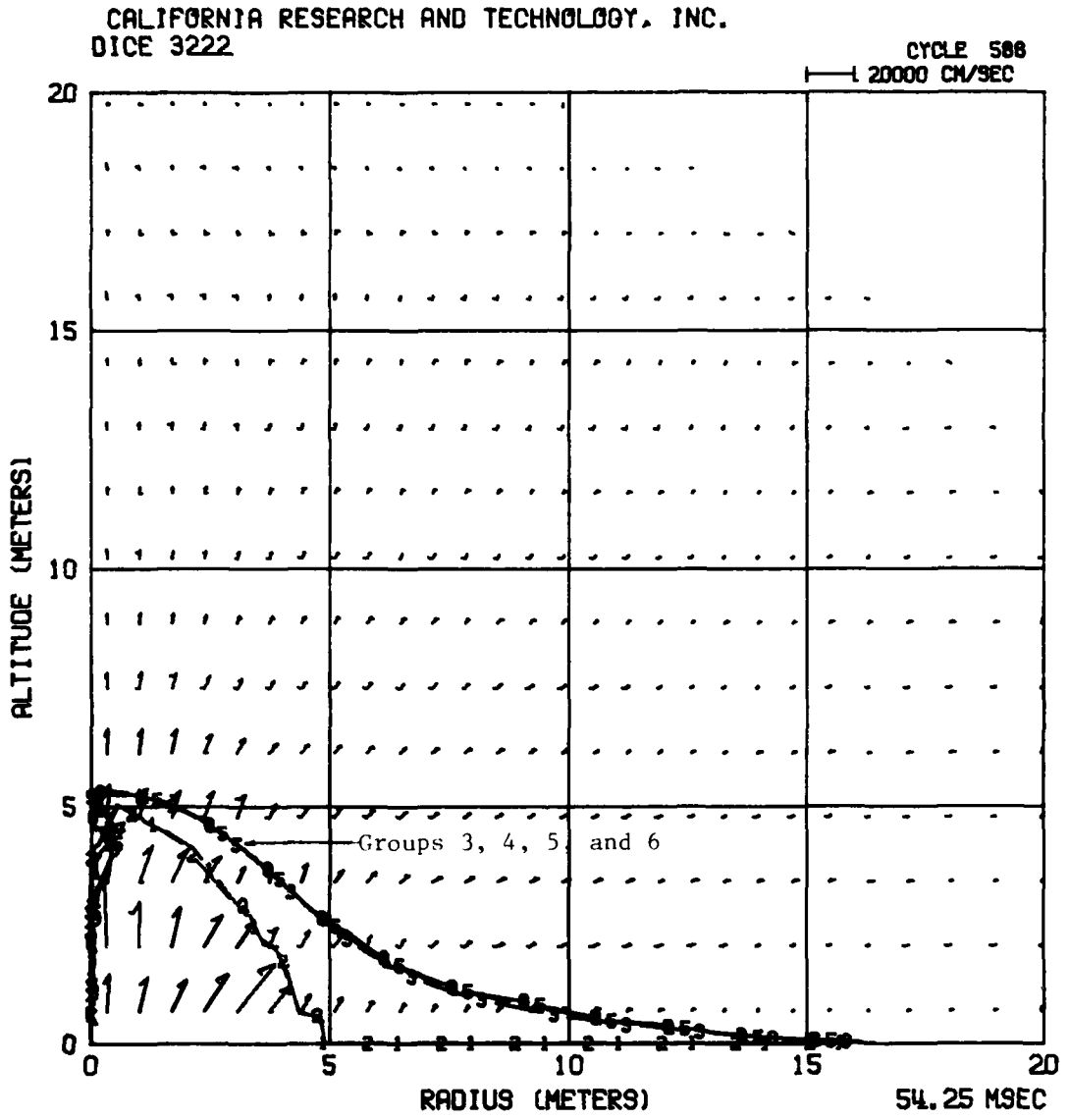

Figure 3.15 Air Velocity Field at 54 ms for a 10-ton HE Burst Buried 6 Meters in a Dry Soil (Case 3222).

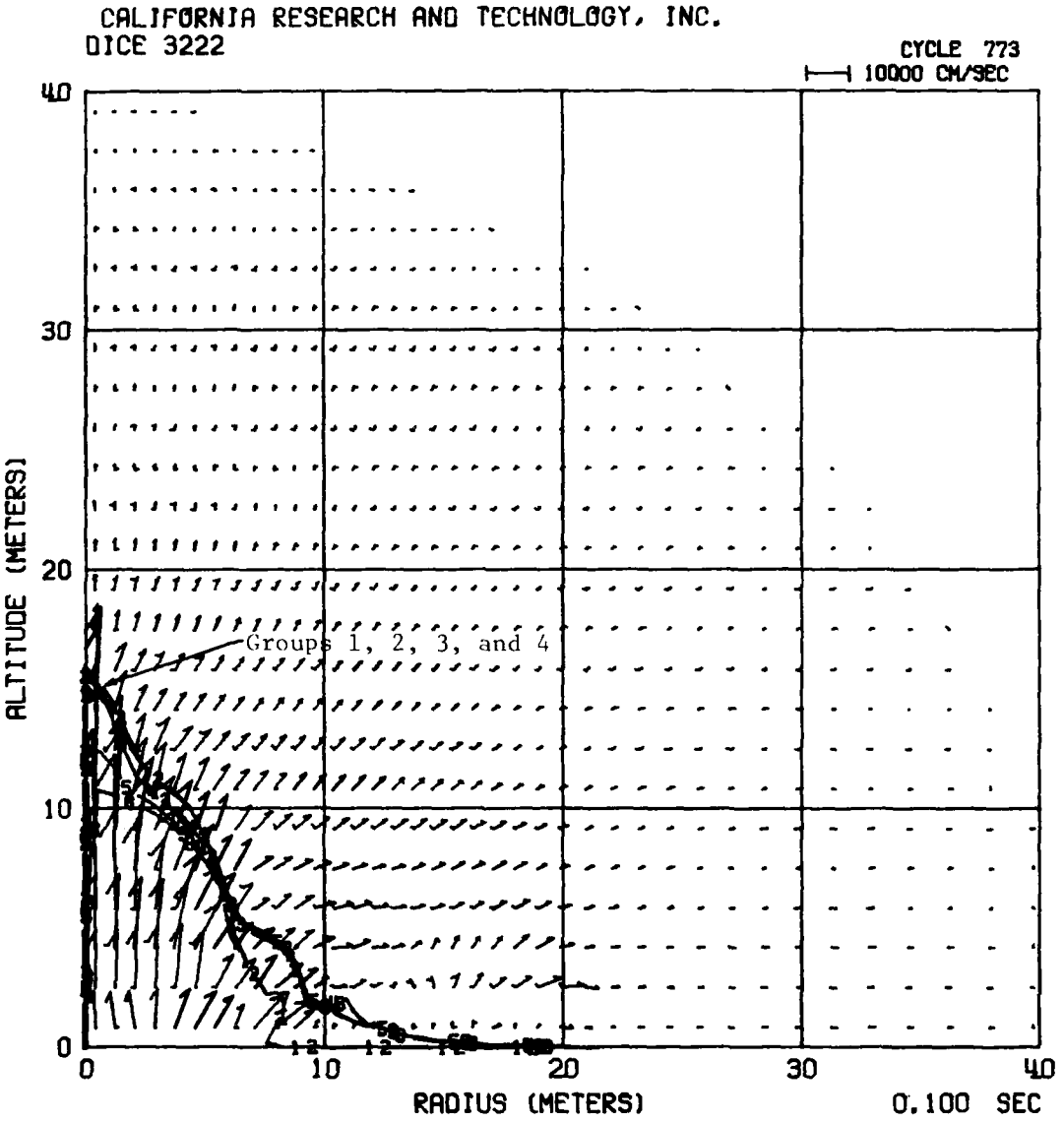

Figure 3.16 Air Velocity Field at 100 ms for a 10-ton HE Burst Buried 6 Meters in a Dry Soil (Case 3222).

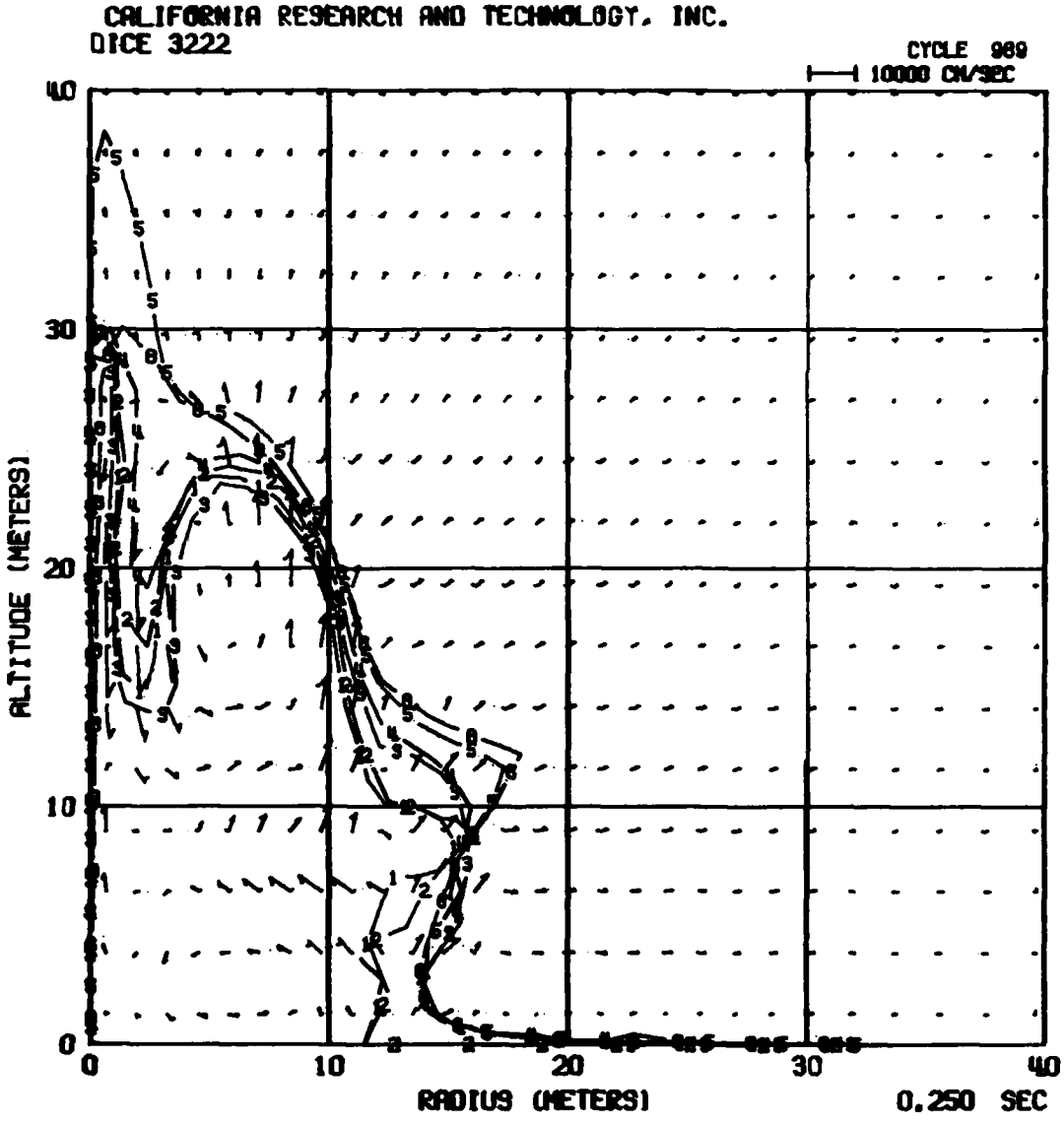

Figure 3.17 Air Velocity Field at 250 ms for a 10-ton HE Burst Buried 6 Meters in a Dry Soil (Case 3222).

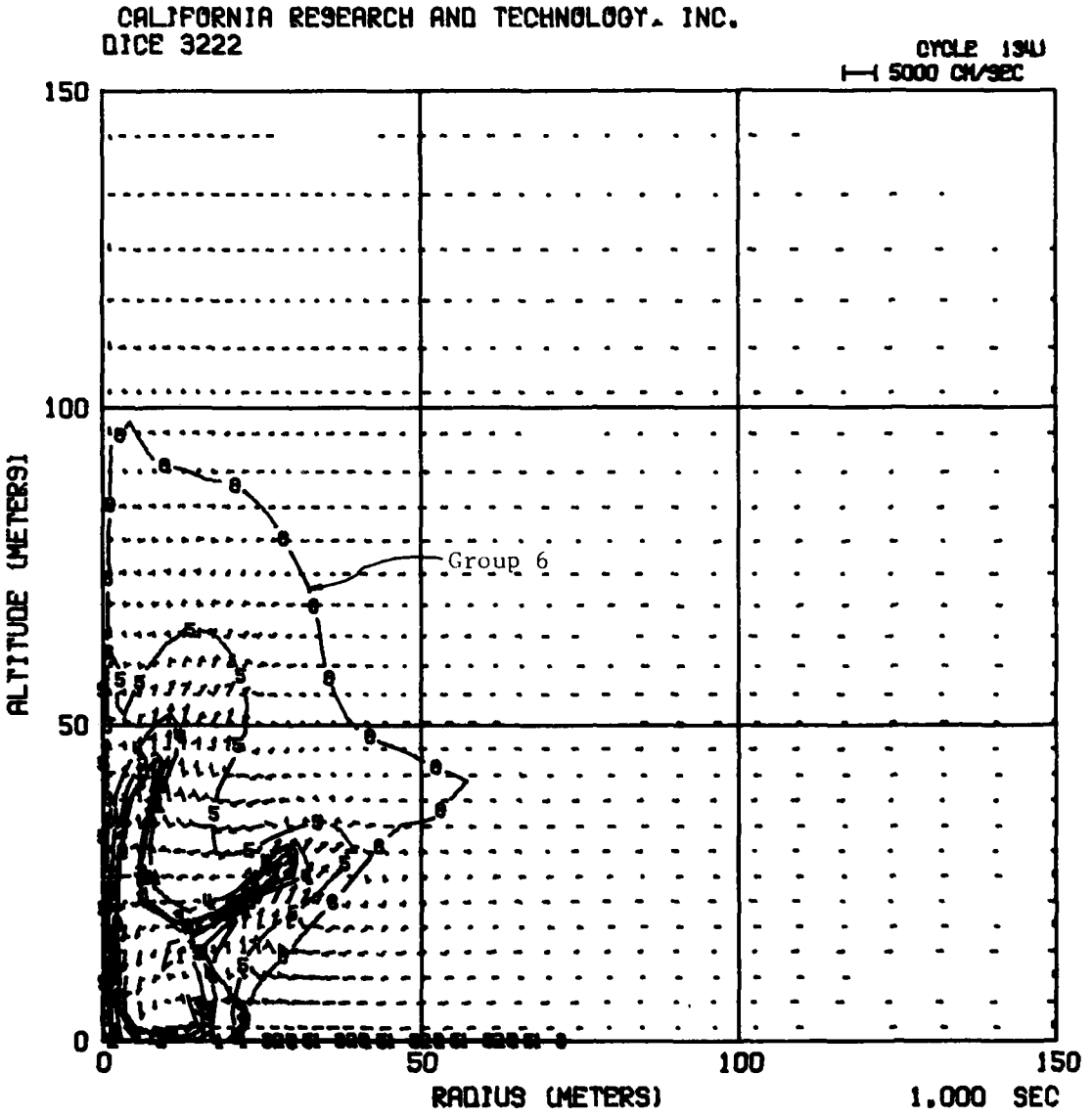

Figure 3.18 Air Velocity Field at 1 second for a 10-ton HE Burst Buried 6 Meters in a Dry Soil (Case 3222).

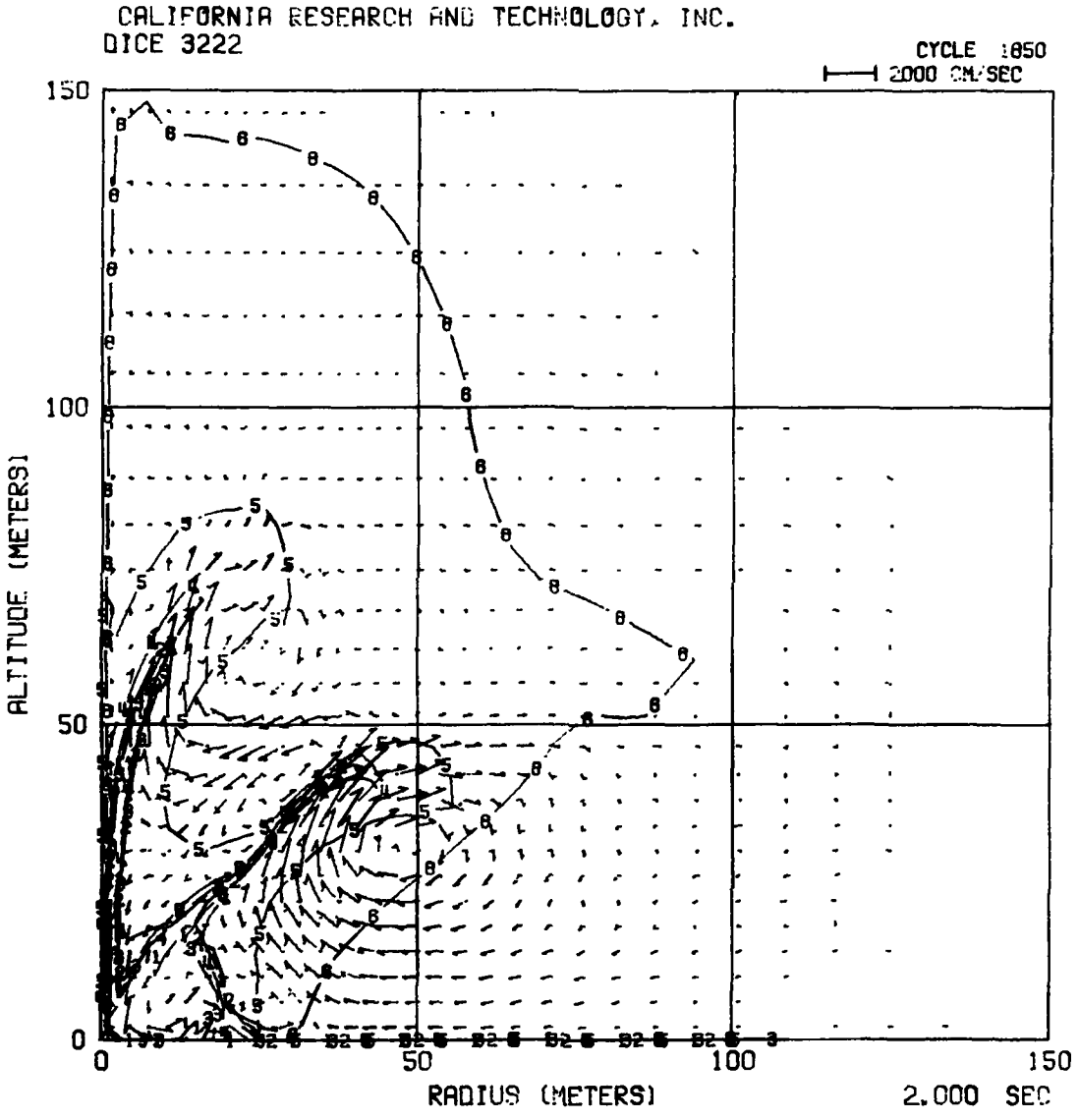

Figure 3.19 Air Velocity Field at 2 seconds for a 10-ton HE Burst Buried 6 Meters in a Dry Soil (Case 3222).

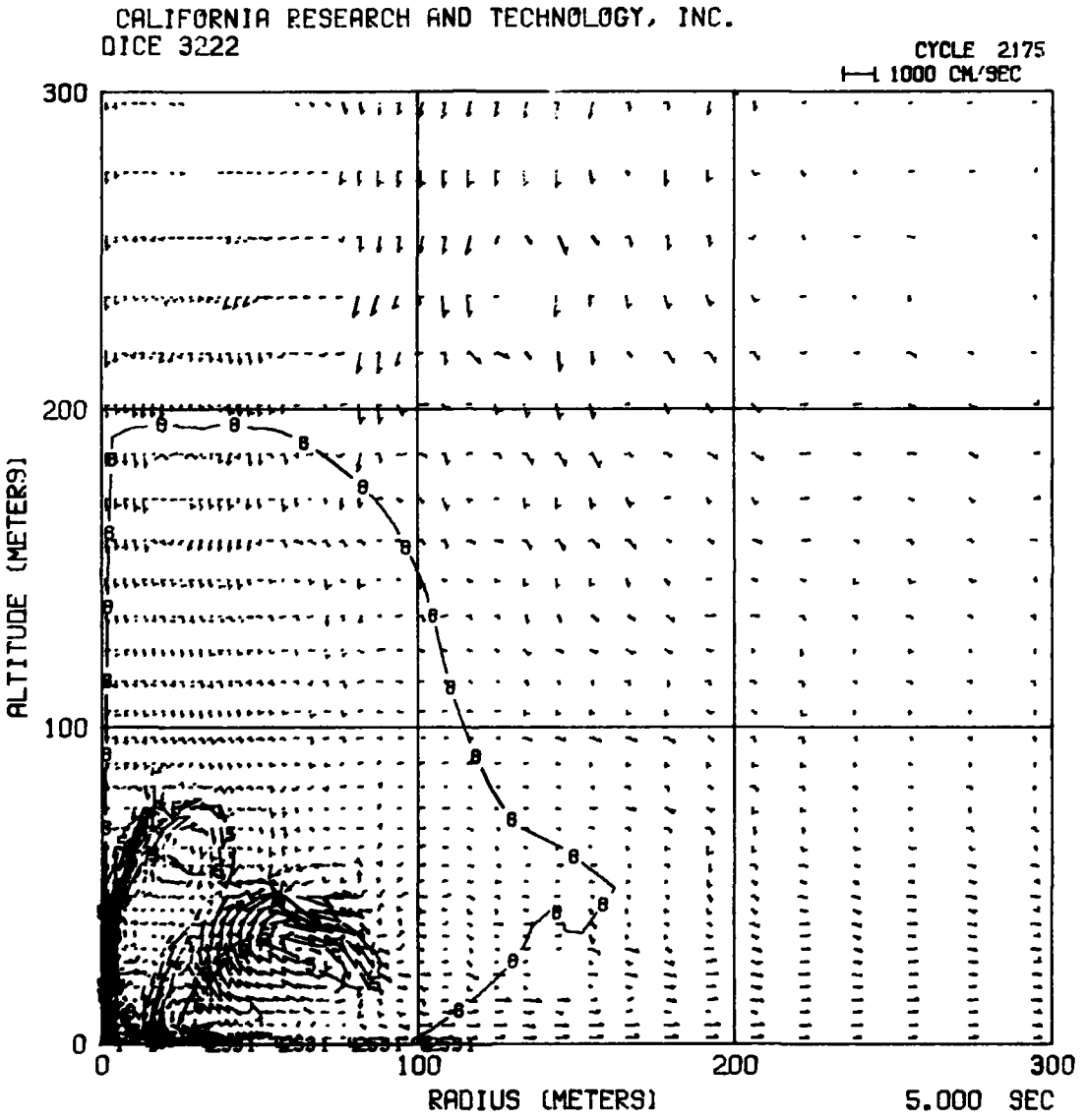

Figure 3.20 Air Velocity Field at 5 seconds for a 10-ton HE Burst Buried 6 Meters in a Dry Soil (Case 3222).

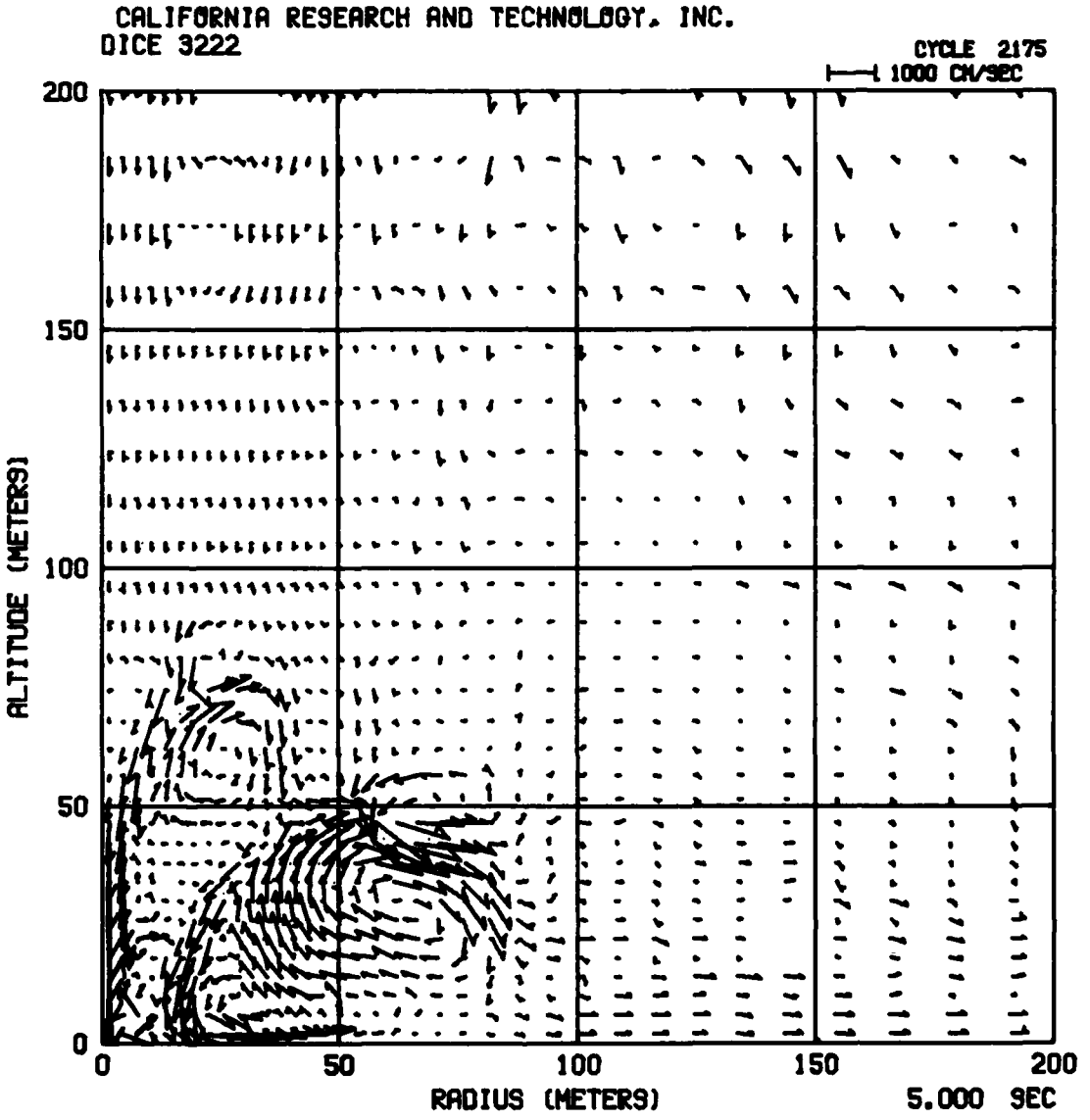

Figure 3.21 Air Velocity Field at 5 Seconds for a 10-Ton HE Burst Buried 6 Meters in a Dry Soil (Case 3222).

Table 3.3

PARTICLE SIZE CHARACTERISTICS
FOR A DRY GEOLOGIC MEDIA[11] (CASE 3223)

Group	Particle Type	Diameter d_p (cm)			Initial Mass Fraction of Solid Incipient Ejecta
		Minimum	Maximum	Representative Diameter	
1	Soil	.0050	.01	.007	.1
2	Soil	.01	.1	.032	.3
3	Soil	.1	1	.32	.3
4	Soil	1	10	3.2	.3
5	Soil Vapor	-	-	-	-

proceed, this soil vapor reaches the original ground surface where its subsequent flow is represented in the DICE code as group 5. The vaporized soil material cools and eventually condenses as it mixes with the colder soil overburden and air; the latent heat of vaporization is released into the atmosphere during this condensation phase. Due to problems with the equation of state in the CRALE calculation of this event (as discussed in Section 2.4) a small latent heat of vaporization (1.5×10^{10} ergs/gm) was included in the internal energy of the vaporized dirt. A value of 1.4×10^{11} ergs/gm (Reference 15) was therefore added to the internal energy of the one metric ton of soil shocked to $P > 1$ Mbar to provide the energy absorbed in vaporizing this mass. This energy was added as the one ton of vapor flowed into the DICE solution at the lower boundary.

Figure 3.22 shows the solid soil and soil vapor ejecta as a function of time. Almost 4 kt of total soil mass crosses the ground surface for times up to 200 msec. This ejecta mass is 1.6 times greater than in the equivalent HE dry media case (3222), but less than 75% of the mass ejected in Case 3221 (HE/Wet). Soil vapor stops flowing into the atmosphere at about 45 msec.

The eventual condensation of this soil vapor and the associated release of the latent heat of vaporization is an important difference between a buried nuclear burst and a buried HE burst. The transfer of this heat into the atmosphere as the soil vapor recondenses results in buoyant lofting of the soil and radioactive materials to altitudes higher than could be achieved by the relatively cold detonation products from a HE source. Pressures from HE detonations do not vaporize any soil. And, for a 6 meter depth of burial, the detonation products have cooled to about $T \sim 300°K$ when they enter the atmosphere.

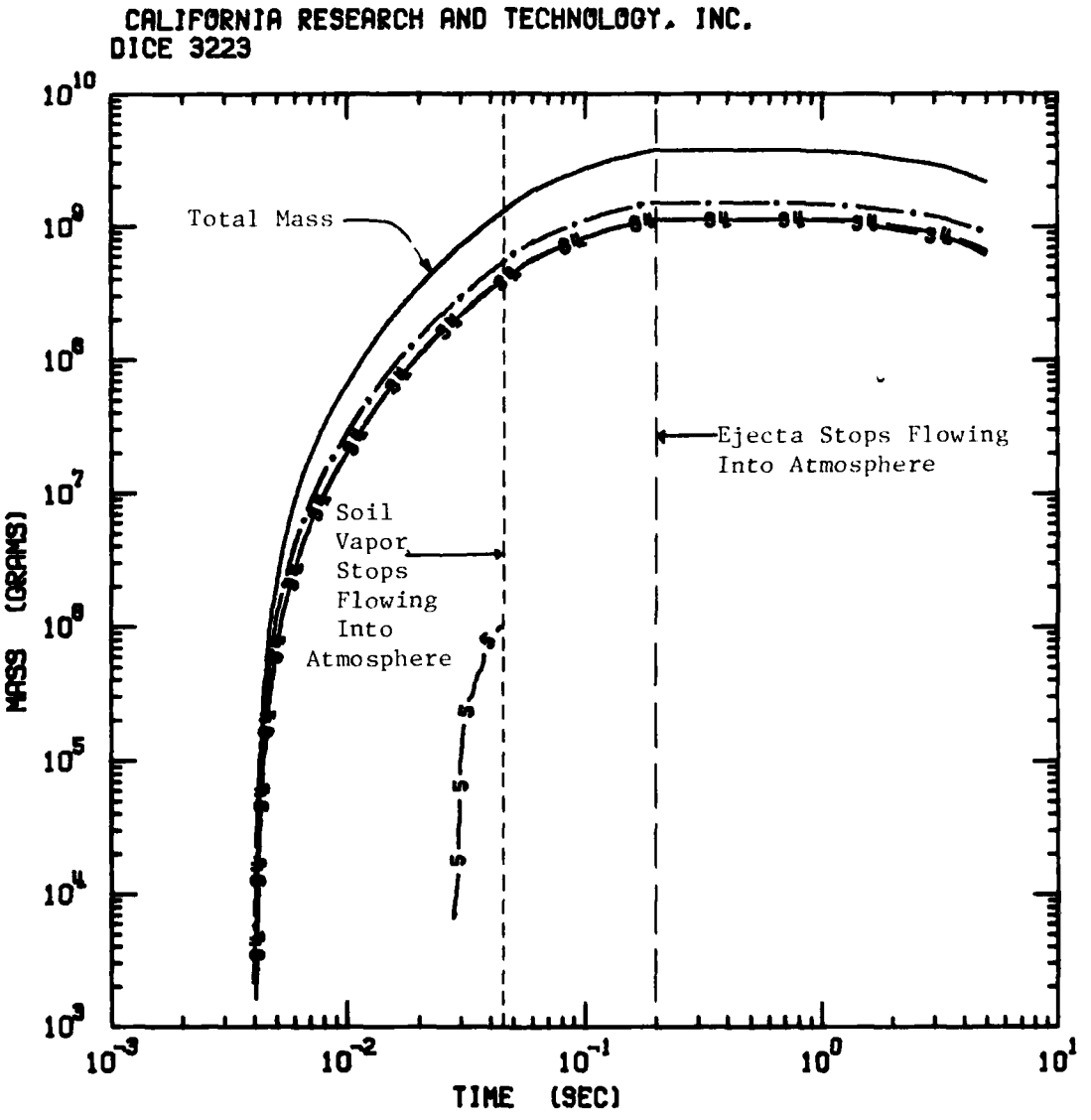

Figure 3.22 Ejecta Mass Flowed Into the Atmosphere as a Function of Time and Particle Size Group for Case 3223 (Nuclear/Dry).

Figure 3.23a shows the maximum increase of air temperature ($\Delta T = T - T_{amb}$) calculated by DICE for the nuclear case as a function of time. The increasing slope of the curve between 30 and 45 msec corresponds to the period when vaporized soil vents into the atmosphere (i.e., enters into the DICE grid). The sharp temperature rise to $\Delta T \sim 2000°K$ is a consequence of rapid condensation of soil vapor and the associated release of latent heat energy into the air near SGZ. By 65 msec, all of the soil vapor has condensed, and maximum temperatures subsequently decay.

Figure 3.23b shows the height and radius of the maximum temperature region at various times. The behavior is as expected, with the hot, low density air rising due to buoyancy. As the hot region of air continues to rise, it entrains cooler air; at 3 seconds, the maximum temperature increase is only several degrees, with its position at an altitude of about 130 m.

Figure 3.24 shows the air flow field at 5 seconds. Strong downflow is seen only near the axis of symmetry below 100 m. The main vortex centered at a height of 140 m dominates the remainder of the air flow field with relatively high maximum upward velocities of about 20 m/sec. In Section 4, the nuclear source case is compared with the HE source cases.

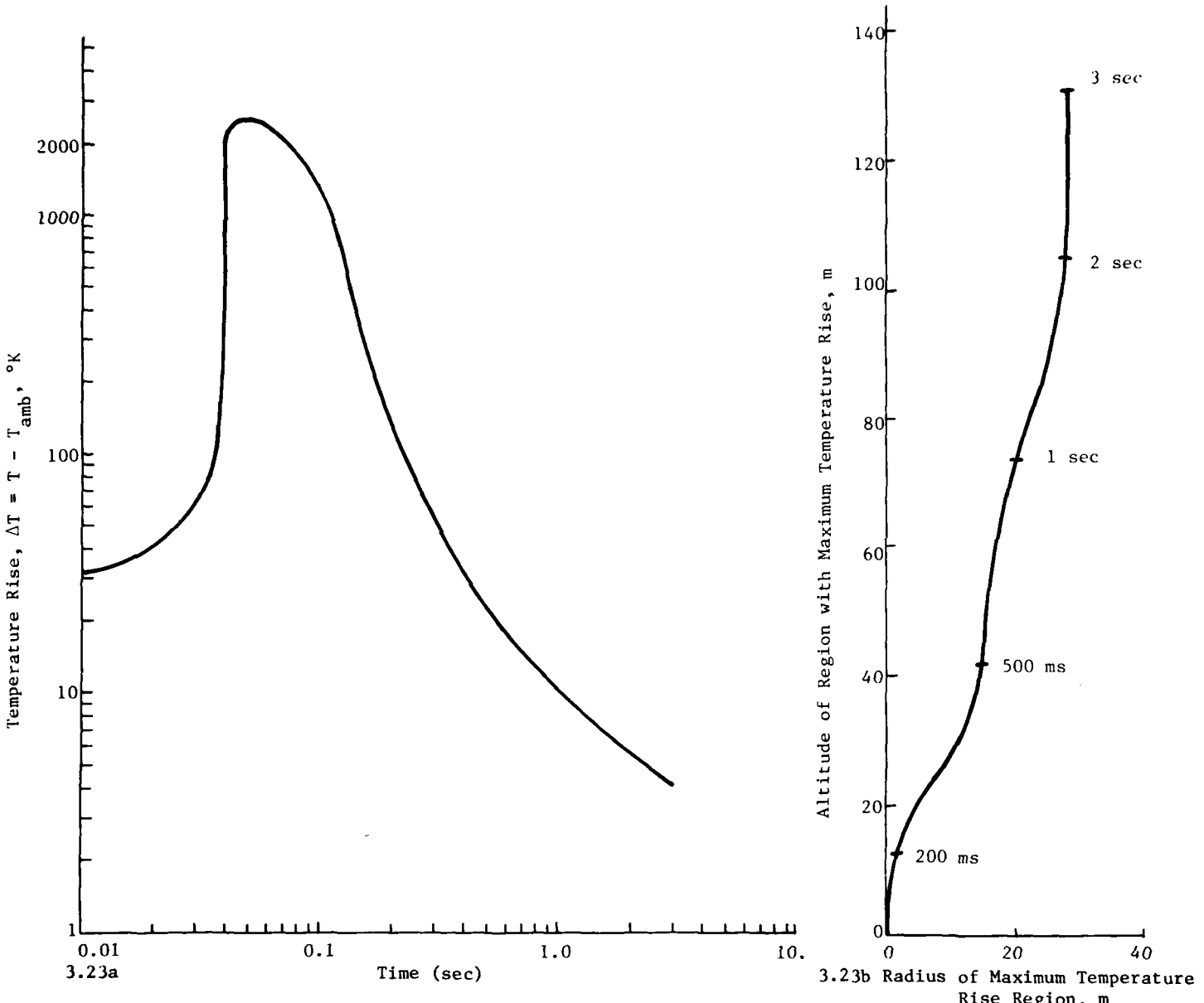

Figure 3.23 Maximum Temperature Rise in the Air for a 20-Ton Nuclear Device Detonated 6 Meters in the Ground (Case 3223 - Nuclear/Dry).

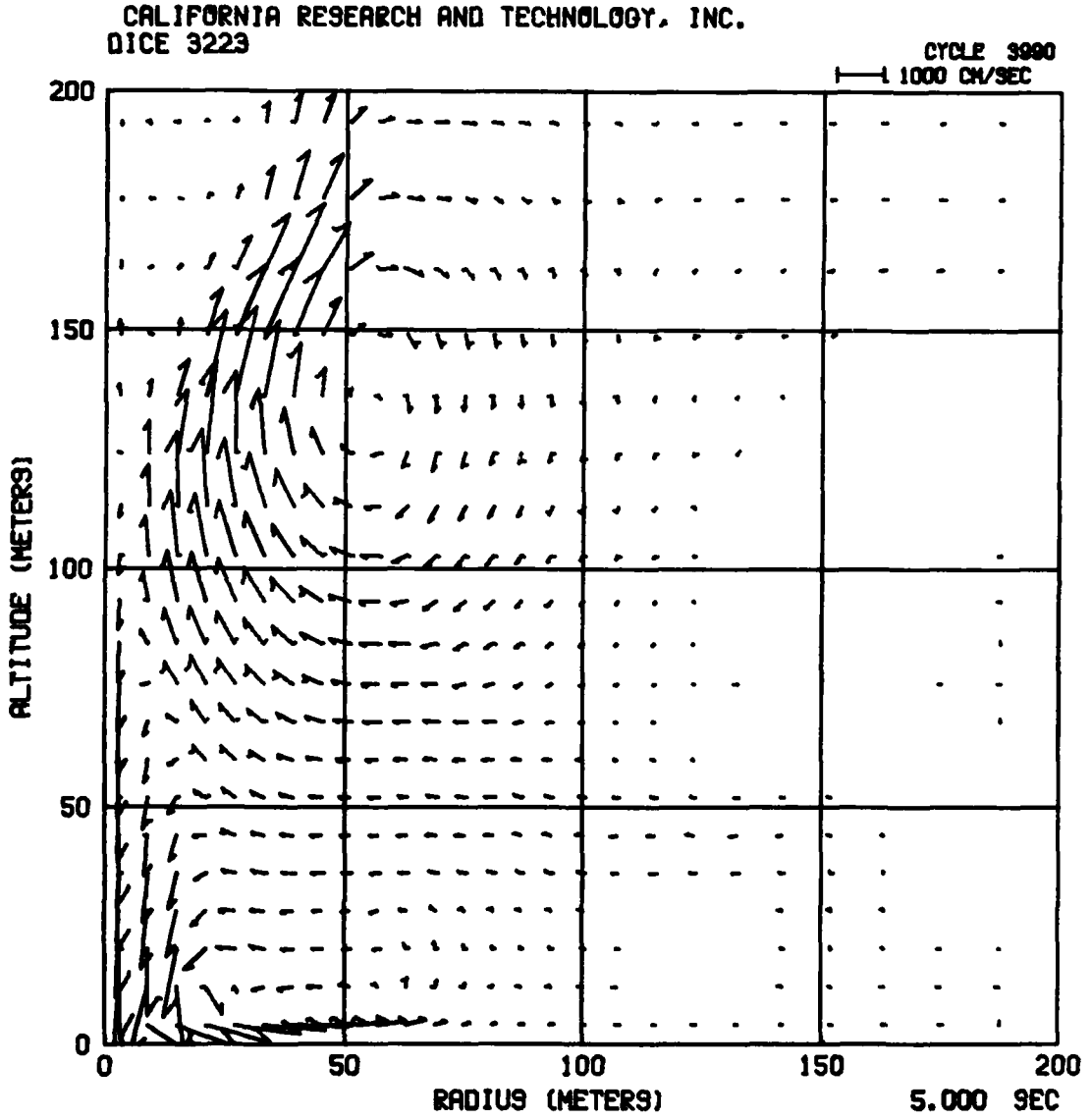

Figure 3.24 Air Velocity Field at 5 Seconds for a 20-Ton Nuclear Device Buried 6 Meters in Dry Soil (Case 3223).

SECTION 4

COMPARISONS OF LOFTED TRACER PARTICLES

In the three numerical calculations, tracer particles are included to follow the movement of iridium-coated sand (Case 3221 and 3222) or radioactive material (Case 3223). The subsequent flow and disposition of these tracers in the lofted cloud is then calculated. Figure 4.1a shows the indexing and initial locations of the 45 iridium tracers for both the wet and dry media HE cases. Those tracers denoted by dots did not cross the original ground surface in the CRALE cratering solution. Figure 4.1b is an analogous plot of the 25 tracers placed in the region of the nuclear source. The iridium tracers initially extend out to just over 1 m radii, whereas the radioactive tracers only extend to 0.1 m.

Figures 4.2 through 4.7 show the positions of the tracer particles at times of .05, .1, .5, 1.0, 2.0, and 5.0 seconds. Each figure compares the tracer particle positions for the three numerical solutions at a specific time.

Figures 4.8 and 4.9 show the maximum tracer altitude and radius as functions of time for the three cases.

4.1 "WET" VERSUS "DRY" SOILS (HE SOURCES)

The iridium tracer motions vary substantially when the HE source is detonated in wet soil versus dry soil. Figures 4.2 through 4.7 show that the iridium is consistently higher in the wet soil case. For example, at 2 seconds (Figures 4.6 and 4.8), the iridium tracers have reached an altitude of about 60 meters in the wet soil case as compared to 30 meters in the dry soil case. With respect to radius, however, note that the tracers reach only 10 m radius in the wet case versus 18 m in the dry case. Thus, an HE burst in a wet soil media leads to iridium tracers, for times up to 5 seconds, which are located higher in altitude and narrower in radial extent than the iridium tracer locations for the HE burst in a dry soil.

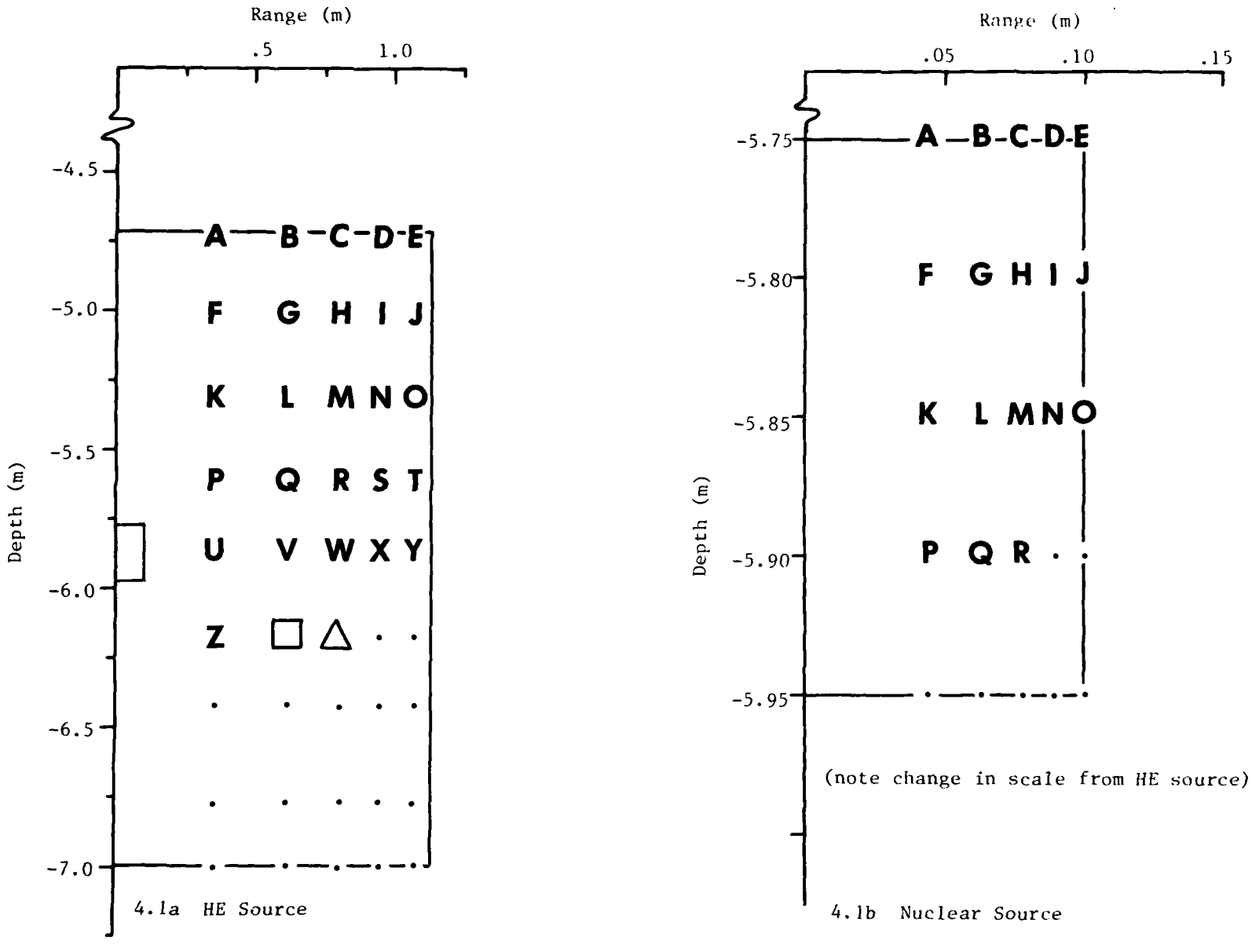

Figure 4.1 Initial Tracer Locations for HE and Nuclear Sources in the Numerical Calculations.

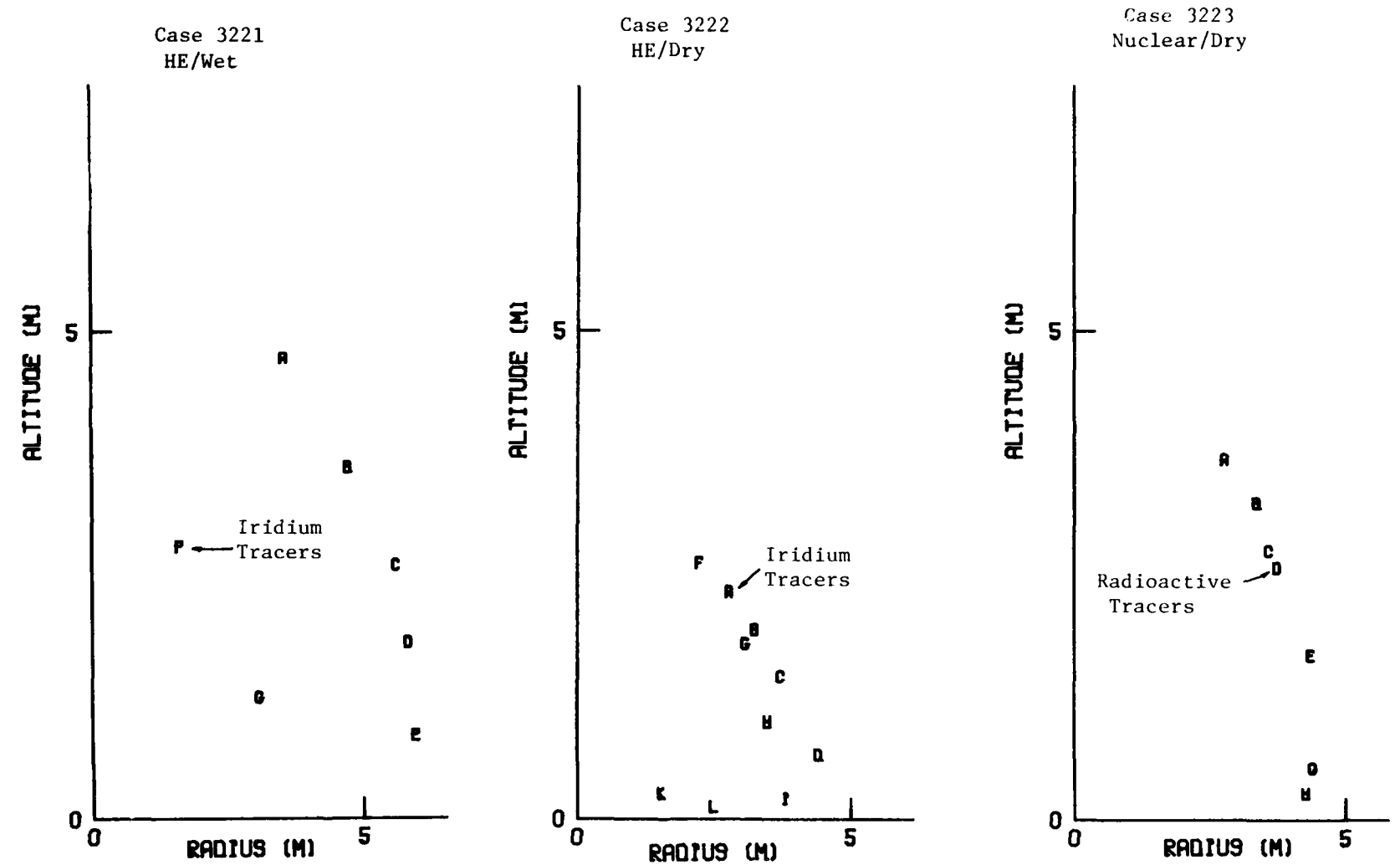

Figure 4.2 Comparison of Iridium and Radioactive Tracer Points at 50 Milliseconds.

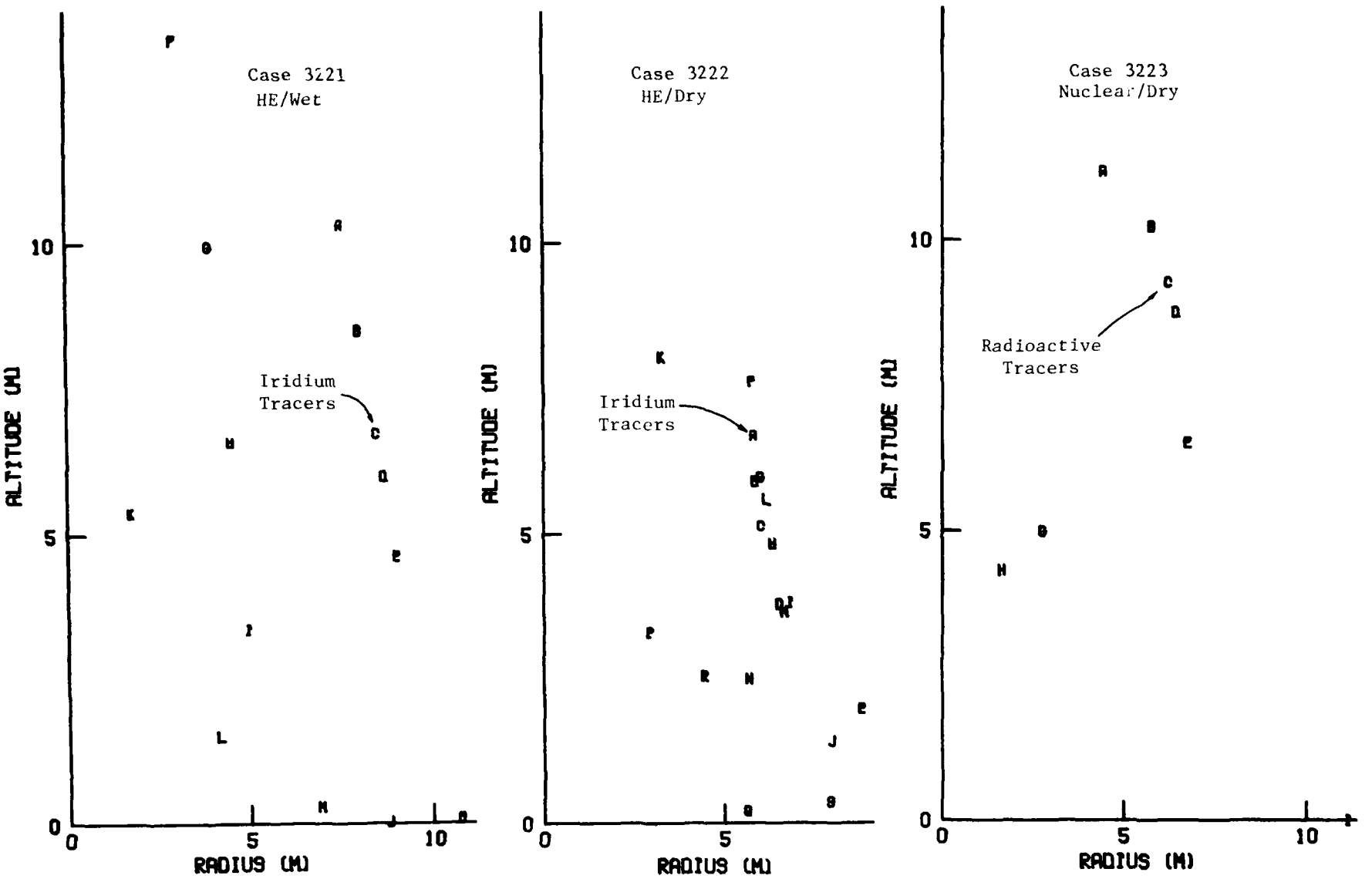

Figure 4.3 Comparison of Iridium and Radioactive Tracer Positions at 100 Milliseconds.

AD-A091 371 CALIFORNIA RESEARCH AND TECHNOLOGY INC WOODLAND HILLS F/G 18/3
INVESTIGATION OF A HIGH EXPLOSIVE TECHNIQUE FOR SIMULATION OF L--ETC(U)
NOV 79 M ROSENBLATT, K N KREYENHAGEN DNA001-78-C-0169
UNCLASSIFIED CRT-322UF DNA-5149F NL

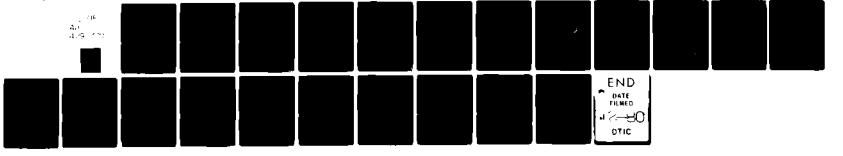

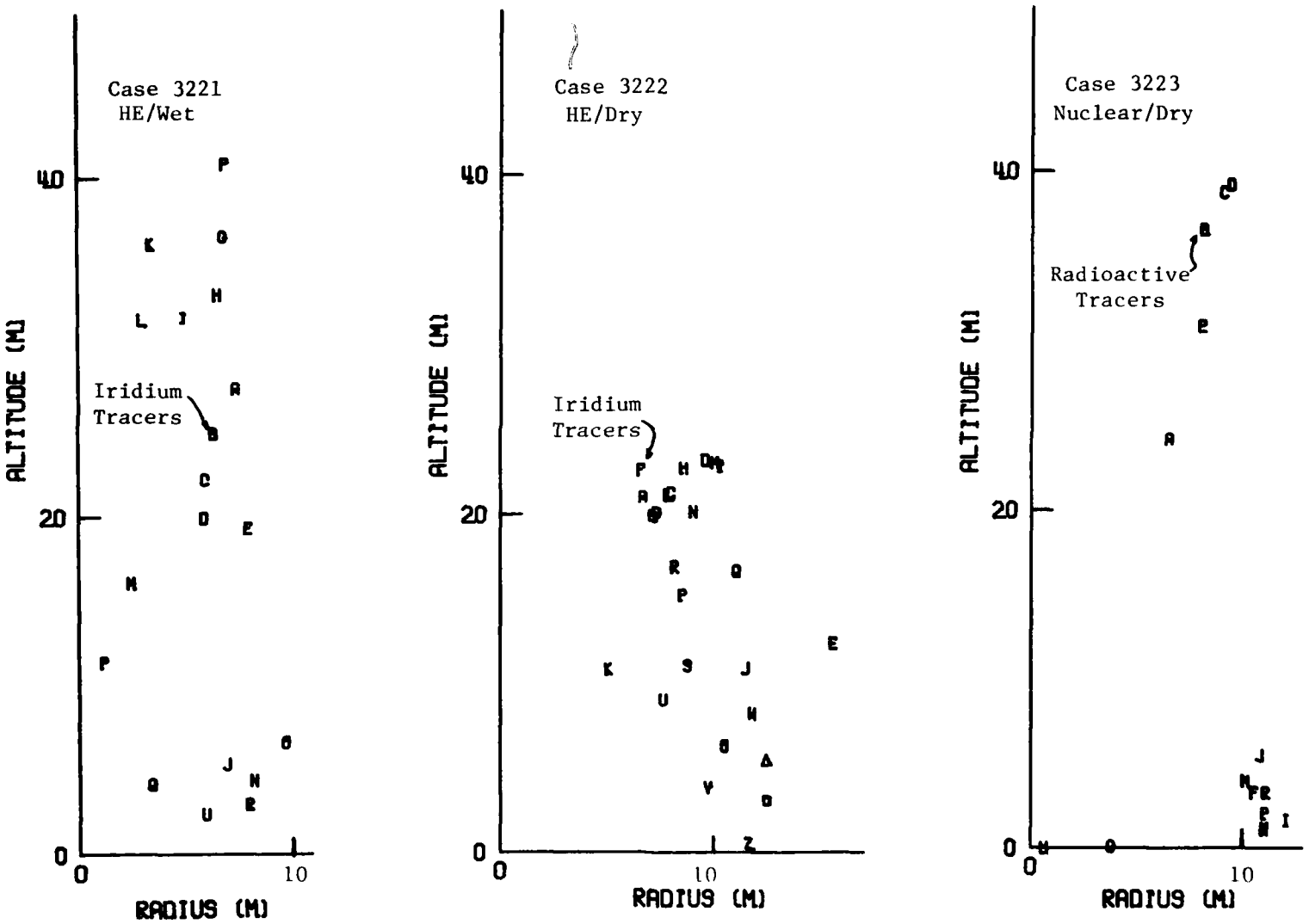

Figure 4.4 Comparison of Iridium and Radioactive Tracer Positions at 500 Milliseconds.

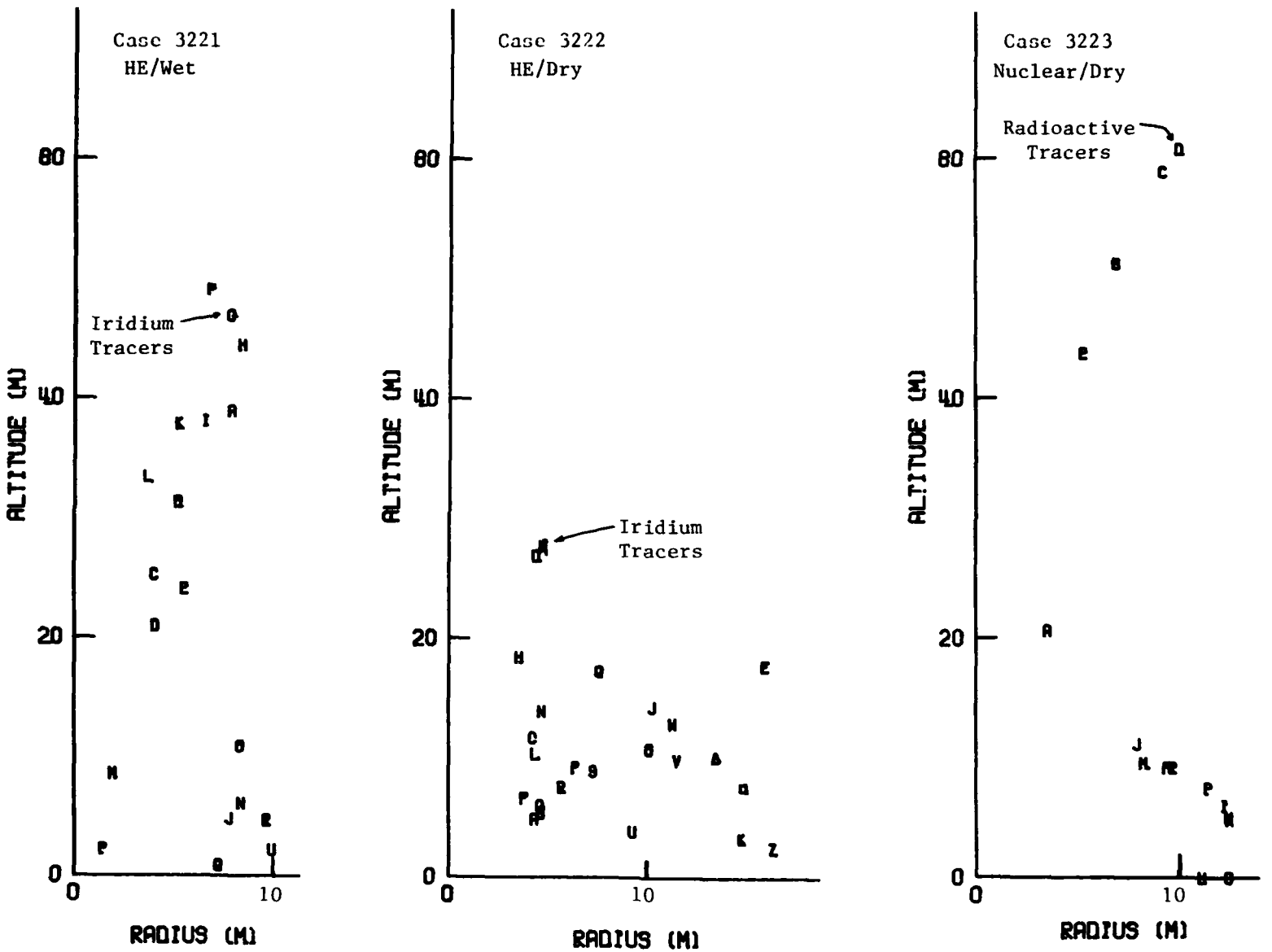

Figure 4.5 Comparison of Iridium and Radioactive Tracer Positions at 1 Second.

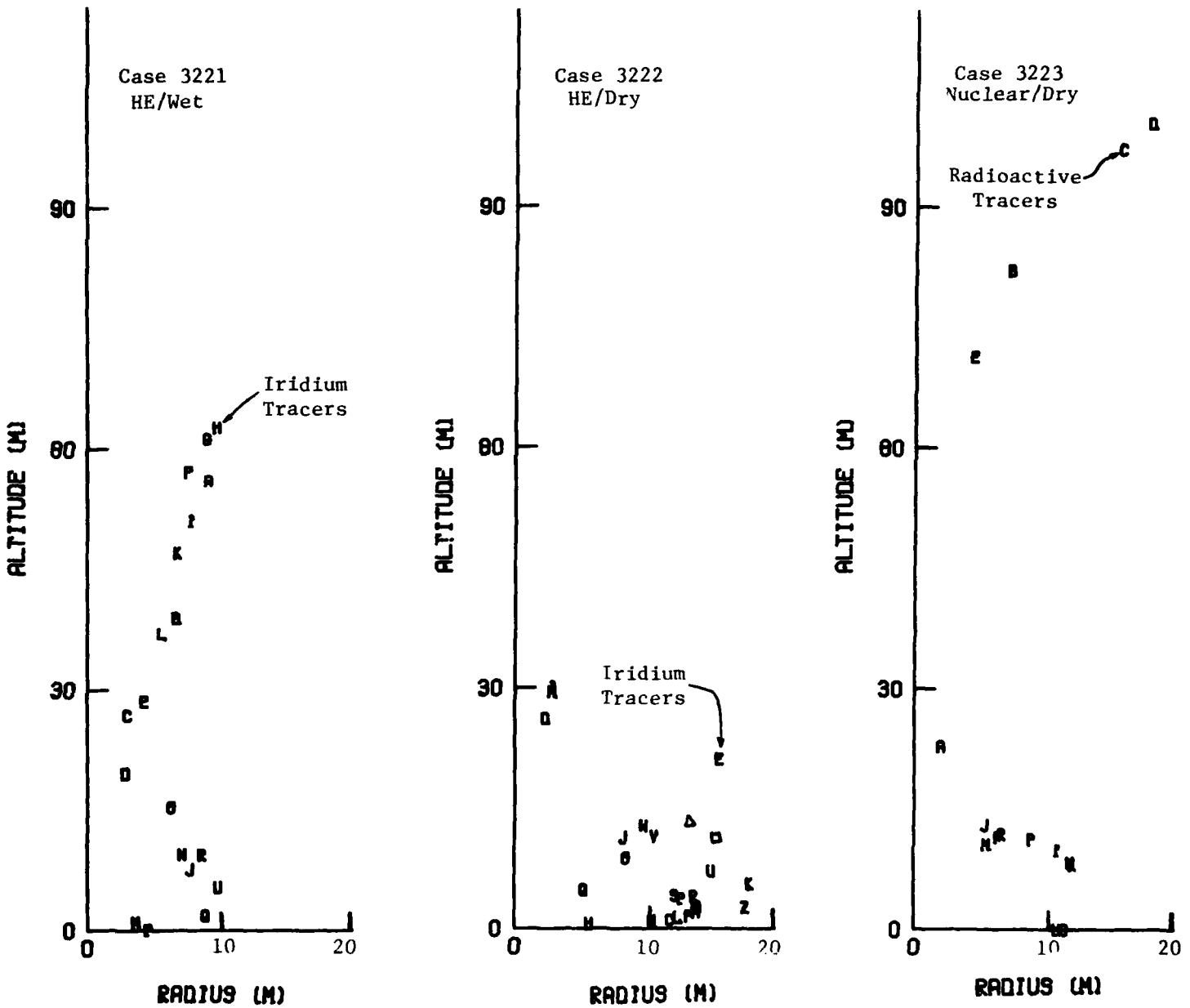

Figure 4.6 Comparison of Iridium and Radioactive Tracer Positions at 2 Seconds.

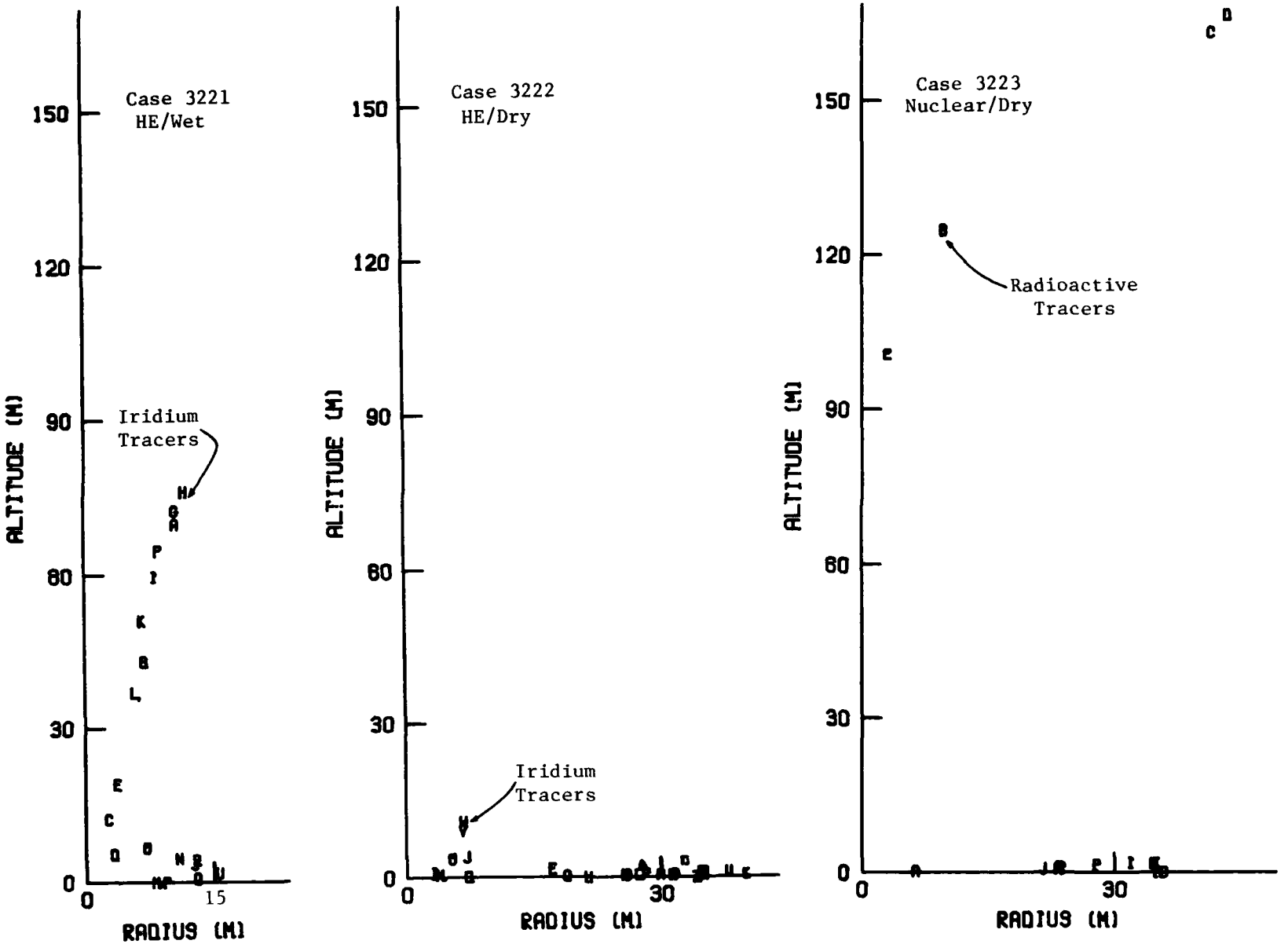

Figure 4.7 Comparison of Iridium and Radioactive Tracer Positions at 5 Seconds.

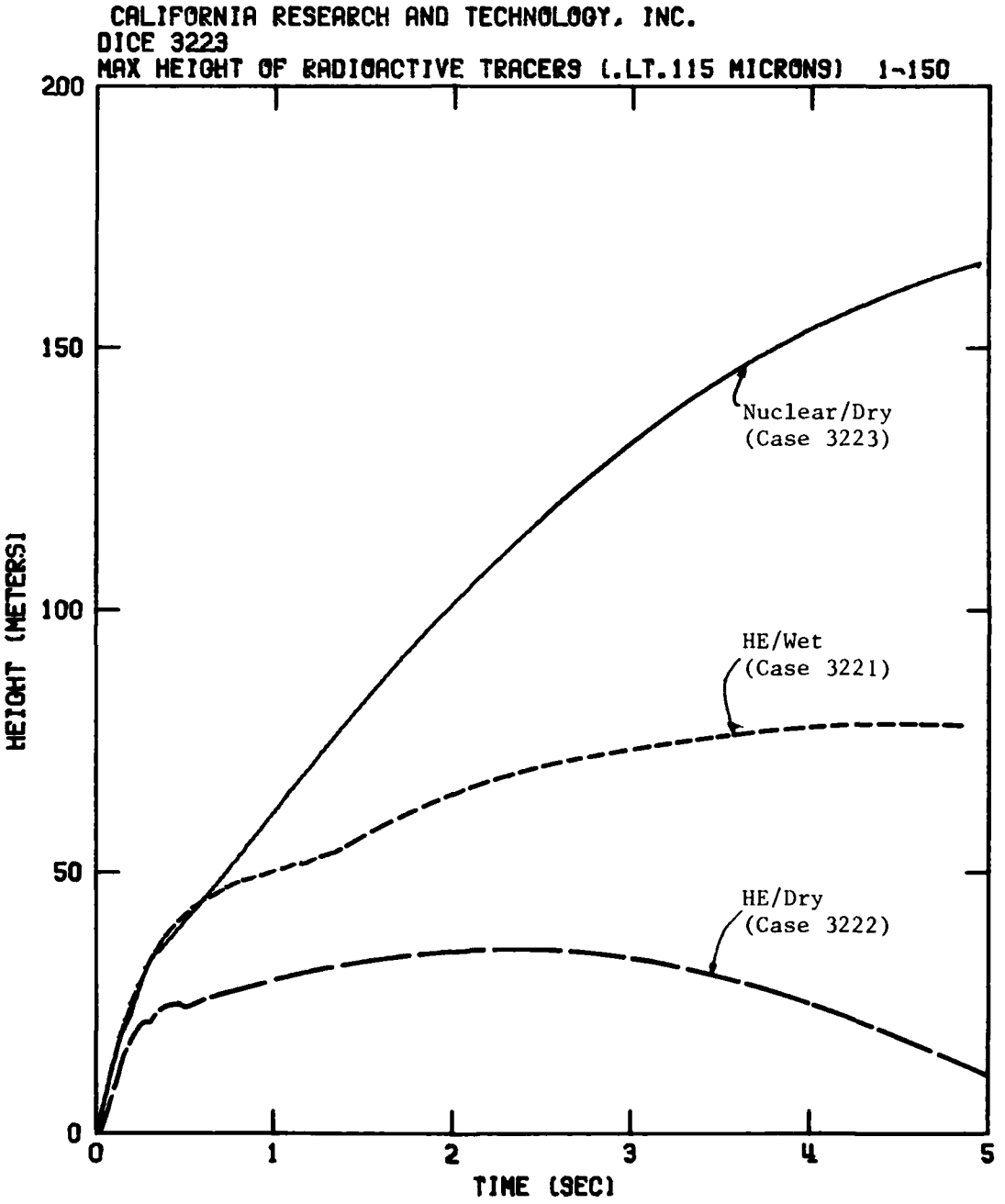

Figure 4.8 Maximum Tracer Altitudes versus Time.

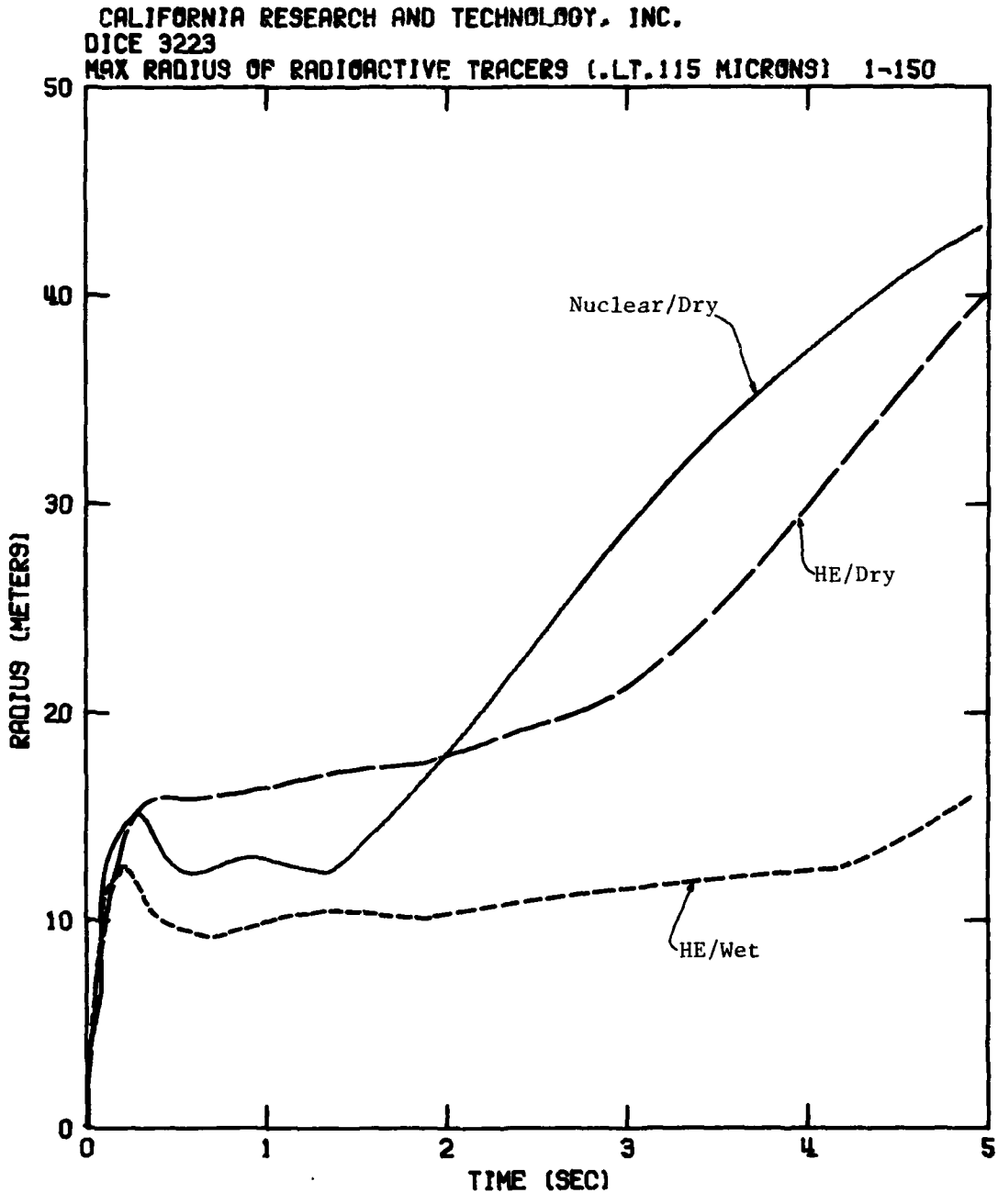

Figure 4.9 Maximum Tracer Radii versus Time.

Possibly the most sensitive soil property affecting the iridium lofting and disposition in the cloud is the particle size distribution of the ejecta. Note that *particles* include cohesive "clumps" of fundamental soil grains. The experimental evidence (Reference 12) indicates that wet soils have a higher percentage of their mass in the larger clumps of particles than do dry soils. For example, Figure 1.5 shows the particle size distributions used for ejecta from the wet and dry soils. In the wet soil, 50% of the mass is in particles greater than 18 cm as compared to a much smaller mass median diameter of .16 cm for the dry soil. This difference in particle size distribution is critical to the aerodynamic drag interactions which determine the rate at which momenta and energy are transferred from the ejecta particles to the atmosphere. (Appendix B summarizes the mutual drag interaction formulation used in mixed phase DICE calculations.) The larger (wet soil) particles transfer momentum to the air much more slowly than the smaller (dry soil) particles. This difference in drag interaction forces leads to the fundamental difference in the air flow fields for the HE/Wet versus HE/Dry cases (compare velocity field Figures 3.16 to 3.21 with Figures 3.5 to 3.12).

Figure 4.10 compares the air velocity fields and particle size positions at 5 seconds for the HE/Wet and HE/Dry cases. This figure shows the intense, localized flow field associated with the dry soil. This flow field, with relatively large radial velocities at earlier times, causes the lofted soil cloud to be larger in radius than the HE/Wet cloud.

4.2 HE VERSUS NUCLEAR BURSTS (DRY MEDIA)

Figures 4.2 through 4.8 show that the radioactive tracers in the Nuclear/Dry case (3223) are always higher than the iridium tracers in the HE/Dry case (3222). At early times, say

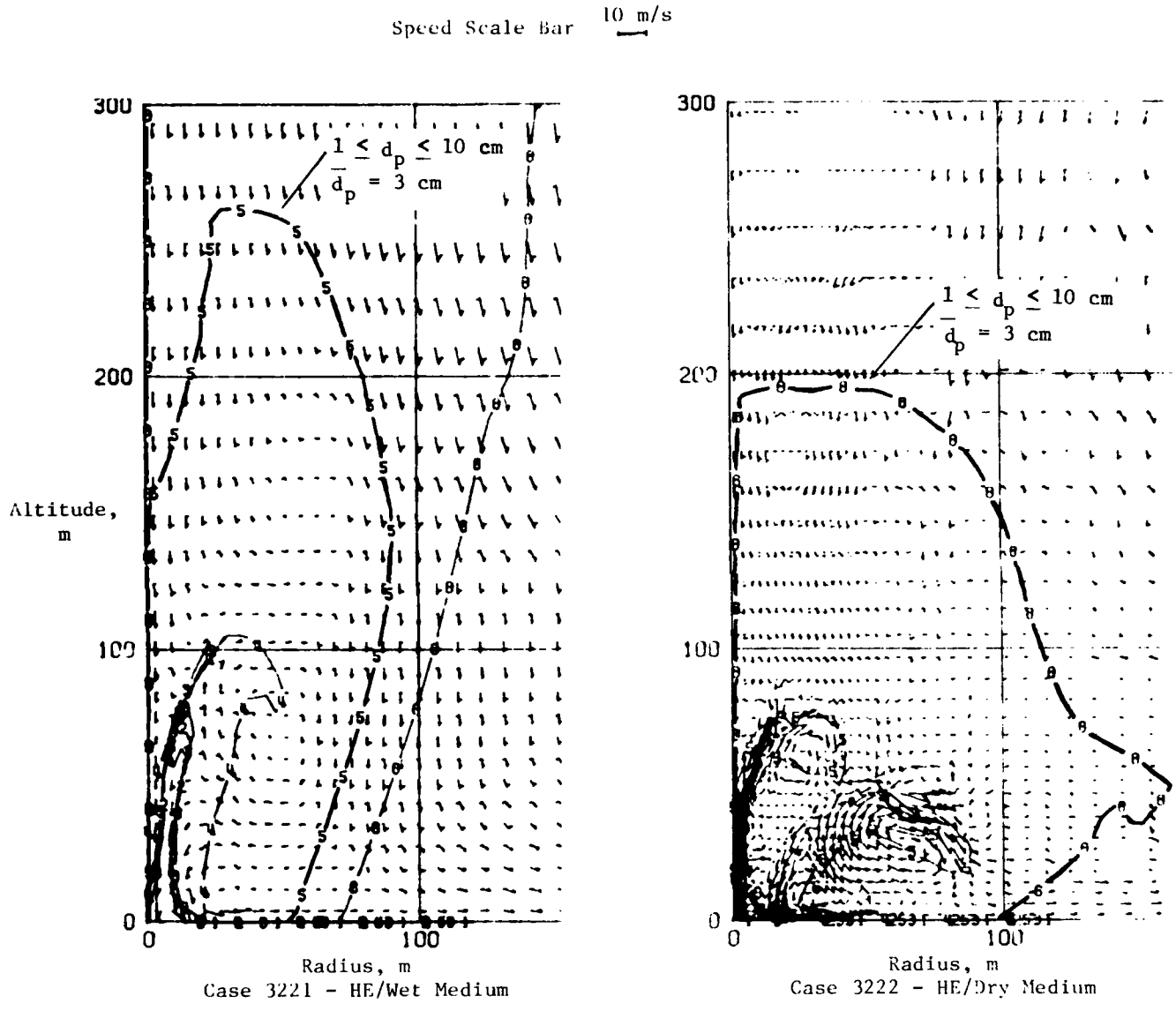

Figure 4.10 Velocity Field and Boundary Positions for Particle Size Groups at t = 5 Seconds.

t < .3 seconds, this difference is primarily due to the higher incipient ejecta velocities from the nuclear burst. At later times in the nuclear case, however, buoyancy dominates the air flow field and the motion of some radioactive tracers.

Figure 4.8 shows that the HE/Dry iridium tracers reach a maximum altitude of about 25 meters in about .3 seconds; after this time the iridium tracers' altitude increases very slowly to a maximum of about 30 meters at t ~2.5 seconds. The "knee" (at t ~.3 seconds) in the tracer altitude curve for the HE cases does not occur in the nuclear case. The maximum altitude of the *radioactive* tracers continues to increase during the 5 second numerical solution, with a gradual decrease in upward velocity.

The release of concentrated latent energy from the condensation of vaporized soil occurs within the developing ejecta-air cloud. The location of this energy transfer to the air enhances cloud lofting through buoyancy.

Figure 4.11 compares the velocity vector fields at t = 5 sec for the HE/Dry versus Nuclear/Dry numerical solution (Case 3222 versus Case 3223). A scale bar representing speeds of 10 m/sec is shown on the figure. The tracer particle positions at 5 seconds are also shown on Figure 4.11.

The 5 second velocity field in the nuclear case shows a toroidal vortex pattern centered at an altitude of ~140 meters and a radius of ~50 meters. The peak speeds are ~20 m/sec. Some of the radioactive tracer particles are entrained in this flow region. In the HE case, at least two vortices are apparent. The altitude of these vortices are a factor of two lower than the main vortex in the nuclear case. The maximum iridium tracer altitude is only ~10 meters, compared to the maximum radioactive tracer altitude of ~160 meters.

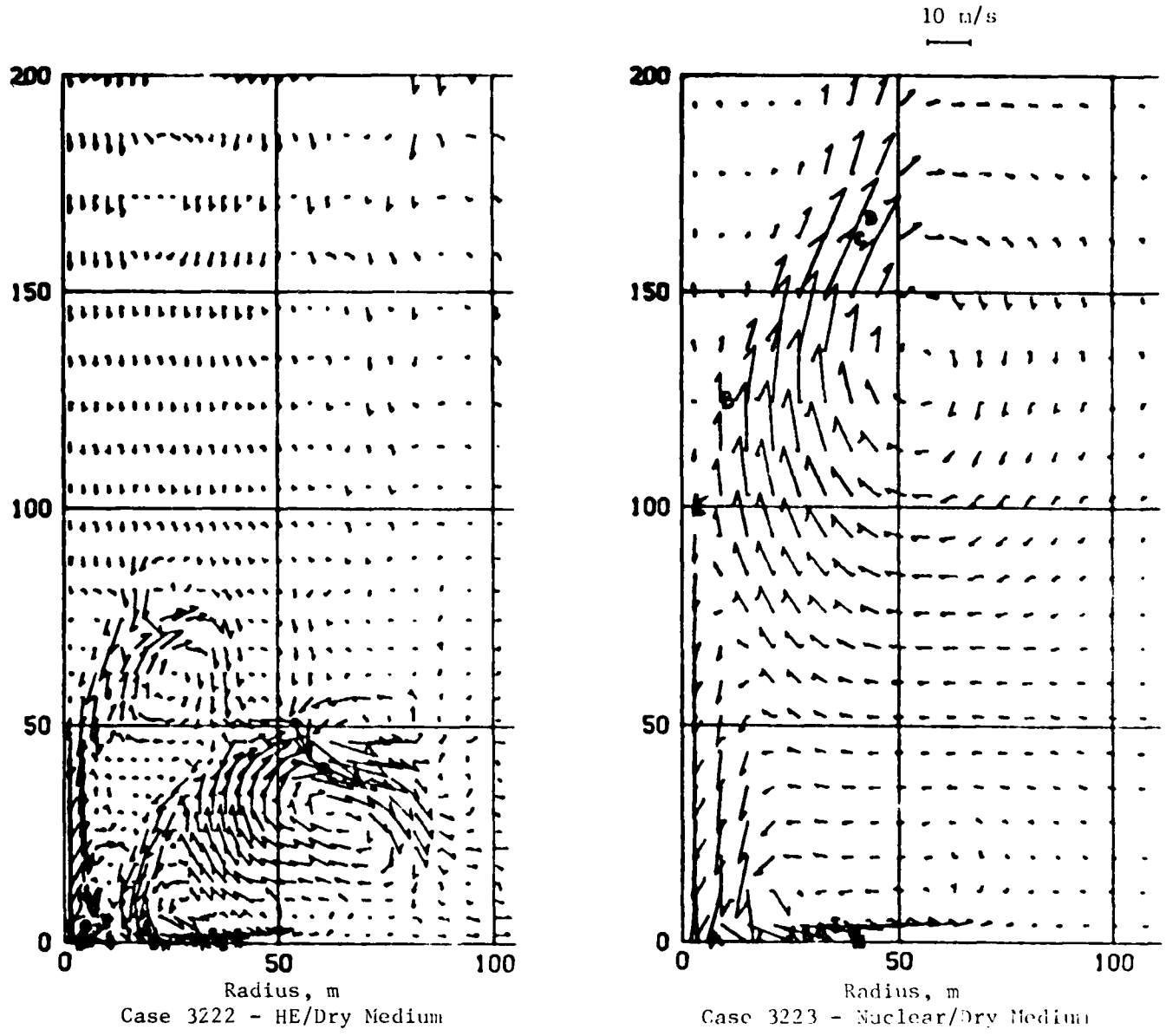

Figure 4.11 Air Velocity and Iridium/Radioactive Tracers at 5 Seconds.

The significant differences in the air flow fields and in the maximum altitude of the iridium versus radioactive tracer particles will lead to different tracer fallout patterns for an HE shallow-buried burst compared to a nuclear shallow-buried burst. The primary cause of these physical differences is the buoyant cloud rise which occurs in the nuclear case when vaporized soil condenses at a temperature of about 2500°K and the latent heat of vaporization is released to the atmosphere. This fundamental difference in phenomenology is expected to persist for all shallow-buried bursts which vent vaporized soil to the atmosphere.

APPENDIX A

ZONING

A-1 CRALE

Initial Zoning

Reference should be made to Figure 1.4 during this discussion.

The high explosive sources (problems 3221 and 3222) were represented by six 19-cm radial zones and twelve 19-cm vertical zones.

The small initial nuclear source (problem 3223) was modeled by two 5-cm radial zones and four 5-cm vertical zones.

Initially, the computational zones outside the explosive sources were rectangular. Zone heights and widths generally increased slightly with distance from the source. Such expansion of the dimensions of the initial grid allows maximum resolution nearest the source.

The boundaries indicated in Figure 1.4 for problem 3221 are material interfaces. The computational grid was designed so that these interfaces coincided with horizontal or vertical zone boundaries.

Motion of the Computational Grid

Motion of the computational grid falls in two broad categories. During the first few milliseconds after source detonation the grid motion was Lagrangian. That is, the grid velocity field is identical to the field of material velocity.

Large material distortions in these problems soon make Lagrangian zoning impractical. Thus, after the first few milliseconds we specify a field of grid velocity independent of the material velocity field. This ability to impose a generalized (neither Lagrangian nor Eulerian) scheme of grid motion is a characteristic of CRALE.

Restrictions must be applied to the generalized grid motion if the simulation is to remain valid. In particular, material boundaries must be respected.

The generalized grid contains a scheme that closely approximates Lagrangian boundaries between materials. Problem 3221 has such "pseudo-Lagrangian" boundaries between the five soil types, the grout, and the expanding cavity filled with the gaseous products of detonation. Problem 3222 has a pseudo-Lagrangian boundary between the HE products and the surrounding alluvium. All three problems have such a boundary at the ground surface, thereby holding all material within the problem domain.

Note that problem 3223 has no internal material boundaries. We simulate the nuclear device by giving high energies to a small amount of alluvium. Thus, the gases at the beginning of the problem as well as those produced by shock vaporization are all soil vapor.

The Dezone Procedure

Maintenance of material boundaries, though necessary, causes problems in the zoning scheme. As the cavity of gas grows in calculations 3221 and 3222 and distorts the surrounding material, serious numerical problems develop. Specifically, sliver-shaped zones hold down the time step and present the danger of doubly-degenerate cells.

The dezone procedure was developed to ease distortion problems. This procedure involves the removal of a few rows of grid points and the redistribution of properties associated with those rows. Grid congestion can thus be relieved and the problem run to completion.

Dezoning was invoked in Cases 3221 at 10.8 msec and in 3222 at 24.7 msec. Due to its lack of internal material boundaries, Case 3223 required no rezoning.

A-2 DICE

A computational grid which expands in both axial and radial directions as a prescribed function of time (Reference 8) was employed in the DICE solutions. Figure A-2.1 shows the height and width of a cell in the uniform region near SGZ of the DICE grid. An approximate 10% grid expansion is used outside the uniform region. Minimum cell heights and widths for all cases were 1.0 and 0.5 m, respectively. Final cell heights for Cases 3221 and 3223 were 8.0 m. For Case 3222, the final height was 6.0 m.

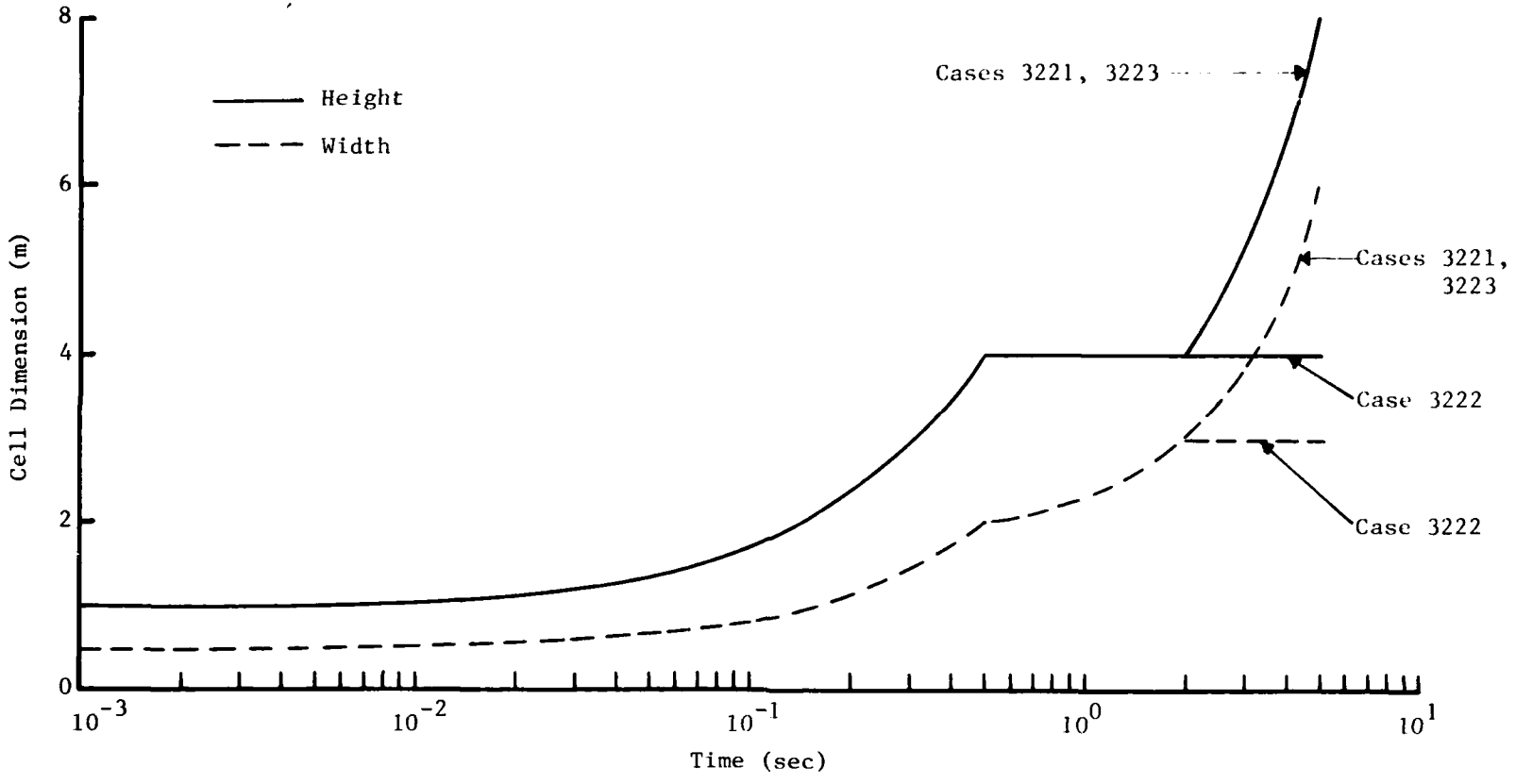

Figure A.2.1 Height and Width of DICE Computational Cell for Cases 3221, 3222, and 3223.

APPENDIX B

AERODYNAMIC DRAG

In DICE mixed phase flow calculations, the soil particles and air experience mutual drag interactions. The equation used in this study for the drag interaction force (F_D) on a particle of diameter (D_p) moving with velocity ($\vec{V}_p$) in a gas stream of density (ρ_g) and velocity ($\vec{V}_g$) is:

$$F_D = \tfrac{1}{2}\rho_g \, (\vec{V}_p - \vec{V}_g) \; | \; \vec{V}_p - \vec{V}_g \; | \; C_D \left(\frac{\pi D_p^2}{4}\right) \tag{B.1}$$

where the drag coefficient (C_D) is defined by:

$$C_D = 0.6 + \frac{36}{Re} \tag{B.2}$$

and Re is the particle Reynold's number

$$Re = \frac{D_p \; | \; \vec{V}_p - \vec{V}_g \; | \rho_g}{\mu} \tag{B.3}$$

where

$$\mu = (2.42T)^{0.78} \times 10^{-6} \text{ poise} \quad (T \text{ in } °K)$$

The relative masses of particles and gas in a computational cell are used to guarantee that changes in the soil particle momentum are compensated by oppositely-directed changes in the air momentum. (See Reference 9 for additional details for this model.)

REFERENCES

1. K. E. Sprague and others, "Middle Course II Cratering Series", Technical Report E-73-3, Explosive Excavation Laboratory, U.S. Army Engineer Waterways Experiment Station, July 1973.

2. J. M. O'Connor, T. J. Dolan and D. E. Burton, "Explosive Selection and Fallout Simulation Experiments, Nuclear Cratering Device Simulation (Project Diamond Ore)", Technical Report E-73-6, Explosive Excavation Laboratory, U.S. Army Engineer Waterways Experiment Station, October 1973.

3. N. J. Adams, W. B. Lane and L. C. Webster, "A Preliminary Assessment of the Radiation Simulation Experiments of Project ESSEX I", Technical Report N-77-4 (DNA PR 0029), U.S. Army Engineer Waterways Experiment Station, August 1977.

4. J. M. Thomsen, "Numerical Cratering Studies for Project ESSEX I: Phase 2, The 3MS and 3MU Experiments", UCRL 51903 (DNA PR 0024), Lawrence Livermore Laboratory, August 1975.

5. T. R. Blake and D. E. Wilkins, "Simulation of Low Yield, Buried Nuclear Explosions by High Explosive Detonations: ESSEX I, Phase I Calculations", Defense Nuclear Agency, April 1975, Unpublished.

6. S. H. Schuster, "Results of Pre-Test Prediction Calculations of Middle Gust I, II, and III", AFWL-TR-76-284, Air Force Weapons Laboratory, April 1977.

7. J. G. Trulio, "Ejecta Formation Calculated Motion from a Shallow-Buried Nuclear Burst and Its Significance for High Velocity Impact Cratering," in Impact and Explosion Cratering, edited by D. J. Roddy, et. al., Pergamon Press, 1977.

8. M. Rosenblatt and G. E. Eggum, "DICE - A Two-Dimensional Implicit Code for Treating Compressible Flow in a Fluid-Particle Mixture", Defense Nuclear Agency, March 1973, Unpublished.

9. M. Rosenblatt and G. E. Eggum, "Analyses of Nuclear Dust and Condensed Water Clouds Including Effects of Drag and Thermal Interactions", Defense Nuclear Agency, May 1975, Unpublished.

10. M. Rosenblatt, G. E. Carpenter and G. E. Eggum, "Lofted Mass Characteristics and Uncertainties for Nuclear Surface Bursts", Defense Nuclear Agency, November 1978, Unpublished.

11. A. D. Rooke, G. B. Clark and J. N. Strange, "Operation Sun Beam Shot Johnie Boy, Mass Distribution Measurement", Defense Nuclear Agency, February 1965, Unpublished.

12. A. J. Piekutowski, "Cratering Mechanisms Observed in Laboratory-Scale High-Explosive Experiments", in Impact and Explosion Cratering, edited by D. J. Roddy, et. al., Pergamon Press, 1977.

13. J. G. Jackson, Letter to Major R. Gates, "Transmittal of Recommended Profiles Representative Constitutive Properties for ESSEX I", December 21, 1972.

14. W. T. Harvey, "Summary Report, ESSEX I, Phase I: Nuclear Crater Simulation", U.S. Army Engineer Waterways Experiment Station, June 1975, Unpublished.

15. R. T. Allen, "Equation of State of Rocks and Minerals", GAMD-7834, General Dynamics, Special Nuclear Effects Laboratory, March 1967.

DISTRIBUTION LIST

DEPARTMENT OF DEFENSE

Assistant to the Secretary of Defense
Atomic Energy
ATTN: Executive Assistant

Defense Advanced Rsch Proj Agency
ATTN: TIO

Defense Intelligence Agency
ATTN: DB-4C, E. O'Farrell
ATTN: DT-1C
ATTN: DB-4N

Defense Nuclear Agency
2 cy ATTN: SPSS
4 cy ATTN: TITL

Defense Technical Information Center
12 cy ATTN: DD

Field Command
Defense Nuclear Agency
ATTN: FCPR
ATTN: FCTK

Field Command
Defense Nuclear Agency
Livermore Division
ATTN: FCPRL

Interservice Nuclear Weapons School
ATTN: TTV

Joint Strat Tgt Planning Staff
ATTN: NRI-STINFO Library
ATTN: JLA

NATO School (SHAPE)
ATTN: U.S. Documents Officer

Under Secy of Def for Rsch & Engrg
Department of Defense
ATTN: Strategic & Space Systems (OS)

DEPARTMENT OF THE ARMY

BMD Advanced Technology Center
Department of the Army
ATTN: ATC-T
ATTN: 1CRDABH-X

Chief of Engineers
Department of the Army
ATTN: DAEN-RDM
ATTN: DAEN-MCE-D

Harry Diamond Laboratories
Department of the Army
ATTN: DELHD-N-P
ATTN: DELHD-I-TL

U.S. Army Ballistic Research Labs
ATTN: DRDAR-BLV
ATTN: DRDAR-BLT, W. Taylor
ATTN: DRDAR-TSB-S
ATTN: DRDAR-BLE, J. Keefer

DEPARTMENT OF THE ARMY (Continued)

U.S. Army Concepts Analysis Agency
ATTN: CSSA/ADL

U.S. Army Engineer Center
ATTN: DT-LRC

U.S. Army Engineer Div Huntsville
ATTN: HNDED-SR

U.S. Army Engineer Div Ohio River
ATTN: ORDAS-L

U.S. Army Engr Waterways Exper Station
ATTN: WESSA, W. Flathau
ATTN: Library
ATTN: WESSD, G. Jackson
ATTN: J. Strange
ATTN: WESSE, L. Ingram

U.S. Army Material & Mechanics Rsch Ctr
ATTN: Technical Library

U.S. Army Materiel Dev & Readiness Cmd
ATTN: DRXAM-TL

U.S. Army Missile Command
ATTN: RSIC

U.S. Army Nuclear & Chemical Agency
ATTN: Library

DEPARTMENT OF THE NAVY

David Taylor Naval Ship R & D Ctr
ATTN: Code L42-3

Naval Construction Batallion Center
Civil Engineering Laboratory
ATTN: Code L51, S. Takahashi
ATTN: Code L08A

Naval Electronic Systems Command
ATTN: PME 117-21

Naval Facilities Engineering Command
ATTN: Code 03T
ATTN: Code 04B

Naval Material Command
ATTN: MAT 08T-22

Naval Postgraduate School
ATTN: Code 0142 Library

Naval Research Laboratory
ATTN: Code 2627

Naval Sea Systems Command
ATTN: SEA-09G53

Naval Surface Weapons Center
White Oak Laboratory
ATTN: Code F31

DEPARTMENT OF THE NAVY (Continued)

Naval Surface Weapons Center
ATTN: Tech Library & Info Services Branch

Naval War College
ATTN: Code E-11

Naval Weapons Evaluation Facility
ATTN: Code 10

Office of Naval Research
ATTN: Code 715
ATTN: Code 474, N. Perrone

Office of the Chief of Naval Operations
ATTN: OP 03EG
ATTN: OP 981

Strategic Systems Project Office
Department of the Navy
ATTN: NSP-43

DEPARTMENT OF THE AIR FORCE

Air Force Institute of Technology
Air University
ATTN: Library

Air Force Systems Command
ATTN: DLW

Air Force Weapons Laboratory
Air Force Systems Command
ATTN: NTE, M. Plamondon
ATTN: DYT
ATTN: NTES-C, R. Henny
ATTN: SUL

Assistant Chief of Staff
Intelligence
Department of the Air Force
ATTN: INT

Ballistic Missile Office
Air Force Systems Command
ATTN: MMH

Deputy Chief of Staff
Research, Development & Acq
Department of the Air Force
ATTN: AFRDQSM

Deputy Chief of Staff
Logistics & Engineering
Department of the Air Force
ATTN: LEEE

Foreign Technology Division
Air Force Systems Command
ATTN: NIIS, Library

Rome Air Development Center
Air Force Systems Command
ATTN: TSLD

DEPARTMENT OF THE AIR FORCE (Continued)

Strategic Air Command
Department of the Air Force
ATTN: NRI-STINFO Library

DEPARTMENT OF ENERGY

Department of Energy
Albuquerque Operations Office
ATTN: CTID

Department of Energy
Nevada Operations Office
ATTN: Mail & Records for Technical Library

OTHER GOVERNMENT AGENCIES

Central Intelligence Agency
ATTN: OSI/NED, J. Ingley

Department of the Interior
Bureau of Mines
ATTN: Tech Lib

Federal Emergency Management Agency
ATTN: Hazard Eval & Vul Red Div

DEPARTMENT OF ENERGY CONTRACTORS

Lawrence Livermore National Laboratory
ATTN: W. Crowley
ATTN: J. Nutt
ATTN: L-10, H. Kruger
ATTN: Technical Information Dept Library

Los Alamos National Scientific Laboratory
ATTN: MS 362, Librarian
ATTN: MS 670, J. Hopkins
ATTN: M. Henderson
ATTN: G. Spillman
ATTN: MS 364
ATTN: R. Bridwell

Oak Ridge National Laboratory
ATTN: Central Research Library
ATTN: Civil Def Res Proj

Sandia National Laboratories
Livermore Laboratory
ATTN: Library & Security Classification Div

Sandia National Laboratories
ATTN: 3141
ATTN: A. Chabai

DEPARTMENT OF DEFENSE CONTRACTORS

Acurex Corp
ATTN: J. Stockton

Aerospace Corp
ATTN: Technical Information Services

Agbabian Associates
ATTN: M. Agbabian

DEPARTMENT OF DEFENSE CONTRACTORS (Continued)

Applied Theory, Inc
2 cy ATTN: J. Trulio

AVCO Research & Systems Group
ATTN: Library A830

BDM Corp
ATTN: Corporate Library
ATTN: T. Neighbors

Boeing Co
ATTN: R. Schmidt
ATTN: Aerospace Library

California Research & Technology, Inc
ATTN: K. Kreyenhagen
ATTN: Library
ATTN: S. Schuster

California Research & Technology, Inc
ATTN: D. Orphal

Calspan Corp
ATTN: Library

Civil Systems, Inc
ATTN: J. Bratton

University of Denver
Colorado Seminary
Denver Research Institute
ATTN: Sec Officer for J. Wisotski

EG&G Washington Analytical Services Center, Inc
ATTN: Library

Eric H. Wang Civil Engineering Rsch Fac
University of New Mexico
ATTN: N. Baum

Gard, Inc
ATTN: G. Neidhardt

General Electric Company—TEMPO
ATTN: DASIAC

IIT Research Institute
ATTN: Documents Library

Institute for Defense Analyses
ATTN: Classified Library

Kaman AviDyne
ATTN: Library

Kaman Sciences Corp
ATTN: Library

Lockheed Missiles & Space Company, Inc
ATTN: T. Geers
ATTN: Technical Information Center

Lockheed Missiles & Space Company, Inc
ATTN: TIC-Library

DEPARTMENT OF DEFENSE CONTRACTORS (Continued)

McDonnell Douglas Corp
ATTN: R. Halprin

Merritt CASES, Inc
ATTN: Library
ATTN: J. Merritt

Nathan M. Newmark Consulting Eng Svcs
University of Illinois
ATTN: N. Newmark

Pacific-Sierra Research Corp
ATTN: H. Brode

Pacifica Technology
ATTN: R. Allen

Physics International Co
ATTN: Technical Library
ATTN: J. Thomsen
ATTN: E. Moore
ATTN: F. Sauer
ATTN: L. Behrmann

R & D Associates
ATTN: C. MacDonald
ATTN: R. Port
ATTN: A. Latter
ATTN: J. Lewis
ATTN: W. Wright, Jr.
ATTN: J. Carpenter
ATTN: Technical Information Center
ATTN: P. Haas

Science Applications, Inc
ATTN: H. Wilson
ATTN: Technical Library

Science Applications, Inc
ATTN: D. Bernstein
ATTN: D. Maxwell

Southwest Research Institute
ATTN: A. Wenzel
ATTN: W. Baker

SRI International
ATTN: G. Abrahamson
ATTN: B. Gasten

Systems, Science & Software, Inc
ATTN: T. Riney
ATTN: K. Pyatt
ATTN: D. Grine
ATTN: R. Lafrenz
ATTN: T. Cherry
ATTN: Library

Terra Tek, Inc
ATTN: Library
ATTN: S. Green

Tetra Tech, Inc
ATTN: Library
ATTN: L. Hwang

DEPARTMENT OF DEFENSE CONTRACTORS (Continued)

TRW Defense & Space Sys Group
ATTN: Technical Information Center
ATTN: I. Alber
ATTN: R. Plebuch
ATTN: D. Baer
2 cy ATTN: N. Lipner

TRW Defense & Space Sys Group
ATTN: P. Dai
ATTN: E. Wong

Universal Analytics, Inc
ATTN: E. Field

DEPARTMENT OF DEFENSE CONTRACTORS (Continued)

Weidlinger Assoc, Consulting Engineers
ATTN: J. Wright
ATTN: M. Baron

Weidlinger Assoc, Consulting Engineers
ATTN: J. Isenberg

Westinghouse Electric Corp
Marine Division
ATTN: W. Volz

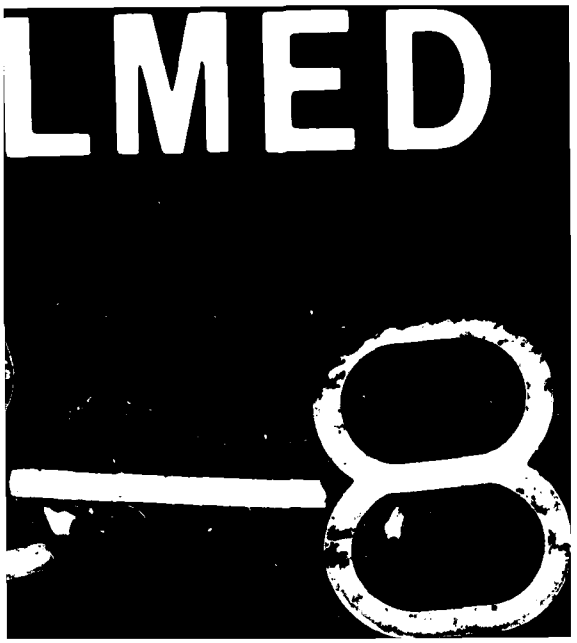
LMED